2018-07-20

The Sedimentation and Diagenesis of a Miocene-Pliocene Mixed-System: Cibao Basin, Dominican Republic

Brandon Burke
University of Miami, brandon.g.burke@gmail.com

Follow this and additional works at: https://scholarlyrepository.miami.edu/oa_theses

UNIVERSITY OF MIAMI

THE SEDIMENTATION AND DIAGENESIS
OF A MIOCENE-PLIOCENE MIXED-SYSTEM:
CIBAO BASIN, DOMINICAN REPUBLIC

By

Brandon G. Burke

A THESIS

Submitted to the Faculty
of the University of Miami
in partial fulfillment of the requirements for
the degree of Master of Science

Coral Gables, Florida

August 2018

UNIVERSITY OF MIAMI

A thesis submitted in partial fulfillment of
the requirements for the degree of
Master of Science

THE SEDIMENTATION AND DIAGENESIS
OF A MIOCENE-PLIOCENE MIXED-SYSTEM:
CIBAO BASIN, DOMINICAN REPUBLIC

Brandon G. Burke

Approved:

_____   _____
James Klaus, Ph.D.   Donald McNeill, Ph.D.
Associate Professor of Marine Geosciences   Scientist, Marine Geosciences

_____   _____
Peter K. Swart, Ph.D.   Guillermo Prado, Ph.D.
Professor of Marine Geosciences   Dean of the Graduate School

_____
André W. Droxler, Ph.D.
Professor of Earth Science
Rice University

BURKE, BRANDON G.   (M.S., Marine Geology and Geophysics)

(August 2018)

The Sedimentation and Diagenesis of a Miocene-Pliocene Mixed-System:
Cibao Basin, Dominican Republic.

Abstract of a thesis at the University of Miami.

Thesis supervised by Dr. James S. Klaus.
No. of pages in text. (100)

The diverse settings in which carbonate and siliciclastic sediments mix provides a challenge in developing predictive models of lithofacies distribution and sedimentologic heterogeneity. The skeletal carbonate and siliciclastic mud deposits of the Cibao Basin, in the northern Dominican Republic, are examined to better understand the dynamics of shelf sedimentation within a mixed-system and its diagenesis. The study examines the sedimentary components within the Gurabo Formation deposited during the late Miocene to early Pliocene. Deposition occurred during the time of a eustatic transgression known as the Zanclean Flood.

This outcrop study examines the variations in the sediment grain composition through three shelfal depositional sequences. The advantage to these outcrops is that the majority of the lithofacies can be disaggregated, providing unusual grain-specific information. There is a mixing of carbonate and siliciclastic content within each of these sequences. In general, the bulk sediment within the transgressive cycles contained a greater abundance of quartz grains (fine sand and mud), and that of the regressive cycles were predominately skeletal carbonate grains. It is noteworthy that in this mud-dominated mixed system there was prominent reef development.

The diagenetic susceptibilities within each of the depositional cycles differ due to changing hydrodynamic conditions. These conditions are likely more turbulent in transgressions than regressions (Mount, 1984). This creates a lithofacies distribution along the shelf that is not simply position-related, but must also be hydrodynamically considered due changing to physiographic and bathymetric conditions imposed through hydrodynamic cyclicity. In general, the transgressive cycles contained a greater abundance of quartz grains, and the regressive cycles were predominately comprised of skeletal carbonate grains.

Diagenesis within this mixed-system was dynamic in that there was microbiologically-mediated marine precipitation of calcite cements within the siliciclastic-rich intervals to produce composite cemented grains. The carbonate-rich intervals experienced typical (tropical) meteoric diagenesis with dissolution of aragonite, and precipitation of secondary calcite and dolomite cements.

Hydrodynamics were a key influence for the lithofacies changes along the shelf as described through transgressive and regressive cycles within the restricted shelf setting. The results of the sedimentology and geochemistry study comprise the necessary framework to illustrate the mixing of the components through temporal changes along the compressed shelf (~6 km wide inner shelf to outer shelf) tropical depositional system. This research along the inner to middle shelf provides a case study for the sedimentological dynamics within restricted water-circulation settings for carbonate-siliciclastic mixing, depositional lithofacies characterization, and the subsequent diagenetic tendencies therein.

Acknowledgements

The choice to begin degree came with many sacrifices – leaving a job and family in Houston to pursue higher education. I would like to thank my family and friends for their moral support as I went to Miami for this pursuit. My grandparents for their advice and for providing confidence that I was ready to focus on developing my geological skills by attending graduate school.

The University of Miami and the Rosenstiel School was a supportive institution that provided me the resources to learn and experiment with my data in a way that exceeded all my expectations. I would like to thank my advisors, Dr. James Klaus and Dr. Donald McNeill for their relentless support in this sedimentology study. I would also like to thank Dr. Peter Swart and the isotope laboratory for use of their equipment, their oversight, trust, and interest in my research. There are many other people that provided their resources, time, and taught me lessons in their respective focuses including Dr. Ali Pourmand, Amel Saiid, Amanda Oehlert, Brooke Vitek, Talib Oliver Cabrera, Philip Staudigel, Anieri Morales Rivera, and many others from the University of Miami that contributed to this research effort.

I have great appreciation to all at the Rosenstiel School for the lessons and experiences that went beyond the degree program. Miami will always be home to me, and I will be forever thankful for the opportunities afforded to me through Marine Geology and Geophysics.

TABLE OF CONTENTS

List of Figures

List of Equations

List of Tables

Chapter 1. Introduction

Mixed-system sedimentology and stratigraphy along the shelf has been well-established and studied for many decades (Maxwell & Swinchatt, 1970; Mount, 1984). Mixed carbonate-siliciclastic systems commonly occur in tropical, low-latitude regions (Dunbar & Dickens, 2003; Purdy & Gischler, 2003; Tcherepanov et al., 2008). It is not always apparent that mixed-systems are comprised of coeval deposition between the carbonate and siliciclastic end-members. However, it is evident that these systems have considerable depositional facies heterogeneity along the shelf, and there are established sedimentological trends observed in their deposition between proximal and distal positions such as grain size tendencies that are more coarse proximally to their source and fine more distally (Flood et al., 1978). This study deconstructs the distribution of the admixed carbonate and siliciclastic grains to assist in paleo-shelf lithofacies reconstruction.

Examples of modern mixed carbonate-siliciclastic deposition include regions such as Australia's Great Barrier Reef (Francis, 2007), Papua New Guinea (Droxler & Jorry, 2011; Maxwell & Swinchatt, 1970; Puga-bernabe et al., 2015), and Belize (Purdy & Gischler, 2003). Ancient shelf margin mixed-systems have been recently documented in Angola (Eichenseer et al., 1999), Panama (McNeill et al., 2013), southeast Spain (Reolid et al., 2014), and Papua New Guinea (Droxler & Jorry, 2013). Each of these systems documents the dynamics of eustatic change, turbidity, climate, subsidence, sediment types, supply rates, and shelf physiography as depositional controls for sedimentation. Many of these studies present a disconnect between input on the shelf to that of the basin is often due to localized climate and weather conditions, its near-shore depositional processes, which causes the shelf environment to be less understood than the basinal eustatic and supply-

driven models. This near-shore mixed-system setting has considerable variability that exemplify that the simplified concept of pure end-member systems is not realistic because there is mixing throughout the successions (Schlager et al., 1994). In general, this study corroborates that each sequence favors a tendency for proportional changes from predominate siliciclastic influence at the base of the sequence to predominately carbonate at the top of the sequence.

Few shallow water sedimentary systems have remained unconsolidated beyond the Holocene time period, and one of those is the easily accessible late Miocene to Pliocene outcrops of the Cibao Basin. Here, sediments are amenable to disaggregation and examination of individual grains. The composite vertical succession of outcrops, included in this study, provides predominately a vertical means of interpreting the overall paleo-shelf lithofacies changes, to assess the coeval deposition of both skeletal and siliciclastic grains along the paleo-shelf, and to integrate those observations into a context of relative sea level fluctuations.

This study assesses the sedimentation of a narrow shelf mixed-system in order to illustrate temporal mixing and diagenetic susceptibility. The main goal of this study is to illustrate the sedimentological mixing of carbonate relative to siliciclastic sediments. A secondary objective is to assess how changes in the nature and abundance of the constituent sedimentary components and their surrounding matrix influence the susceptibility of the different lithologic units to diagenesis. This approach can provide the necessary tools to determine which of the sedimentary components contribute most to the bulk isotopic signature and what drives the bulk isotopic responses of the mixed-system.

1.1 Regional Geologic Setting

The island of Hispañiola is part of the Greater Antilles island chain that includes from west to east: Cuba, Hispañiola, and Puerto Rico (Figure 1). Island arc subduction has been inactive since the collision with the Bahama platform in the Eocene and early Oligocene and the initial opening of the Cayman Trough (Heubeck et al., 1991). Transpression began in the middle to late Miocene and continues today (Figure 2). There is strike-slip movement along both the Septentrional fault zone (SFZ) in the north at 12.8 mm/yr and the Enriquillo-Plantain Garden fault zone (EPGFZ) at 9 mm/yr in the south (Calais et al., 2002). The geology of the Hispañiola can thus be considered part of a mature island arc formed in an intra-oceanic setting (Bowin, 1966).
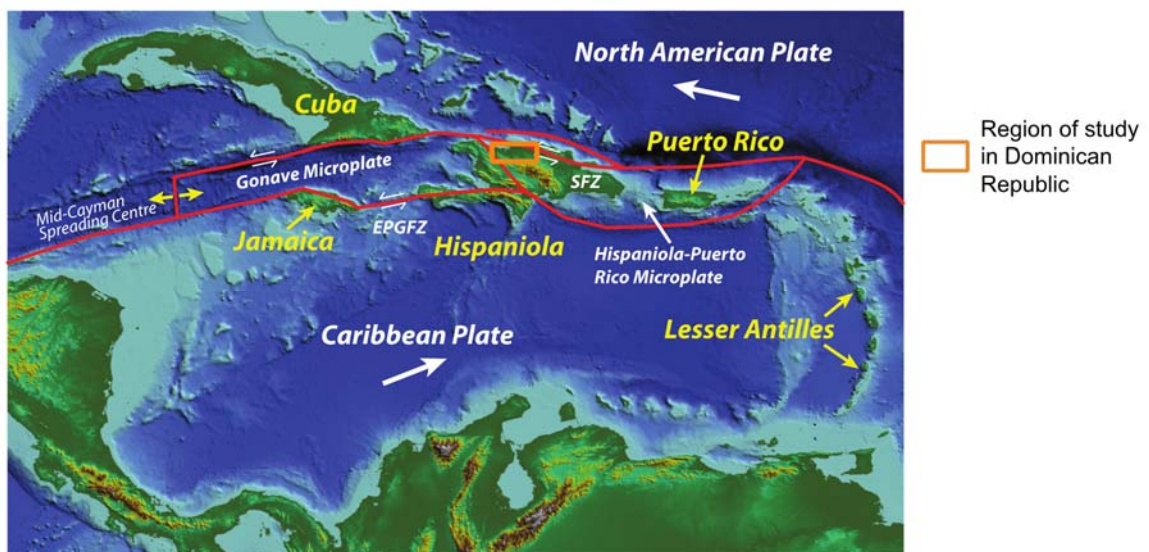
Figure 1: Regional location and tectonic setting of the Hispañiola-Puerto Rico microplate and their relation to the transpressional movement along the SFZ and EPGFZ.

Hispañiola consists of four northwest-southeast trending mountain ranges. From north to south, these are the Cordillera Septentrional, Cordillera Central, Sierra de Neiba, and Sierra de Bahoruco. These mountain ranges are separated by low-lying valleys or basins, from north to south, these include the Cibao Valley, the San Juan Valley, and the

Enriquillo Valley. The main basement of the island is composed of Cretaceous-early

Eocene igneous and metamorphic age rocks formed as part of the aforementioned volcanic

island arc and forearc.
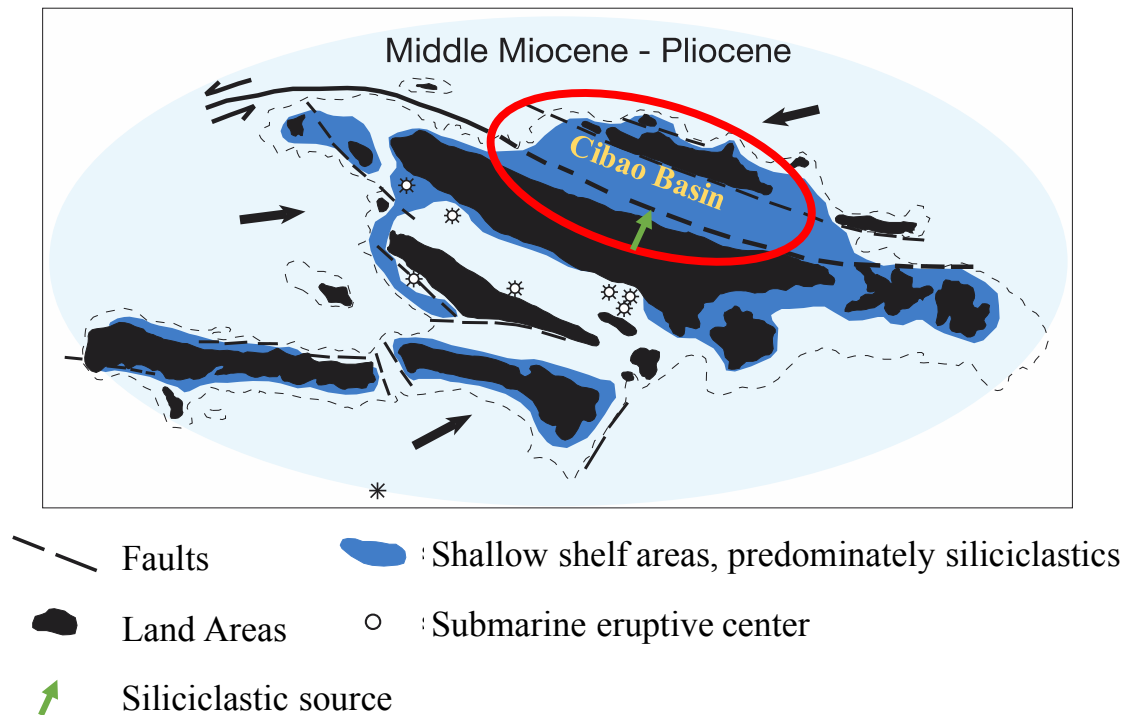
Figure 2: Illustration depicting the major tectonic boundaries of Hispañiola and the distribution of the shallow marine shelf area during the Miocene and Pliocene. This time period precedes the closure of the shallow shelf due to subsequent transpressional uplift and narrowing of the Cibao Basin seaway. Figure modified from McNeill et al. (2012) and Maurrasse et al. (1982).

The Cibao Basin lies between the Cordillera Septentrional mountain chain to the

north and Cordillera Central mountain chain to the south (Figure 3). The basin is a result

of compressional and sinistral transpression caused by the eastward motion of the

Caribbean Plate relative to the Greater Antilles Deformed Belt (Draper et al., 1994)

(Figure 2). The Septentrional strike-slip fault bounds the northern edge of the Cibao Basin

(Figure 2). During the middle Miocene to Pliocene the Cibao Basin consisted of a shallow

marine shelf composed of mixed carbonates and siliciclastics (Figure 2). The Cibao Basin

was at one time an open marine shelf and seaway where siliciclastic sediments were shed from the mountains of the Cordillera Central and mixed with local biogenic carbonate (Figures 2 and 3). Siliciclastic sediments were produced by the weathering of metamorphic and igneous rocks of the basement complex and transported by a series of rivers into the marine waters; whereas, carbonates were produced *in situ* through biogenic activities during times of marine inundation. McNeill et al. (2012) confirmed Saunders (1986) conclusions that the Cibao Basin consists of three distinct formational units that include: late Miocene Cercado Fm, late Miocene and early Pliocene Gurabo Fm, and the early Pliocene Mao Fm (Evans, 1986; Saunders, 1986; Vokes, 1979) (Figure 4). In the mid-Pliocene, the basin was uplifted due to compressional forces, exposing a thick section of Neogene marine shelf deposits (McNeill et al., 2012) (Figure 2).
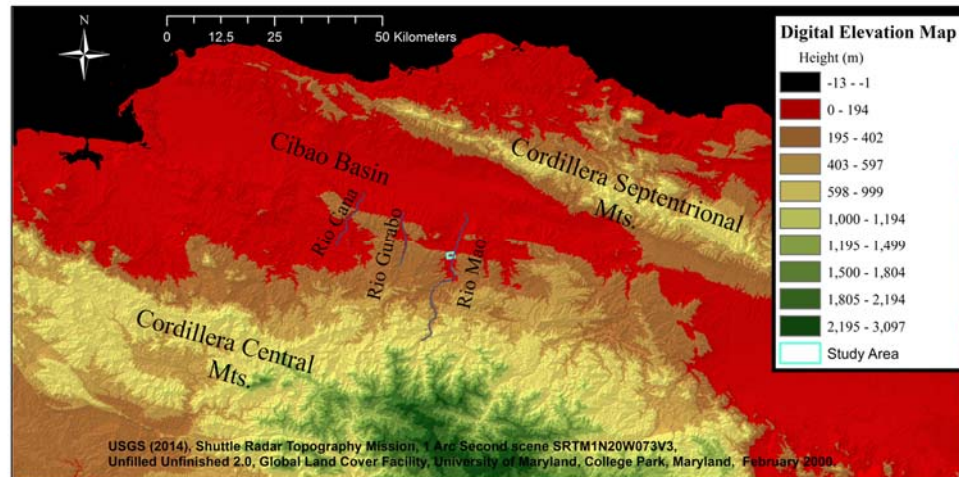
Figure 3: Regional digital elevation model (DEM) displaying the Cibao Basin (red). DEM downloaded from USGS (2014).
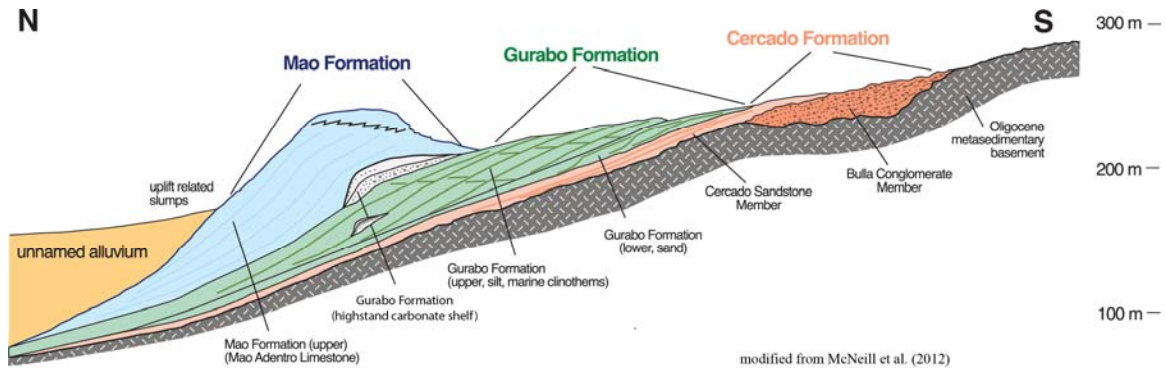
Figure 4: The generalized stratigraphy within the Cibao Basin shelf margin, including the Cercado Fm., Gurabo Fm., and Mao Fm. Figure is modified from McNeill et al. (2012).

1.2 Framework of Sea Level Changes During Gurabo Fm. Deposition

The Gurabo Fm. deposits record shelf deposition across the Miocene-Pliocene boundary, a time period in Earth history that contains several major sea level events. The section examined in this study provides a record of deposition across the transition from the Messianian sea level lowstand (where desiccation occurred in the Mediterranean Basin) to a subsequent rise in sea level (Zanclean Flood event) that flooded many of the world's continental shelves and isolated reef platforms (Van Couvering et al., 2000).

The Zanclean Flood event has worldwide potential for correlation and the rapid redistribution of the global water mass (Van Couvering et al., 2000). This event has mainly been tied to the Mediterranean Sea due to the reflooding of the Mediterranean that ended the Messinian Dessication event (Hsu et al., 1973).

As there was no Messinian dessication event outside of the Mediterranean, the event is often marked by a lowered sea level, seaward shift in the shoreline position, and subaerial exposure in the relatively higher elevations (Hodell & Kennett, 1986). The eustatic sea level rise associated with the Zanclean flood event produced a landward shift in the shoreline position, a transgression on many continental shelves and margin back-stepping in carbonate systems. This transgressive surface may be erosional, so a distinct

change in the lithologic record, the diagenetic record, and perhaps the isotopic composition may be the key in identifying this boundary.

The Zanclean Flood is hypothesized to consist of two pulses of eustastic rise according to (Haq et al., 1987) (Figure 5). These pulses of eustastic deepening had estimated magnitudes of ~132 m and ~89 m based on seismic data and their sequence interpretation (Haq et al., 1987). Other estimates of sea level magnitude have been more difficult to ascertain and confirm (Gornitz, 2008), but based on the aforementioned seismic methodology, these two sea level transgression events, are separated by a fall in sea level estimated at ~122 m. The total transgression corresponds to a sea level rise of ~100 meters between 6 and 3.8 Ma (McNeill et al., 2012; Tcherepanov et al., 2008).

Miller et al. (2011) further refined the eustatic sea level curve to higher order cycles (Figure 5). There are at least three major transgressions during the time of the Gurabo Fm. deposition (Miller et al., 2005). They indicate eustatic inundations of approximately 93.3 m, 69.2 m, and 46 m between 5.755 Ma and 4.155 Ma (Miller et al., 2005) (Figure 5). Miller reconstructed these sea level curves by applying backstripping using reefs, continental margin strata, and oxygen isotopes from global database records. These oxygen isotope records were used as a proxy for water temperature and thereby continental ice sequestration and eustatic sea level (Burgess & Steel, 2017).
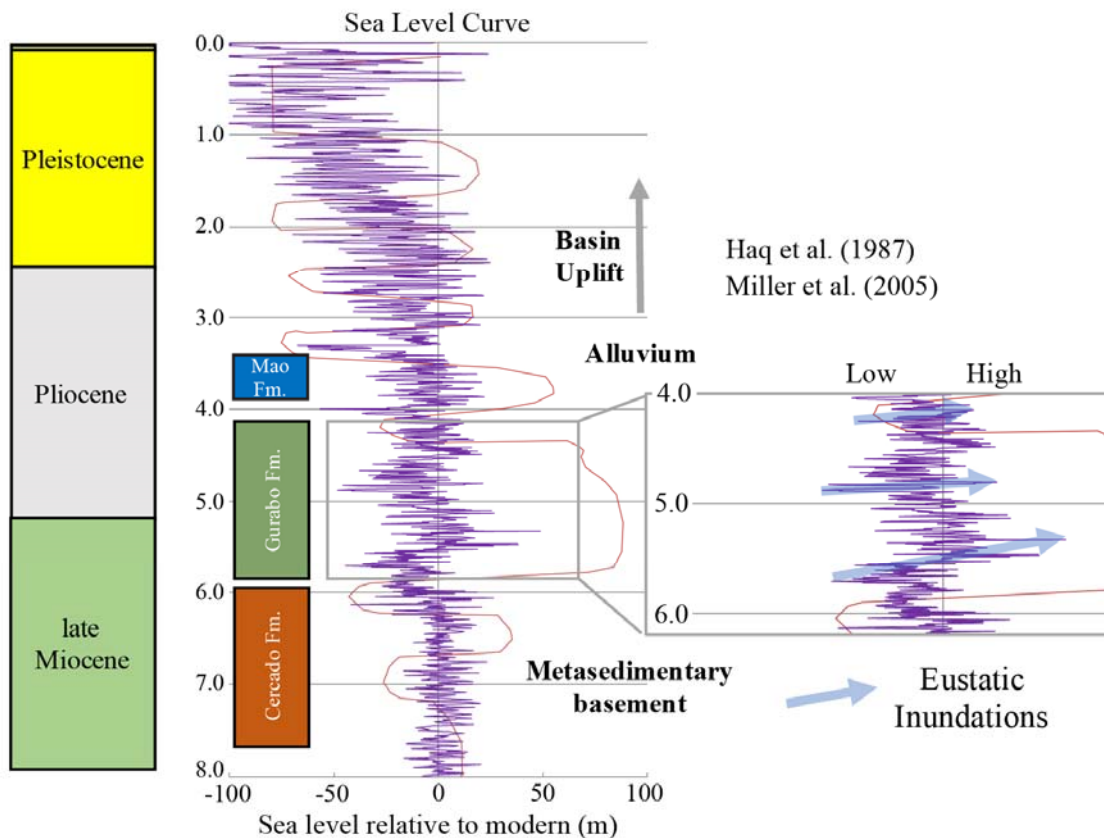
Figure 5: An age summary of the Cibao Basin depositional formations with respect to eustatic sea level fluctuations. The formation ages are from McNeill et al. (2013). The sea level curves are from Haq et al. (1987) shown by red line and Miller et al. (2005) shown as purple line, and the primary eustatic inundations are in three general pulses indicated by the blue arrows.

Chapter 2. Sampling and Analytical Methods

2.1 Field Sampling

The outcrops examined for this study are generally located south and west of the town of Mao, in the Valverde province. Deposition spans from the late Miocene to the Pliocene and is associated with three formations including the Cercado Fm., the Gurabo Fm., and the Mao Fm. Each of the three subsequent formations is characterized by progradation and aggradation in a more basinward position (north-northwest) (Figures 4, 5, and 6). There are eight studied outcrops near the Rio Mao (Figure 6). One Cercado Fm. outcrop is located to the south, whereas seven Gurabo Fm. outcrops labeled RM-1, RM-2, …, RM-7 are located further to the north (Figure 6). Among the seven Rio Mao outcrops, the first six were manmade through excavation for a road, a hydrologic dam, power and water treatment plants. The seventh outcrop to the east is not well understood in terms of its correlation to the other studied outcrops, and therefore will not be assessed in the present study (Figure 6).

The Gurabo Fm comprises the units of the Rio Mao stratigraphic section and was measured using a Jacob's staff, Brunton compass, and sight-balance tool to calibrate the bedding thicknesses and contacts over large lateral offsets (Figure 7). The section was measured and main lithofacies were logged using a hybird textural classification of the simple siliciclastic grain-size type (mud, silt, sand, gravel) and the Dunham (1962) carbonate classification (mudstone, wackestone, packstone, grainstone, rudstone, framestone). Mud-size to fine sand sediments comprise the bulk sedimentary matrix for the majority of the section.
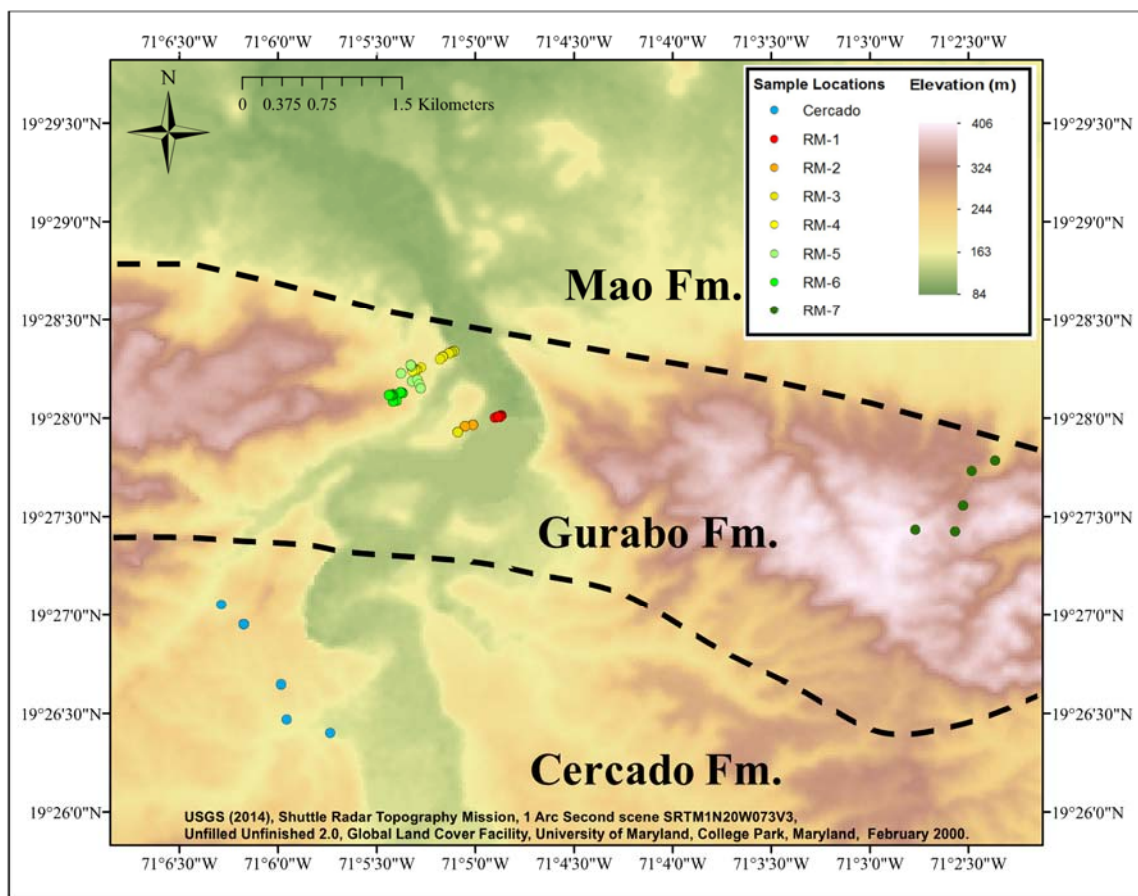
Figure 6: Digital elevation model (DEM) for outcrops of the Cercado, Gurabo, and Mao Formations in the area of the Rio Mao. DEM downloaded from USGS (2014).

The Formation is largely unconsolidated matrix sediment with more cemented reefal intervals. The unconsolidated matrix is ideal to study the sedimentology and stratigraphy of this mixed system. The cohesive sediments of the matrix were collected with a small gas-powered drill. Six-inch plug samples were drilled so that fresh, unweathered sediment was accessible. The plug samples, although weakly consolidated, provide less diagenetically-altered material than the exposed outcrop. In areas where the sediments were not cohesive enough to drill, hand-samples were collected with a rock hammer after 5-10 cm of the weathered surface was removed. Samples were typically

collected in 1 to 2 meter intervals where the section was exposed through the Gurabo Fm. In total, 128 samples were collected through the ~160-meter-thick measured section.

2.2 Sedimentological Analyses

Sediment samples were soaked in 4% sodium hexametaphosphate to help disaggregate the siliciclastic matrix. The remaining sediment clumps were gently broken by hand, or placed in a sonicator. Of the 128 samples, 84 were amenable to disaggregation. The remaining 44 samples included concretions as well as other lithified beds, mainly in the upper carbonate-dominated part of the section. These samples were too indurated with secondary cements to fully disaggregate.

The unconsolidated sediment was wet sieved (1 mm, 0.5 mm, 0.25 mm, 0.125 mm, and 0.063 mm sieves) to isolate the mud (<0.063 mm), sand (0.063-2.0 mm), and gravel (>2 mm) fractions. The washed material was collected from the sieve and dried to determine a weight percent of each fraction.

To determine the sediment composition, each of the sieve fractions greater in size than mud was examined and analyzed by point counting of the grains utilizing a stereomicroscope. If grains were present, each size fraction was point-counted for at least 50 grains, with an average of 57 grains per sample. Point counting has been reconciled to illustrate the percent weight of eight different component types within the section. The assumptions were that all the grains were the same weight and the counts were representative of the entire sample. The dried bulk sample weight per sieve size fraction multiplied by the percent of each components contribution to the sieved sample produces the weight percent of each component type in each sieve size (Equation 1).

Equation 1: Equation for the weight percent of each componenet from point counts within each sieve size.

(Dried bulk wt.) x (% component from whole) = (Wt. % Component in each sieve size)

2.3 Carbonate Mineralogy by X-Ray Diffraction and Thin Section Petrography

Ninety-eight bulk powdered samples were homogenized with a mortar and pestle, mixed with deionized (DI) water and the resultant paste was then mounted on a glass slide. These samples were subsequently analyzed for carbonate mineralogy through X-ray diffraction (XRD) using a PANanalytical X'pert Pro diffractometer. The samples were scanned following the protocol established by Swart et al. (2000). The XRD scans were run from 10° to 40°, this range provided some of the main peaks for the common carbonate minerals (aragonite, low Magnesium Calcite (LMC), high Magnesium Calcite (HMC), and dolomite) and siliciclastic minerals (quartz and feldspars). Each mineral is identified using its 2θ peak positions and its relative intensity. The peak area for each of the carbonate minerals was measured by the PANanalytical software and used to calculate the percentages of aragonite, calcite, and dolomite. These percentages were calculated based on a series of in-house standard mixtures. The standards used in this calculation were compiled from the different compositions of pure aragonite, calcite (LMC, HMC), and dolomite.

Thin sections were prepared for ten bulk sedimentary samples at the University of Miami and were petrographically examined for composition and diagenesis. Seven thin sections were additionally prepared from 3.3 m, 89.1 m, and 125.95 m in the Rio Mao section to investigate possible biologically mediated grains. Primary features of interest were the cement types, replacement, recrystallization, pore types, and mineralogy presence.

2.4 Percent Carbonate, Total Organic Carbon, and $\delta^{13}C$ of Organics

Total percent carbonate and organic carbon (TOC) values were measured for each one of the 78 bulk powder samples. Each homogenized sample was treated with 10% HCl to dissolve the carbonate fraction. Subsequently, four rinses with DI water were applied to remove the acid residue, and then the samples are slowly dried in an oven at or below 50°C. Once dry, the difference between the pre-weighed samples and the post-weighed samples yield the soluble percentage of the sample, which is interpreted to represent the carbonate fraction of the samples. The resultant sediments were then packed into small aluminum foil tins for six separate runs with the initial sample containing weights of 10 to 15 mg and subsequent runs containing sample weights of 20 to 25 mg per sample. The runs utilized both the Thermo Delta V Advantage Mass Spectrometer and a Costech elemental analyzer employing methodology from Mehterian et al. (2017). These runs also provided $\delta^{13}C_{Organic}$ isotope values that are reported in per mil (‰) and are calibrated relative to the PDB standard. A calculation using in-house standard mixtures produced the TOC values.

2.5 $\delta^{13}C$ and $\delta^{18}O$ of Carbonates

The bulk inorganic carbon and oxygen stable isotopes were measured using a Finnigan MAT-251 mass spectrometer employing methodology from Mehterian et al. (2017). The sample's stable-isotope values represent the average value of the grains, matrices, and cements in the bulk sample. The resulting values for $\delta^{13}C_{Inorganic}$ and $\delta^{18}O_{Inorganic}$ isotopes are reported in per mil (‰) and are calibrated relative to the Vienna Pee-Dee Belemnite (PDB).

The individual components that make up the mixed-system had their inorganic stable isotope values measured using the Delta Plus mass spectrometer employing methodology from Mehterian et al. (2017). The components analyzed through the section include: benthic foraminifera, bryozoans, calcite flakes, composite cemented grains (CCG), corals, coral debris, mollusks, planktic foraminifera, urchin spines, and worm tubes.

A composite inorganic isotope curve based on the relative abundance of individual components was generated for comparison to the bulk isotopic signature. The composite curve was developed by multiplying the isotopic signature of the individual component ($\delta^{13}C_{Component}$) by the proportion of the component (**a, b, …, z**) with respect to the whole sample, from point counts (Equations 1 and 2). Each of the proportions add up to 100% of the component distributions to yield a composite inorganic isotope curve. The only values that are not accounted for in the composite curve are the <63 μm inorganic carbon values. The total carbonate content of the mud-size sediment was typically less than 30% carbonate (Appendix D).

$$\delta^{13}C_{Components} = \sum a * \delta^{13}C_a + b * \delta^{13}C_b + \ldots + z * \delta^{13}C_z$$

Equation 2: Composite curve equation for inorganic carbon isotope and proportion of component

The primary (original) signature curve utilized modern $\delta^{13}C_{Carbonate}$ values for each component type to reconstruct a profile that lacks diagenetic alteration based on an identical proportion of sedimentary components that exist within the Miocene-Pliocene Gurabo Fm mixed-system. The primary signature $\delta^{13}C$ values and the proportions for each component as they vary for each of the 18 samples are listed in Appendix C.

2.6 Chronostratigraphy

Three coral and one scaphopod samples were processed by homogenizing the samples in a SPEX CERTI PRGP 8000 mixer/mill. The samples were pre-screened for diagenetic alteration through XRD analysis, and each of the samples contained >93% aragonite content. Samples were analyzed for Sr in a Neptune Mass Spectrometer at the University of Miami, and subsequently scanned following the protocol established by Pourmand et al. (2014). The isotopes of Sr ($^{87}Sr/^{86}Sr$) were dissolved from the skeletal carbonate with nitric acid and analyzed on a ThermoFisher Neptune Plus multi-collection inductively coupled plasma mass spectrometer. Raw data were corrected for mass bias and isobaric interferences and the final ratio was further adjusted relative to the accepted value of 0.710248 for SRM987. Age dates were calculated based on the Sr^{87}/Sr^{86} ratio at two locations within the Gurabo Fm. Calibrated strontium-isotope dates were used as the primary age tie points between 3 Ma and 7 Ma (McArthur et al., 2001).

Chapter 3. Results

3.1 Study Reference Section

A reference section for the Rio Mao outcrops has been compiled from six individual outcrop sub-sections (Figure 7). The individual sub-sections are projected to their relative position using strike and dip information collected at six localities. Slight overlap occurs in some of the sub-sections using this technique and only one minor (~2 m) gap occurs. The six sub-sections within the Rio Mao (RM), or outcrops, are named: RM-1 (base of section at dam), RM-2, RM-3, RM-4, RM-5, and RM-6 (the water plant excavation). The section had a measured thickness of nearly 160 m from the base, near the contact of the underlying Cercado Fm. The reference section is projected to be at the base of the "dam" section (RM-1) on the Rio Mao to the top of the water plant section (top of RM-6) (Figure 7). The composite lithostratigraphic section was divided into seven main units (I-VII) based on the dominant lithology.

3.1.1 Unit I (0-20 m)

Lithostratigraphic Unit I is the lowest part of the reference section and overlies the projected exposure boundary that separates the Gurabo Fm from the underlying Cercado Fm. The unit ranges from 0-20 m in the reference section. The outcrops that comprise the RM-1 location begin at the base of the concrete dam below the lake-like reservoir and continue west up to the asphalt road.
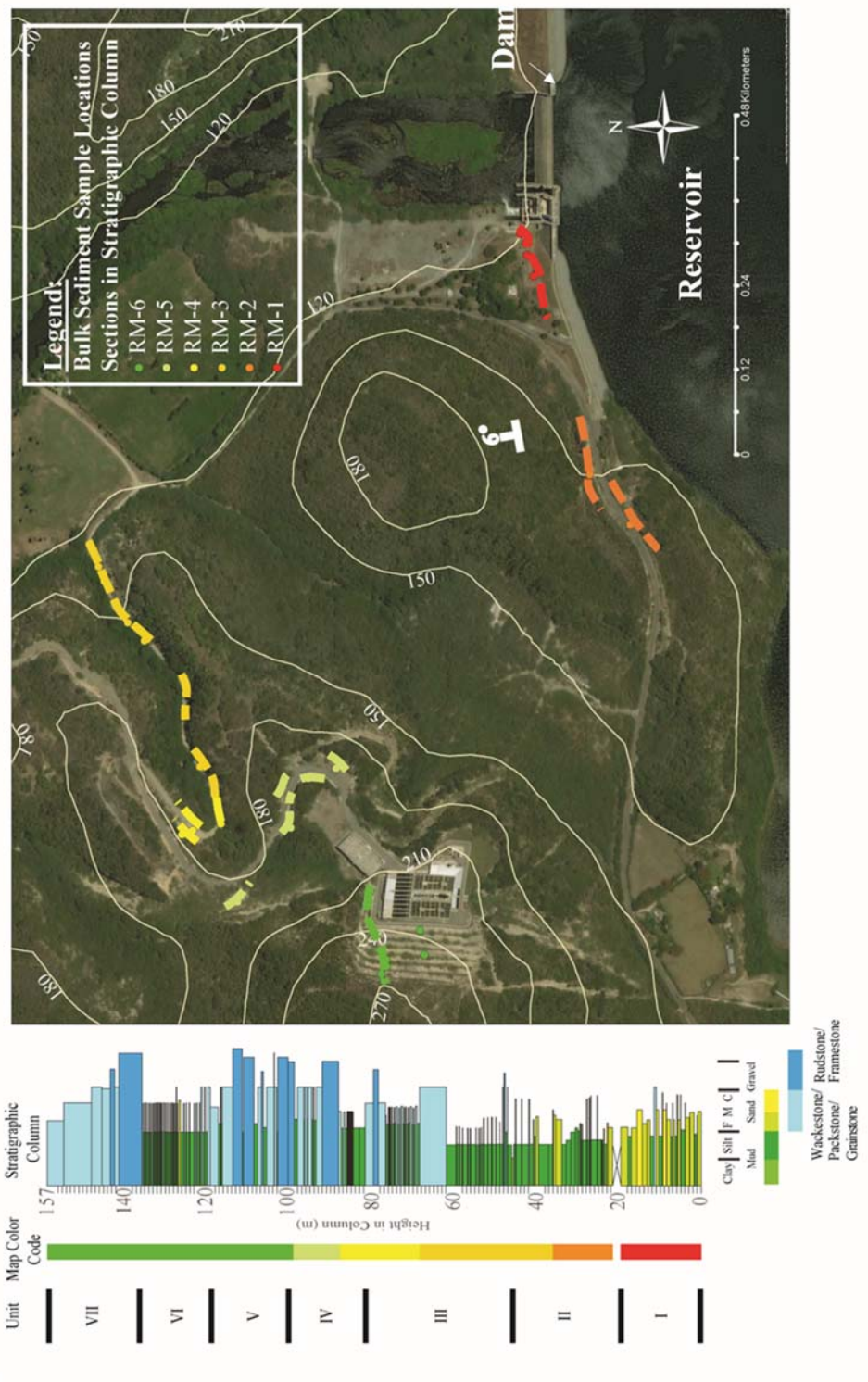
Figure 7: Stratigraphic column, units I-VII, and map of the Rio Mao sections through the Gurabo Fm. Map and contours are from USGS DEM (2014). The left side of the photograph shows the water treatment plant and the top of the section. The base of the section is at the dam, shown at the right center of the photograph.

The main faunal components (Figure 9) throughout the unit are benthic foraminifera with minor amounts of bivalves, gastopods, coral fragments, and crustaceans (crab claws). The benthic foraminifera were ubiquitous throughout the unit and molluscs became more abundant in the upper third of the unit. Most of the sand and mud beds had some degree of bioturbation in the form *Thalassinoides*-type burrow structures. There were also wood oxidation rings seen in the outcrop (Figure 8).
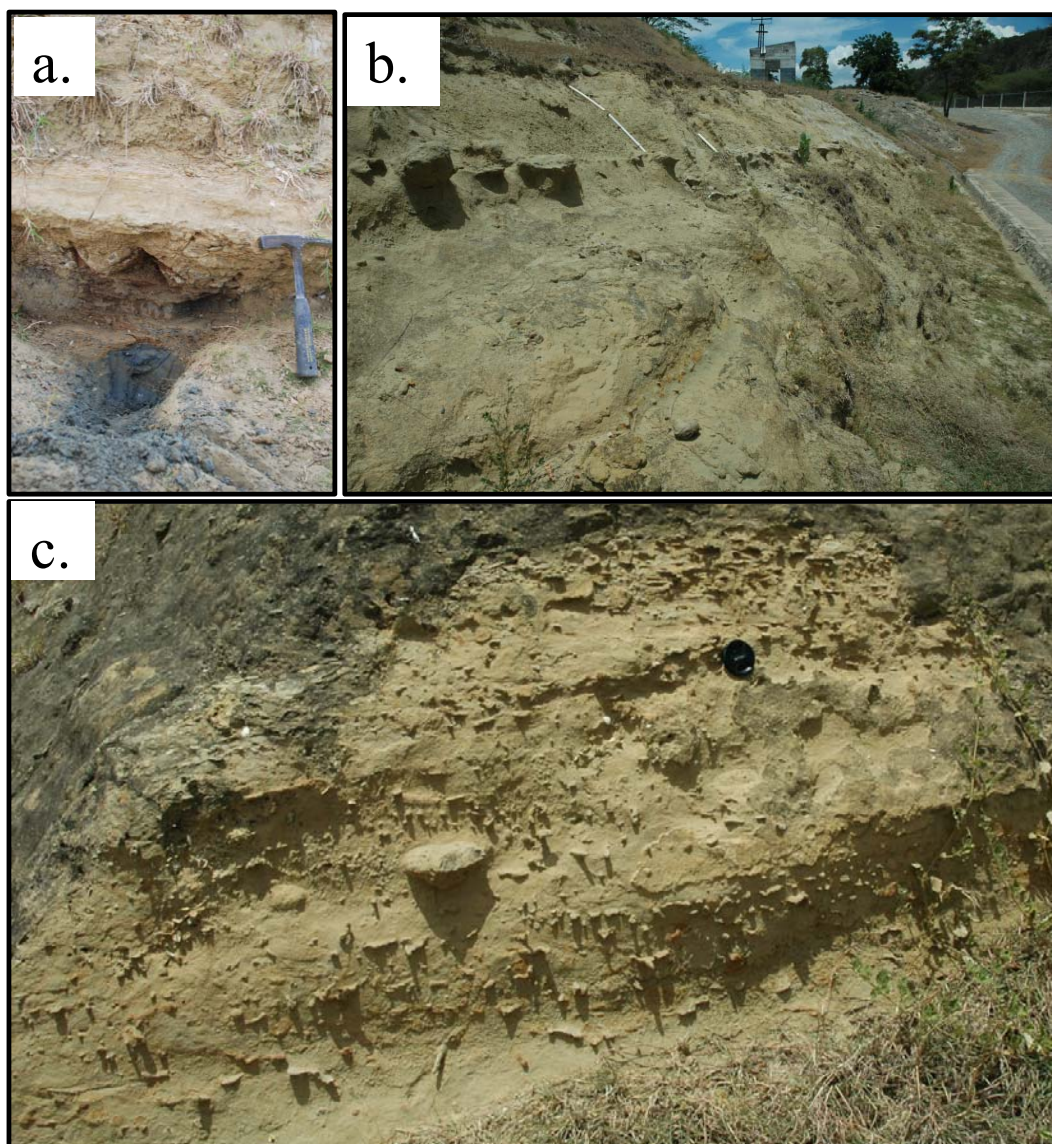
Figure 8: Unit 1 a) (0.85-1.1 m) base of section marked by clay layer overlain by oxidized layer (soil, possible exposure); b) (1-3 m) thick layers of siliciclastic content with bioturbation and concretion bed; c) (12 m) *Thalassinoides* bioturbation and mollusks within sedimentary matrix

Diagenetically, the sand and mud beds show little post-depositional alteration. Thin (1-3 cm) calcite veins occur perpendicular to bedding at the base of the section (0-5 m in reference section).   Concretionary beds are 10 to 30 cm thick and follow the primary bedding. These concretions occur throughout Unit 1. The concretions are knobby and may follow burrow structures (Figure 8b).

3.1.2 Unit II (22 m – 45 m) (Note the 2 m gap between Units I and II)

Unit II is the second lithologic unit from the base of the composite lithostratigraphic column. The interval ranges from 22-45 m in the section, and the unit is found within outcrop section RM-2 and RM-3 (Figure 7). There is a ~0.7 km offset between RM-2 and RM-3, and RM-3 is offset in a down-dip direction (basinward direction to the north).

Within Unit II, the outcrops are composed of mud and fine sand. Beds of more cohesive or indurated nature alternate with softer, recessed silt-mud beds. Most of the beds range from 0.25 to 2.0 m in thickness (Figure 10). The base of Unit II is predominately greenish quartz sand that grades to an increasingly greenish mud-rich composition towards the top of the unit (Figure 10a and 10c).

The main faunal components are benthic foraminifera, mollusks, corals and coral debris, bryozoans, and planktic foraminifera. The benthic foraminifera and mollusks first appeared above the quartz sand at the base of the unit (base of RM-2). There are abundant free-living coral fauna (Klaus et al., 2008) dispersed through the fine sand to silt layers between 22 to 43 m (Figure 10). Free-living coral and other skeletal debris occur also in a 30-50 cm thick debris bed at the base of the RM-3 outcrop (~42 m in section near Figure 10c). Benthic foraminifera are present throughout the unit, and corals, mollusks, and

planktic foraminifera increase in abundance within the interval at ~40-45 m (Figures 9e and 9f).
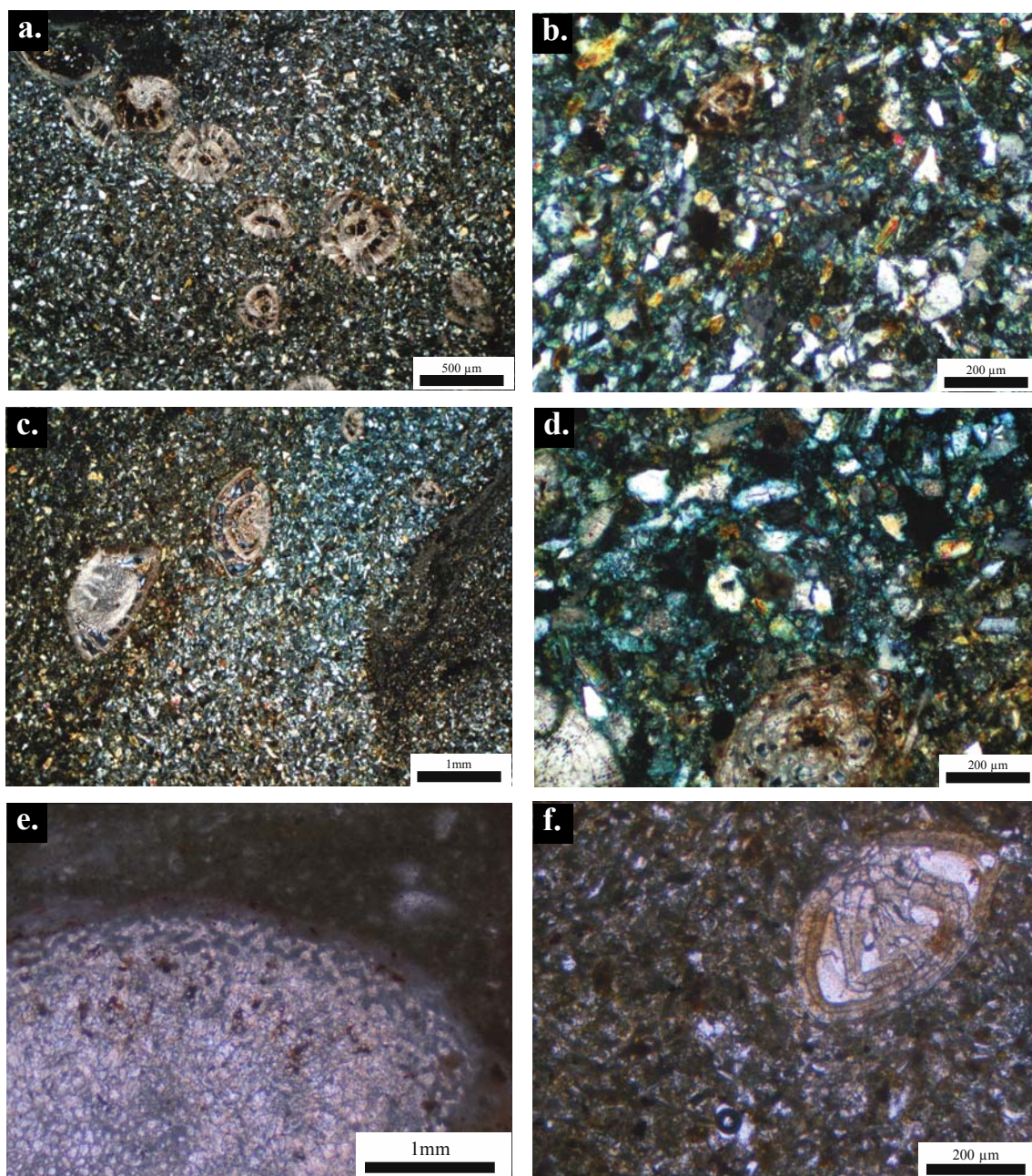
Figure 9: Thin section images under cross-polarized light. Figures a-d from Unit I of Rio Mao section Gurabo Fm (a through c from 9.1 m in section); a) yellow, silt-size quartz dominate the matrix with mica, opaque pyrite, and well preserved benthic foraminifera; b) well-sorted very fine quartz grains, mica, and feldspars within the matrix; c) porosity (indicated by blue dye infiltration) variations in sand that may be bioturbation-related; d) (14.6 m in Mao section) silt and very fine sand with benthic foraminifera (bottom left) and bryozoan (bottom center). Thin section images e-f from Unit III at 68.1 and 68.5 m in Rio Mao section, respectively. e) LMC coral recrystallized within mud matrix; f) fine quartz sand and pyrite within matrix with a benthic foraminifera composed of sparry, calcite cement.
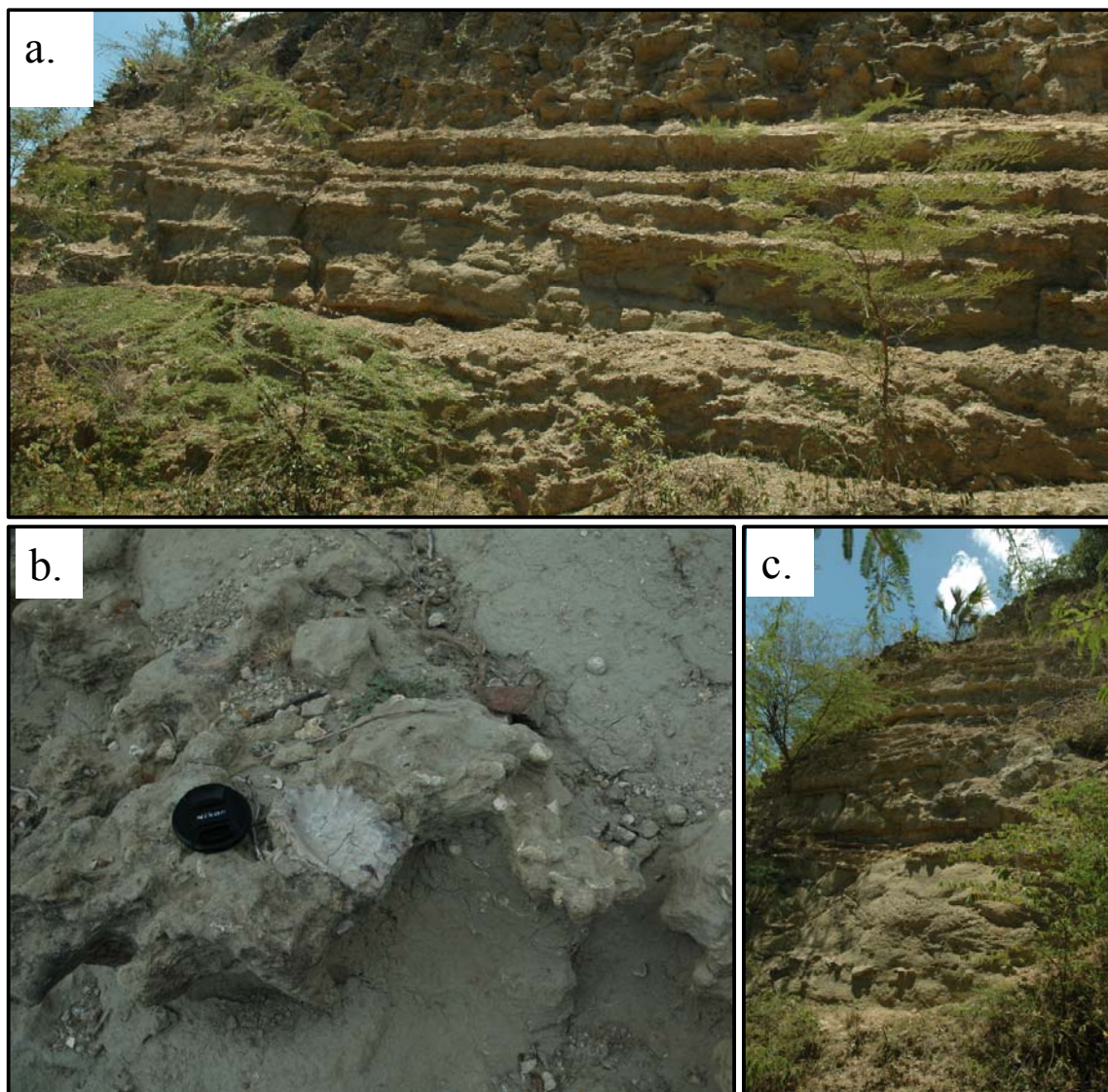
Figure 10: Unit II outcrops a) (26-30 m) succession of beds with low-angle dip to northwest, abundant free-living corals in this low energy environment; b) (45 m) free-living corals and oyster shell; c) (42-46 m) (low part of photograph) massive green silt layers with azooxanthellate free-living corals.

The sand and mud beds had relatively little post-depositional diagenetic alteration. 10-40 cm thick knobby concretions, similar to Unit I, follow the primary bedding through this interval at RM-2 (Figure 10a). Gypsum and calcite veins occur perpendicular to bedding sparingly but extended through the full extent of the outcrop at RM-2. The RM-3 outcrops had no prominent outcrop indicators of diagenetic alteration.

3.1.3 Unit III (45-81 m)

Unit III lies within the RM-3 and RM-4 outcrops between 45-81 m height in the section. The outcrop transverses the lithostratigraphic section by following along a road cut with increasing elevation, to the west, mostly along the strike direction (Figure 7). The base of Unit III comprises a 40 cm thick coral debris layer that is overlain by 50 cm to meter-scale bedforms with low dip angles from 45-60 m height in section (Figure 11a). The beds were predominately composed of mixed mud and quartz sand with mollusks, coral debris, and benthic foraminifera (Figure 11a). The first large reefal unit occurs between 62 m to 72 m in the section. The upper ~7 m of the section contain 10-30 cm thick greenish, cohesive silt-sand beds that alternate with indurated concretion beds (Figures 11b and 11c). Capping the unit is a 2-3 m thick coral-rich unit and a bed of *Thalassinoides* burrows in benthic foraminifera-rich sands (Figure 11d).

The main faunal components throughout Unit III are benthic foraminifera, mollusks, corals and coral debris, mollusks, and planktic foraminifera. The planktic foraminifera and coral debris had heightened presence within the 45-50 m and 60-70 m intervals (Figures 11a and 11b). The mollusk content increases in the interval 45-50 m and in two levels at 60 m and 70 m, which bound the foraminifera-rich and coral debris-rich zones. Within the silty beds, stratigraphically above the reef and concretion deposit (70-75 m), minor amounts of *Thalassinoides*-type burrow structures and concretions followed prominent bedding planes (Figure 11c), and between 75-80 m *Thalassinoides* type bioturbation became more abundant and massive (Figure 11d).

Diagenetically, the carbonate-rich units have been affected by some meteoric diagenesis. The concretionary bedding is thicker in Unit III relative to Units I and II. Some

of the concretions are knobby (~15 cm) through this zone, but others can be up to 60 cm thick and are mostly stratigraphic types (Figure 11c).
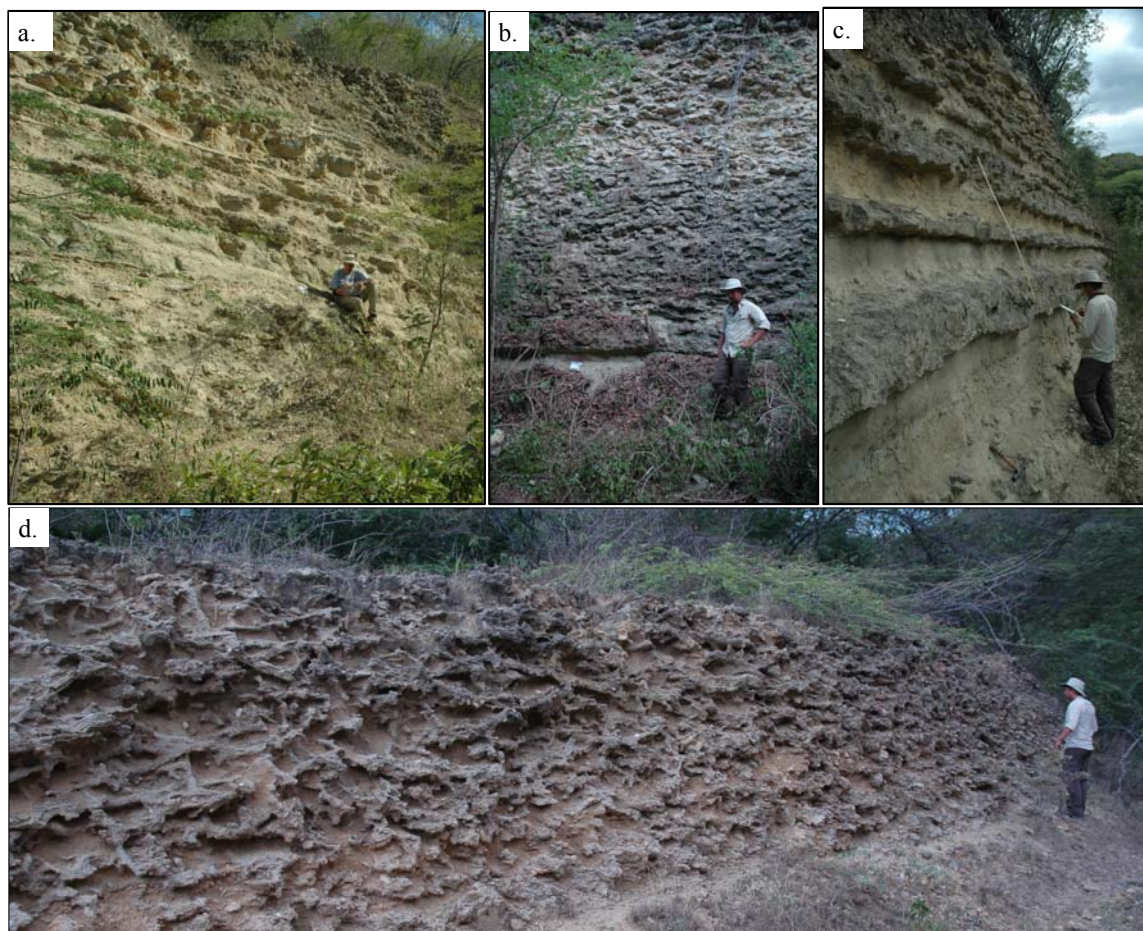
Figure 11: Unit III outcrops. a) (47-50 m) beds that contain high siliciclastic content; b) (62-67 m) first major reef unit with abundant corals marking the initiation of reef development; c) (73-76 m) recessed silt with burrow features, lithified concretions and nodules; d) (78-80 m) extensive *Thalassinoides* bioturbation burrow structures with abundant pectins and scattered free-living corals.

3.1.4 Unit IV (81-96 m)

Unit IV is located within the RM-4, RM-5, and base of RM-6 outcrop locations. These outcrops progress up-section with increasing elevation to the south (Figure 7). The outcrops are composed of massive, fine sand at the base of the unit, and increase in greenish silt and coralline fragments between 83-90.5 m (Figures 12a, 12b and 13). Within the upper portion of the unit, 90.5-96 m, the silt is more light-colored and more carbonate-rich

(Figure 12c). Thin (10-15 cm) lithified, skeletal wackestone-packstone beds are present within the *in-situ* muddy micrite-silt matrix (Figure 12c).

The main faunal components of Unit IV, from most to less common, are benthic foraminifera, mollusks, corals and coral debris, planktic foraminifera, bryozoans, and echinoderms. Quartz sand and mud dominate the basal few meters, and benthic foraminifera, followed by mollusks, and coral debris became more prevalent upward through this unit. Knobby bioturbation nodules occur between 83-90.5 m and follow the primary bedding (Figure 12b). Diagenetically, some erosion is observed within the recessed bedforms of the muddy-sand layers where bioturbation was more prevalent. The lithified wackestone-packestone layers are bound by a calcite cement (Figures 12c and 13).

3.1.5 Unit V (96-116 m)

Unit V spans from 96 to 116 m in the section and is located at the northern portion of the RM-6 outcrop (Figure 7). The outcrop is within terraces 1 through 3 of the massive excavation for the water treatment plant. The stratigraphic column continues upward by traveling west from the base of the terrace, with increasing elevation, along the strike direction (Figure 7). The bedding within this unit varies from 30 cm to meter-scale. The interval begins with a reefal unit that is composed of coral framestone with a few scattered recessed mud layers (Figure 14a). The mud layers are light-tan colored with a single green mud layer towards the center of this unit. Mud dominates the matrix of this unit (~65-70%).
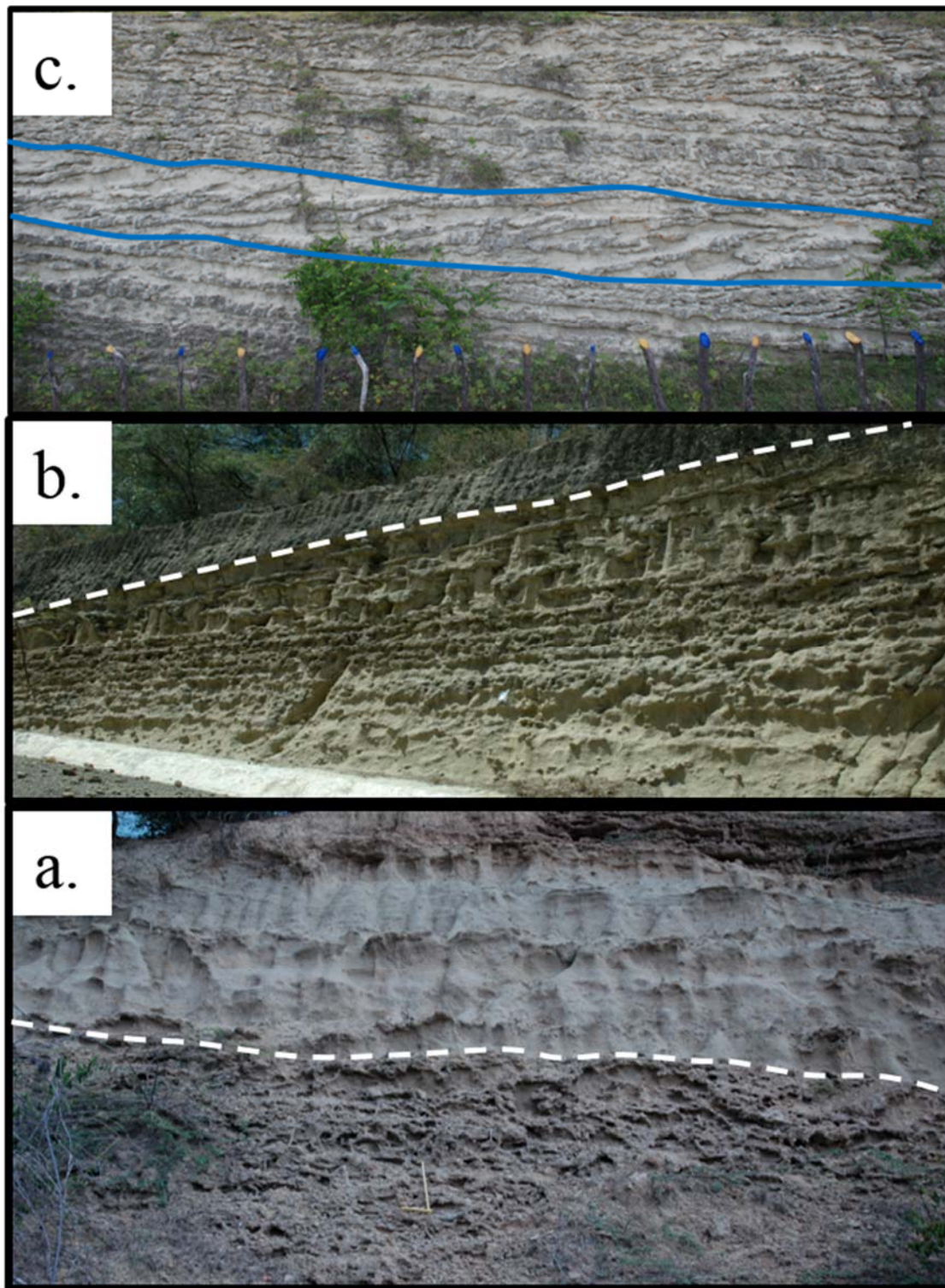
Figure 12: Unit IV deposition a) (78-82 m) shallow *Thalassinoides* bioturbation at base of image (Unit III) overlain by massive fine sand; b) (84-90 m) very fine sand and greenish-mud with bioturbation nodules within *in-situ* silt-micrite matrix with a dense, micrite matrix at top of image that contains large head corals; c) (93-96 m) blue lines outline the thin, lithified beds that show stratigraphic onlap (basin to right, or north) within white-grey *in-situ* muddy-sand and micrite matrix.
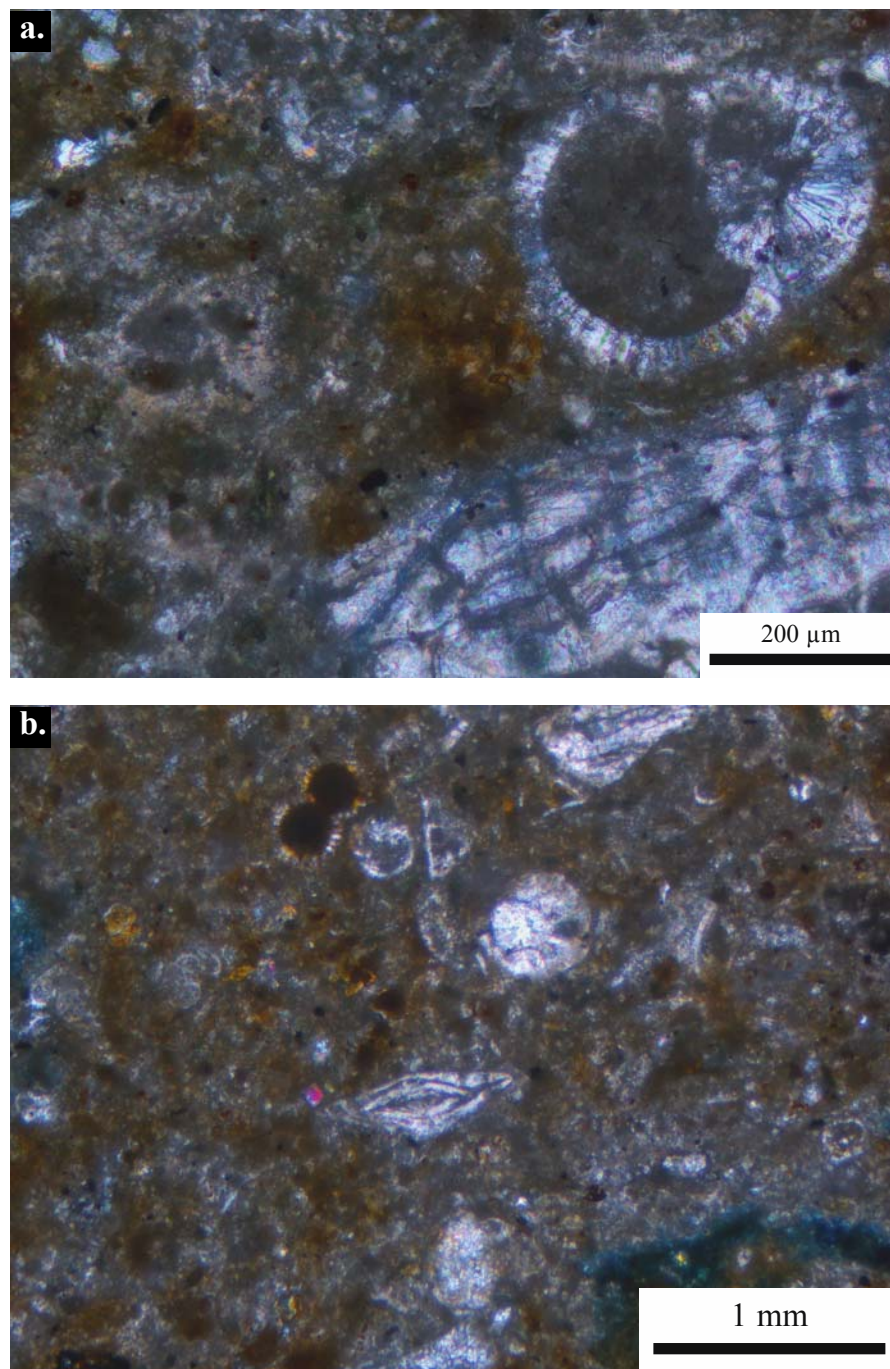
Figure 13: Unit IV sample from 89.1 m in Rio Mao section of Gurabo Fm. a) planktic foraminifera and coral with elongate crystalline LMC replacement within a mud-size quartz and micrite matrix; b) predominately benthic foraminifera and few planktic foraminifera within a matrix of fine quartz and lime mud matrix.
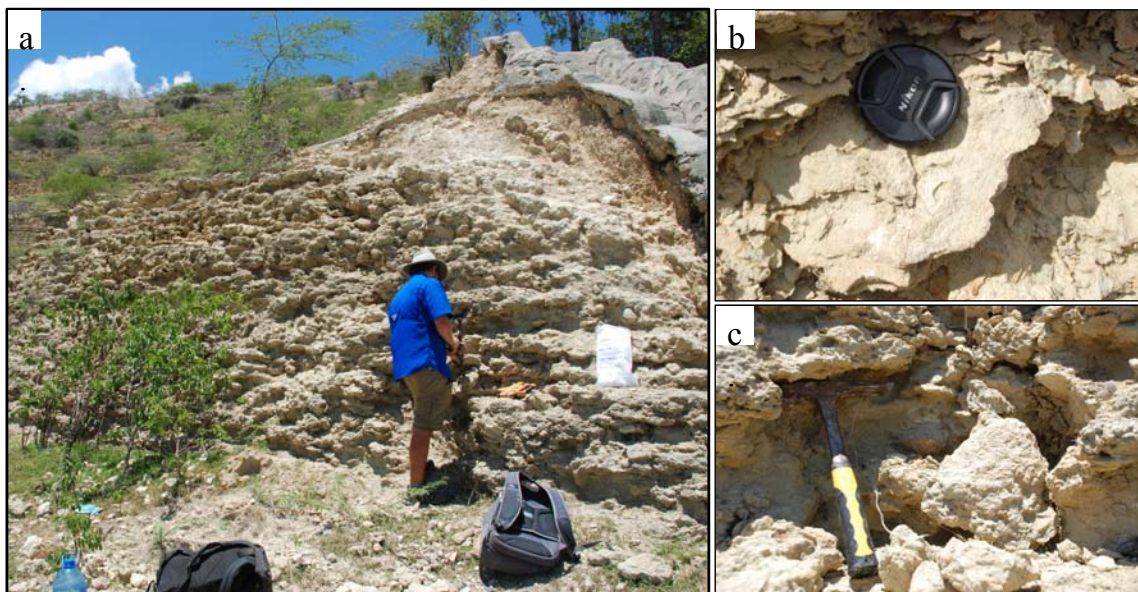
Figure 14: Unit V deposition a) (102-106 m) second major reef outcrop with plethora of corals and large benthic foraminfiera; b) colonial coral; c) spiny oyster within the reef interval at the base of Unit V.

The fauna of Unit V consists predominately of platy and massive coral with coral debris (Figure 14). There are abundant planktic foraminifera (based on washed sediment samples) throughout the unit with decreasing proportions towards to the top of the unit. Mollusks are observed throughout the unit, though rare. Bioturbation structures or apparent diagenetic alteration is not observed in outcrop, although some coral debris has been affected by meteoric alteration.

3.1.6 Unit VI (116 - 136 m)

Unit VI lies midway up the water treatment plant terraced section of RM-6 between 116-136 m (Figure 7). This 20-m thick outcrop lies within terrace 3 to terrace 6 of the outcrop, and like Unit V follows west, along strike, with increasing elevation to expose the stratigraphic succession. The unit is dominated by coherent, mud- to fine-sand layers (50-70 cm thick) that alternate with lithified wackestone-packstone (10-30 cm thick) layers (Figure 15a). A possible channel feature is overlain by an algal mat and root casts within this unit from 123-126 m in the section (Figure 15a).
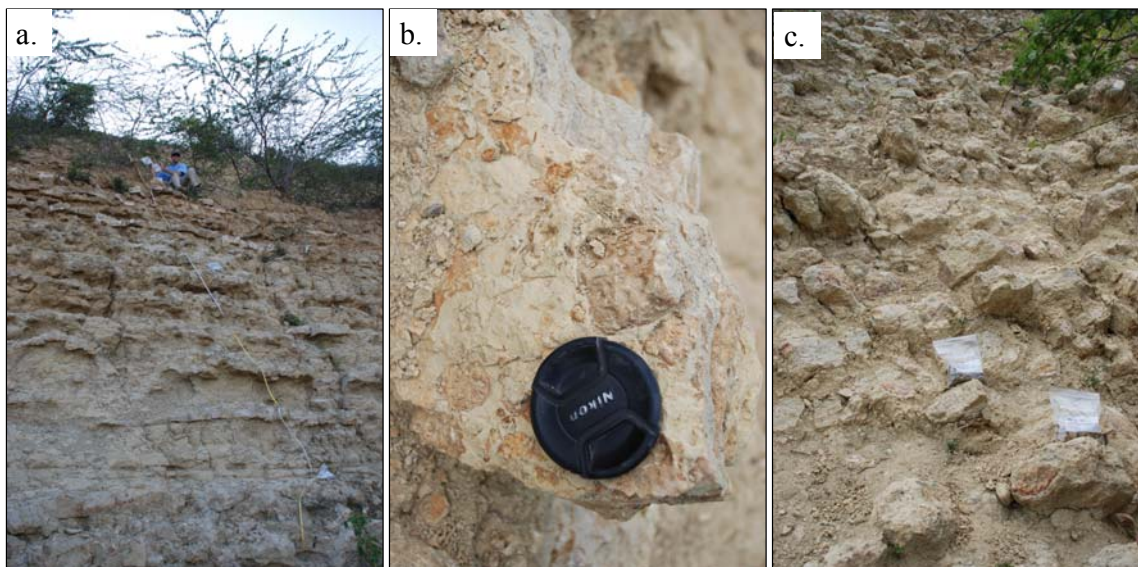
Figure 15: Unit VI deposition. a) (116-126 m) 50-70 cm thick siliciclastic sand layers alternating with thin lithified wackestone-packstone layers; b) (130 m) thick encrusting red algae; c) (130-136 m) lithified boulders that contain encrusting red algae within a silty matrix.

Red algae, leached mollusks, and free-living coral occur within this unit (Figures 15 and 16a,b,c). Benthic foraminifera and mollusks dominate the carbonate skeletal components at the base of the unit (Figures 16a and 16b). A high proportion of fine- to very fine- quartz grains is observed within the matrix of this unit. The diagenetic alteration is seen within the leached mollusks from weathering of the exposed grains, thin calcite veins, and pyrite (Figures 15 and 16a, b, c).
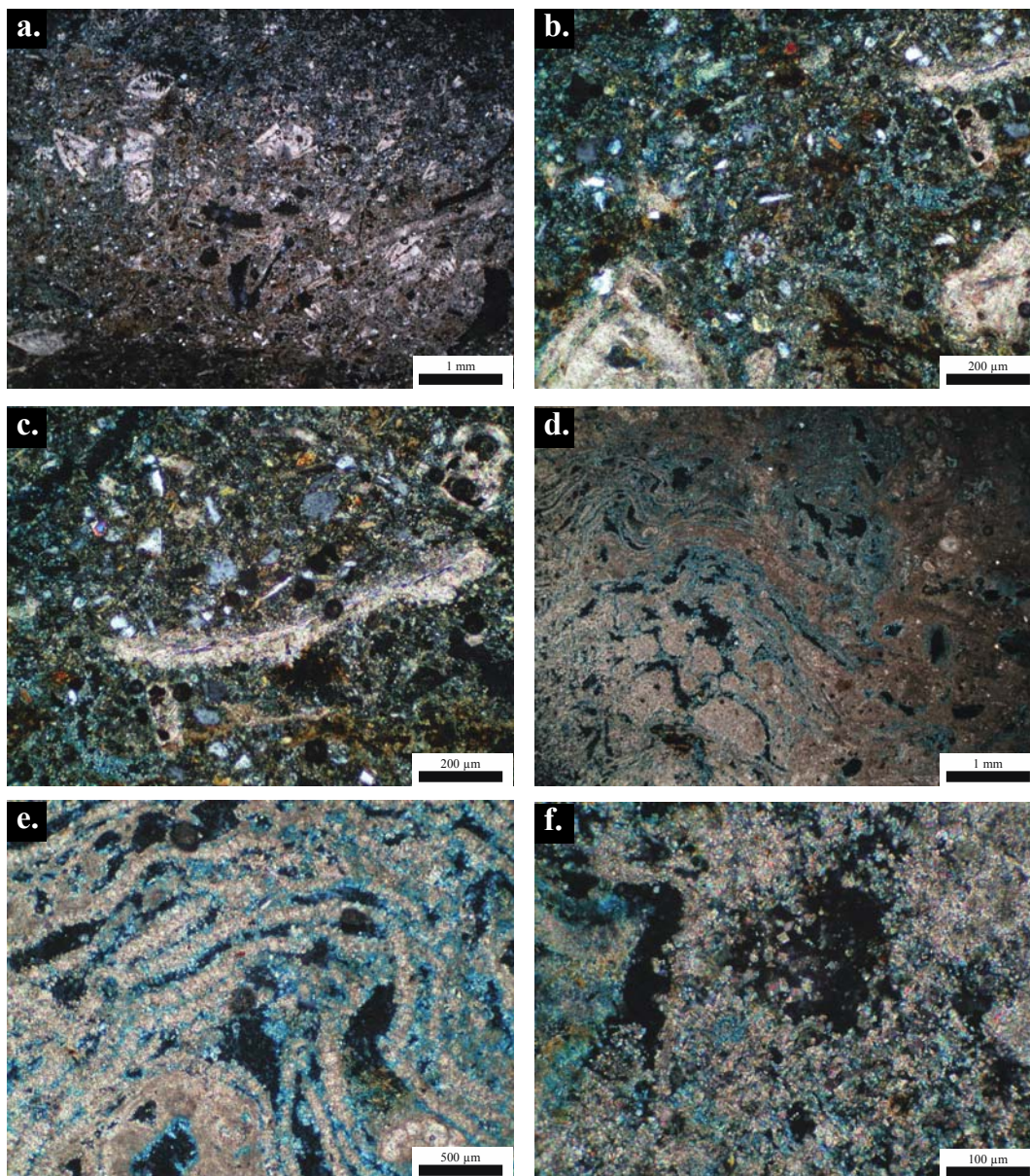
Figure 16: Samples a, b and c are from Unit VI at 118.8 m in Rio Mao section, and all photomicrographs are taken with cross-polarized light. a) the bulk sediment is dominated by abundant benthic foraminifera and scattered mollusks within a wackestone matrix; b) quartz silt within the matrix and benthic foraminifera and echinoderm spines are present; c) mollusk shell (center) and worm tube (top right) within a very-fine quartz sand and LMC cement matrix. Samples d, e and f from Unit VII at 145.3 m in Rio Mao section; d) matrix of predominately encrusting red algae and bryozoans within the wackestone-packestone. e) very fine, elongate spar cements along fringe of red algae; f) very fine dolomitic rhombahedrals (<10 μm diameter) near primary pore space.

3.1.7 Unit VII (136 - 157 m)

Unit VII is within the uppermost portion of RM-6 between 136–157 m in the Rio Mao lithostratigraphic section. This interval is within the excavated terraces of water treatment plant. The Unit is within terraces 6, 7, and 8 from the RM-6 outcrop (Figure 7). This unit comprises a third and uppermost reefal interval where massive corals are contained within a micrite matrix (Figure 17a). The unit is best characterized as a massive wackestone to packstone. The bed thicknesses vary between 1 to 3 m (Figures 17a and 17b). The sedimentary section is capped by a white to dark-gray calcareous mud and coralgal packestone (Figure 17c). In outcrop, there were not any apparent indications of bioturbation, and there was heavy surficial weathering.

The skeletal components with the coralgal interval consist of benthic foraminifera, coral debris, few bryozoans, encrusting red algae, and mollusks. Red algae and benthic foraminifera are most prominent within the coralgal framework (Figure 16d). Diagenetically, there is fringing LMC cement along edges of red algae pore networks (Figure 16e). There are also dolomite rhombohedrals (<10 µm) that have replaced some of the micrite matrix (Figure 16f).
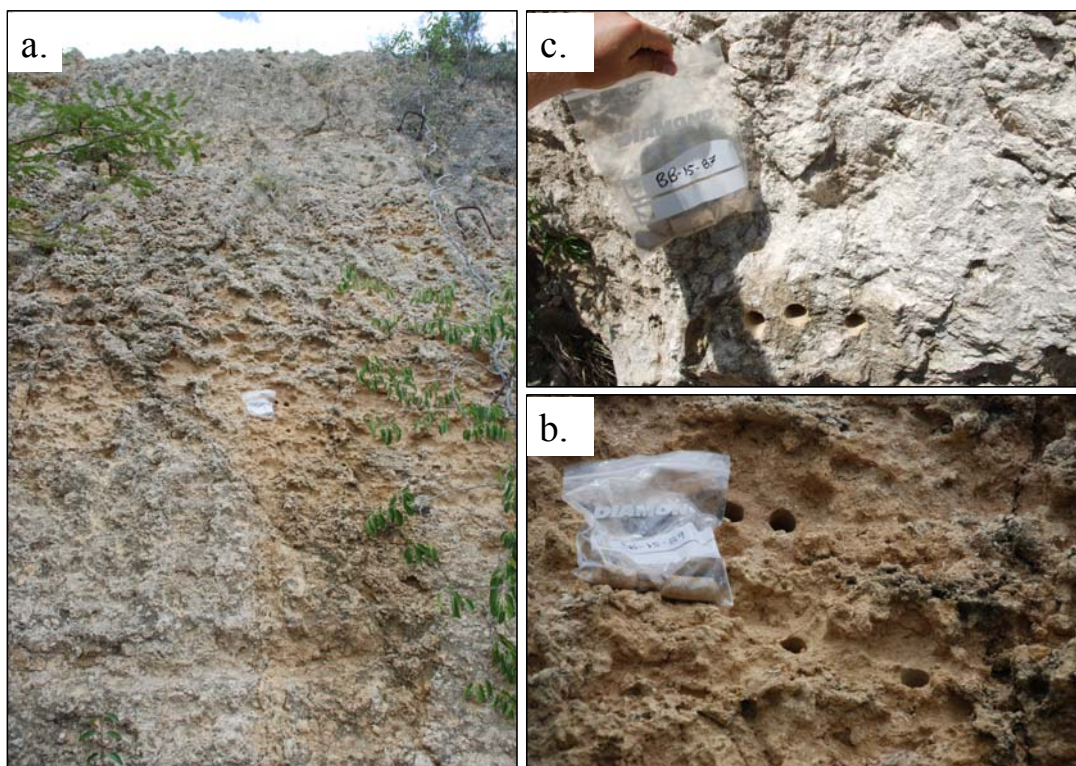
Figure 17: Unit VII deposition. a) (136-157 m) there is a general transition from a wackestone at the base to a packestone at the top of the unit; b) (147.5 m) packstone layer with bag containing plug samples; c) (157.6 m) calcareous mud and coralgal packestone with bag containing plug samples.

3.2 Sediment Analysis

A mixed-system consists of variable proportions of carbonate and siliciclastic sediments. In order to understand the proportions and variances in the deposition of these two components, sediment samples were disaggregated and wet sieved to obtain a grain-size distribution throughout the studied Rio Mao section (Figure 18; Table 2). The bulk sediment was also examined for carbonate content and screened through X-ray diffraction (XRD) to determine variation in carbonate mineralogy through the Gurabo Formation, Rio Mao sections. Sieved sediments (>63 μm) were point counted within their respective size groups. A grain component-type distribution was constructed throughout the mixed-system section. The final portion of the sedimentary analysis involved categorizing the varying coral types and abundances in the Rio Mao section.

3.2.1 Grain Size Distribution

The bulk sediment matrix throughout the section was separated in six different size fractions: less than 63 μm (mud), 63-125 μm (very fine sand), 125-250 μm (fine sand), 250-500 μm (medium sand), 500-1000 μm or 1 mm (coarse sand), and greater than 1 mm (very coarse sand). Overall, the mud-size, <63 μm, sediment fraction is most common through the Rio Mao section. This size fraction ranges from as low as 26.5% to as high as 95.4% of the sediment matrix (Table 1). Greater proportions of mud-size and very fine grains (0-125 μm) occur at the base of the section (0-60 m height in section); whereas, more large grains (250 μm to >1 mm) exist towards the top of the stratigraphic section (>80 m in section; Figure 18).

Table 1: Distribution of grain sizes within the Gurabo Fm at the Rio Mao section, as a percent.

Rio Mao Section	Statistic	>1000 μm	500-1000 μm	250-500 μm	125-250 μm	63-125 μm	<63 μm
Gurabo Fm.	Maximum	27.5	18.5	10.1	33.0	60.5	95.4
	Average	4.1	3.1	3.0	4.9	14.3	70.6
	Standard Deviation	5.0	2.7	2.4	2.6	11	12
	Minimum	0.0	0.0	0.0	0.6	1.9	26.5
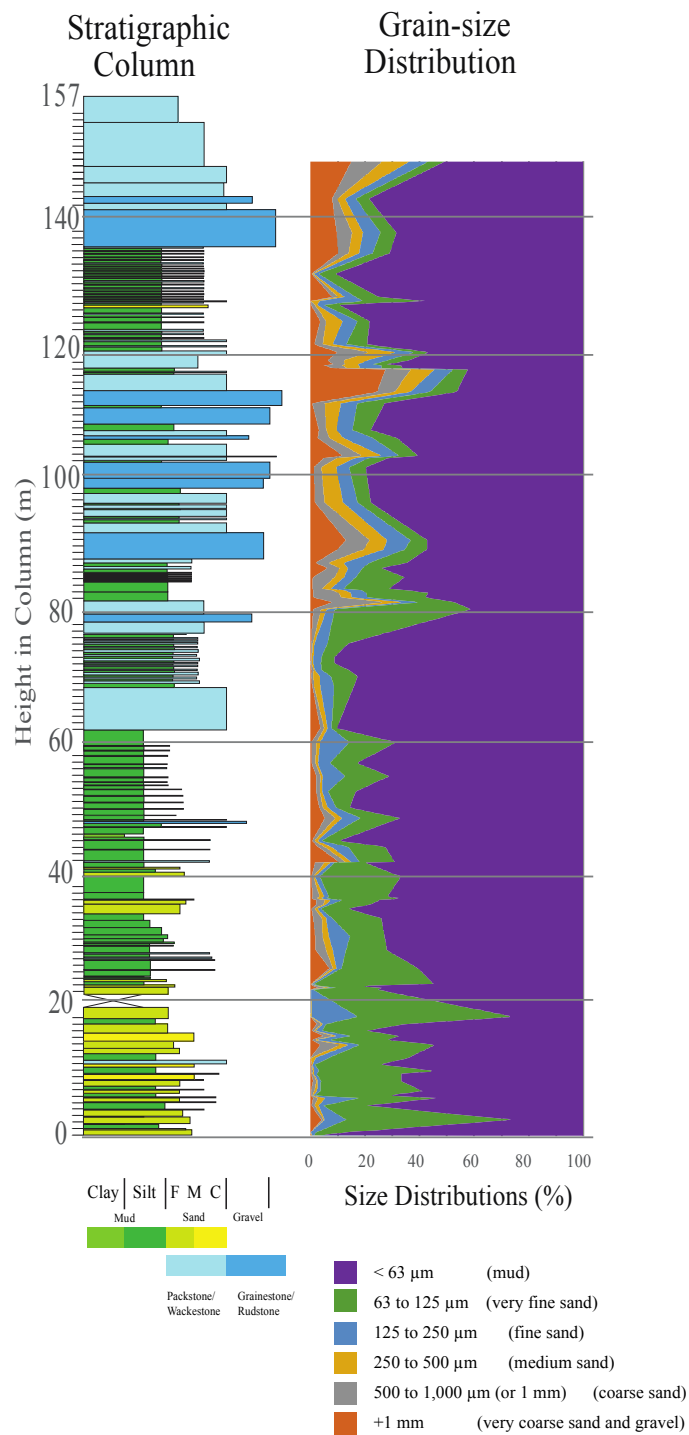
Figure 18: Rio Mao stratigraphic section through the Gurabo Fm and grain size distribution.
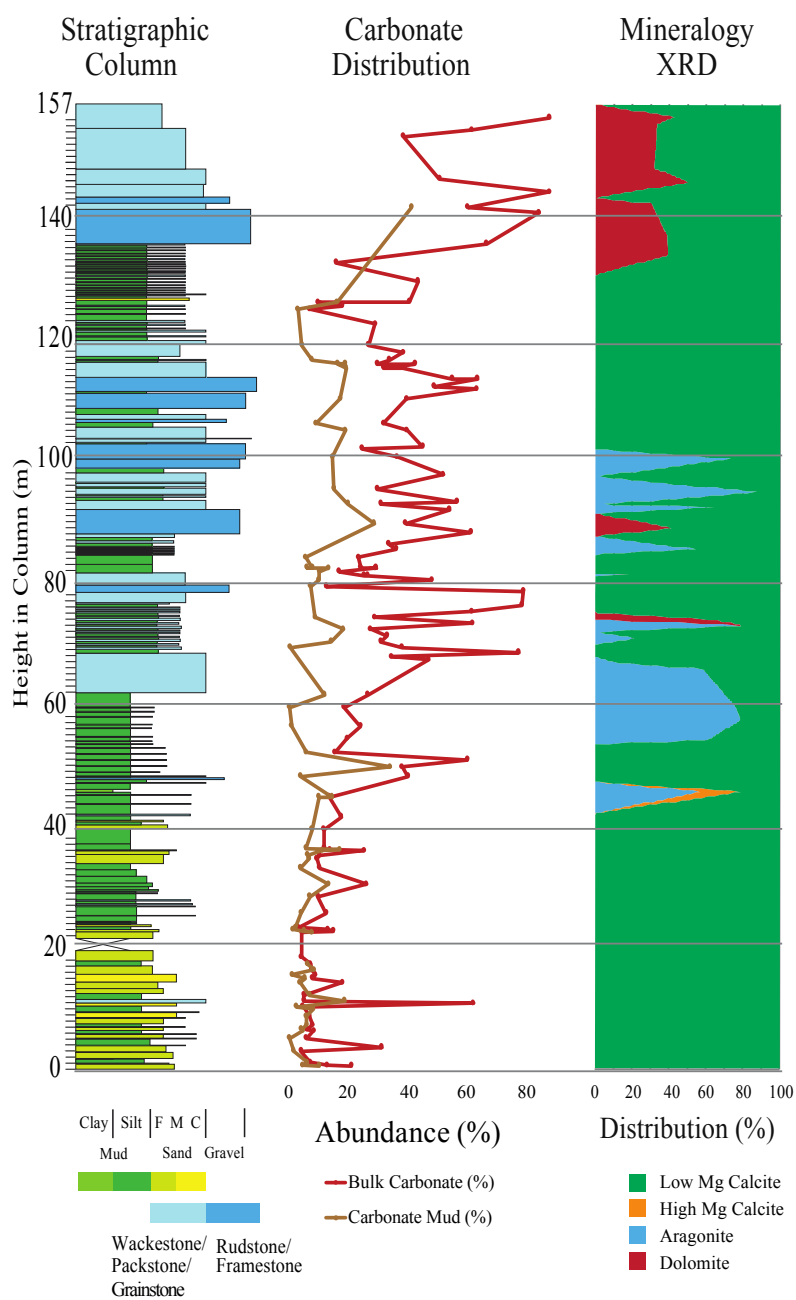
Figure 19: From left to right the data illustrated are: outcrop stratigraphic section, carbonate percentage within mud-size matrix bulk sediment), and the X-ray diffraction data from the Gurabo Fm at the Rio Mao section.

3.2.2 Carbonate Content Through Gurabo Formation

The carbonate content values in the bulk sediment matrix through the section are relatively low at its base, increasing upward with discrete pulses of high values throughout (Figure 19). The lowest values are observed in three distinct intervals: 0-45 m, 80-85 m, and 126-133 m (Figure 19) and the highest values in four distinct intervals: 48-52 m, 67-79 m, 85-120 m, and 136-157 m (Figure 19). Bulk and mud carbonate content values do not correlate (with a $4.9*10^{-9}$ p-value) (Figure 19; Appendix D). Table 2 illustrates that the average bulk matrix carbonate content value in the Gurabo Fm. is 28.6%, within a standard deviation of 21.2%, a minimum value of 1.3%, and a maximum value of 80.9%. The carbonate content of the mud-sized fraction is 8.4% of the total carbonate on average through the Gurabo Fm with a standard deviation of 6% (Table 2). A comparison of the mud-sized carbonate content to the bulk carbonate proportions is located in Appendix D.

Table 2: Bulk carbonate and carbonate mud maximum, average, standard deviation, and minimum percentages through the Gurabo Formation in the Rio Mao section.

	Statistic	Bulk Carbonate Content (%)	Carbonate Mud Content (%)
	Maximum	80.9	37.9
Gurabo	Average	28.6	8.4
Fm.	Standard Deviation	21.2	6.0
	Minimum	1.3	0.0

3.2.3 XRD Mineral Data

X-ray diffraction (XRD) analysis provides carbonate mineralogy variations through the Gurabo Fm as proportions of the entire carbonate fraction within the sample (Figure 19; Table 3). Low magnesium calcite (LMC) is predominant through the section with lesser

occurrence of aragonite and dolomite, and rare high magnesium calcite (HMC) (Figure 19).

LMC is ubiquitous in the bottom 45 m of the section, in addition to intervals between 76-86 m, and 105-130 m. HMC only existed in the bulk sediment matrix between 45-50 m. Aragonite is found intermittently between 45-102 m in the section. Dolomite is predominately at the top of the section between 130-157 m, but also occurs at 76 m and 91 m in the section (Figure 19).

Table 3: Carbonate mineralogy statistics through the Rio Mao section Gurabo Fm.

| | | Carbonate Distribution (%) | | | |
	Statistic	Aragonite	Dolomite	High Mg Calcite	Low Mg Calcite
	Maximum	87.7	61.3	21.9	100.0
Gurabo Fm.	Average	10.3	6.4	0.4	83.0
	Standard Deviation	22.3	13.4	2.3	24.0
	Minimum	0.0	0.0	0.0	12.3

3.2.4 Grain Component Distribution

A grain component-type distribution was measured through point counts of grains that were greater than 63 μm (mud-size) for eighty-two samples throughout the section (Figure 20). The grain component types are: benthic foraminifera, planktic foraminifera, coral debris, mollusks, siliciclastics (feldspar, quartz, and composite cemented grains), recrystallized and unidentifiable, and 'others.' The 'others' recognized are composed of: mica, echinoderms, bryozoans, sea urchin spines, crab fragments, calcite, and red algae fragments. Combined, the 'other' grains were usually less than 10% of the total sample. The analysis of grains >63 μm diameter are detailed in Figure 20 for components that included the following groups: quartz and composite cemented grains (CCG), benthic

foraminifera, planktic foraminifera, coral debris, mollusks, recrystallized and unidentifiable grains, and 'other.'
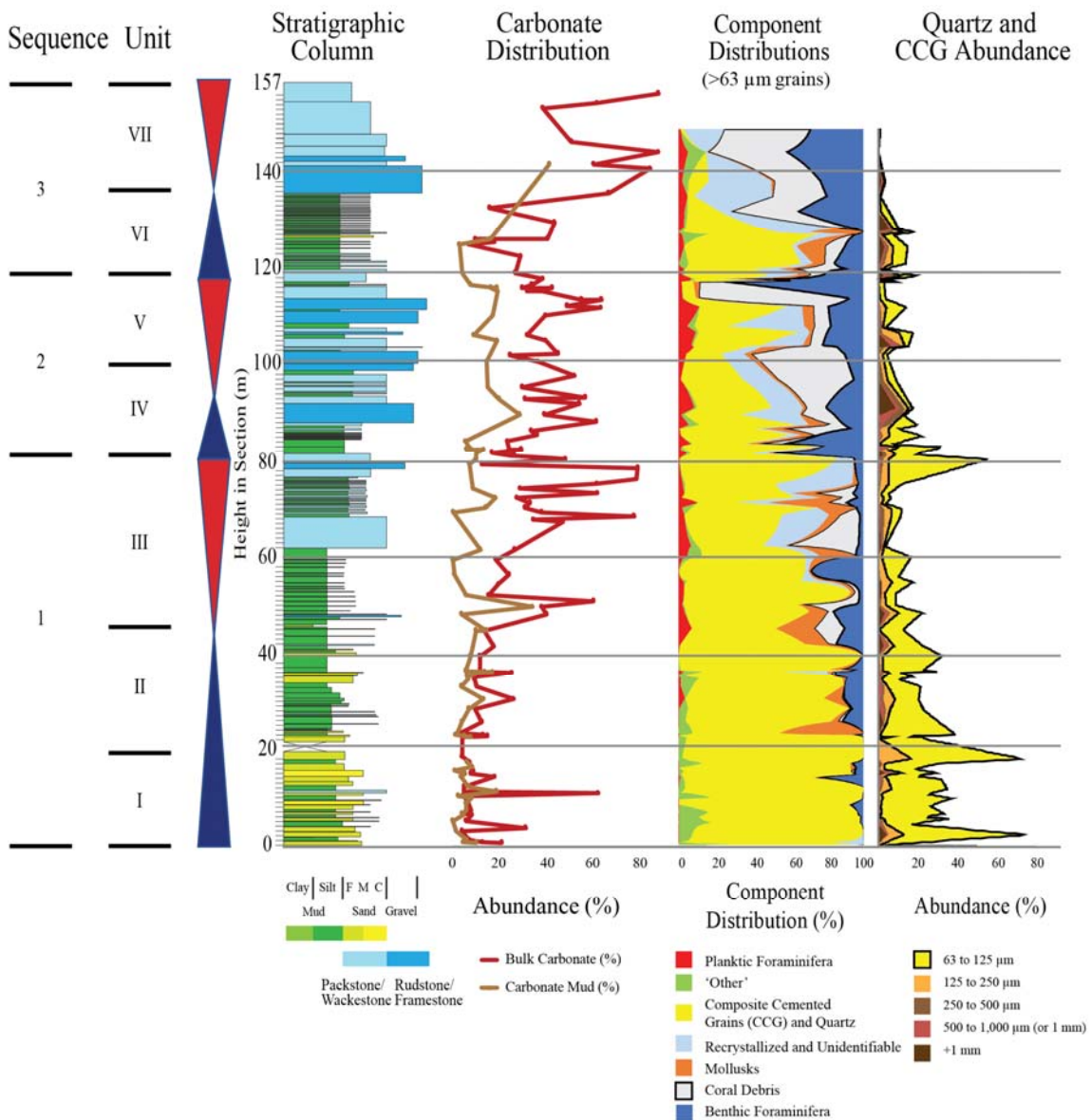
Figure 20: From left to right: stratigraphic column, carbonate content, grain component distributions for grains >63 µm, and the combined quartz and composite cemented grains (CCG) through the Rio Mao section Gurabo Fm.

Quartz and Composite Cemented Grains (CCG)

Quartz and composite cemented grains (CCG) (Figures 21 and 22a) form the majority of >63 µm size grains in the lower half of the Rio Mao section. The grain is

composed of many smaller grains that are predominately quartz, feldspar, and occasionally pyrite. The quartz and CCG grains that were smaller than 125 μm were typically individual quartz grains; whereas, the grains that were larger than 125 μm were commonly CCGs (Figure 20).

Quartz and CCGs occur in all the depositional units (Figure 20) of the the Rio Mao section. Several trends in abundance are recognized where they are higher at the base and decreased in abundance upward through the section (Figure 20). The trends are identified between 3-71 m, 80-112 m, and 120-148 m (Figure 20). Typical variation in composition of CCGs is shown in Figure 21.

Benthic Foraminifera

Benthic foraminifera were present in nearly all samples from the Rio Mao section (Figures 20 and 23). The benthic foraminifera identified in the section are most commonly of the genus *Amphistegina* (Figures 22b and 22c), with *Quinqueloculina* and *Ehrenbergina pacifica* also common within the section (Figure 22c).

Planktic Foraminifera

The most predominant two genera of planktonic (planktic) foraminifera present in the Rio Mao section are *Globigerinoides* (Figure 22d) and *Orbulina*. These foraminifera were commonly still fully intact even after undergoing the wet-sieving process. The planktic foraminifera (in red; Figure 20) occur in pulses and are generally in low abundance relative to the remainder of the grain type. The planktic foraminifera had a maximum of 3.6%, an average of 0.7%, standard deviation of 0.9%, and they were not present throughout the entire formation (Figures 20 and 23; Table 4; Appendix B).
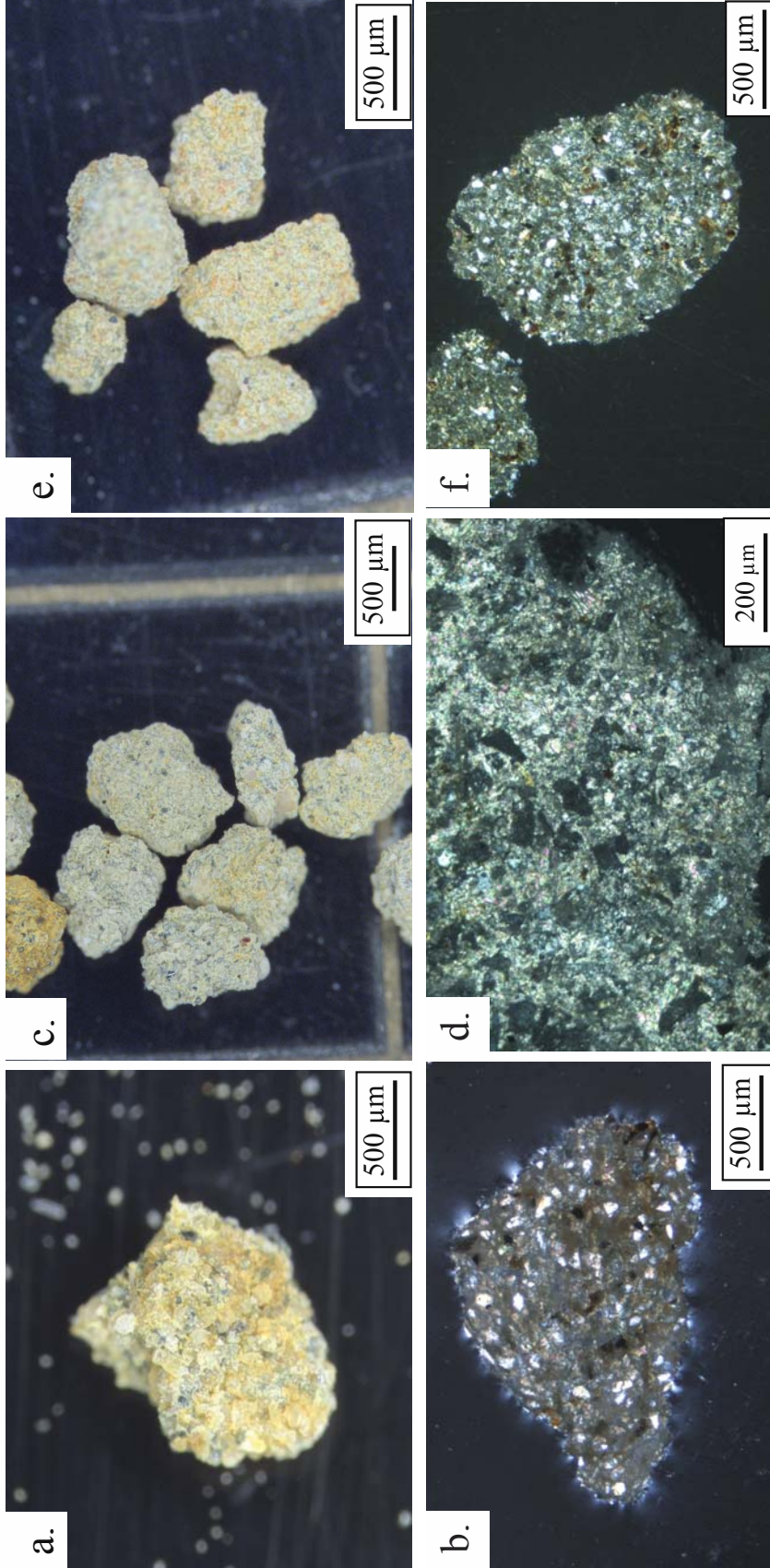
Figure 21: Composite cemented grains (CCG) depicted in image a, c, and e through stereoscope and b, d, and f are corresponding thin section views through the Rio Mao section Gurabo Fm. Images a and b) 3.3 m CCG has quartz and feldspar grains of ~63 μm within mud and micrite matrix. Images c and d) 84.95 m has fewer quartz and feldspar grains with a greater amount of carbonate content and micrite matrix. Images e and f) 125.95 m has similar quartz and feldspar content that were depicted in images a and b.
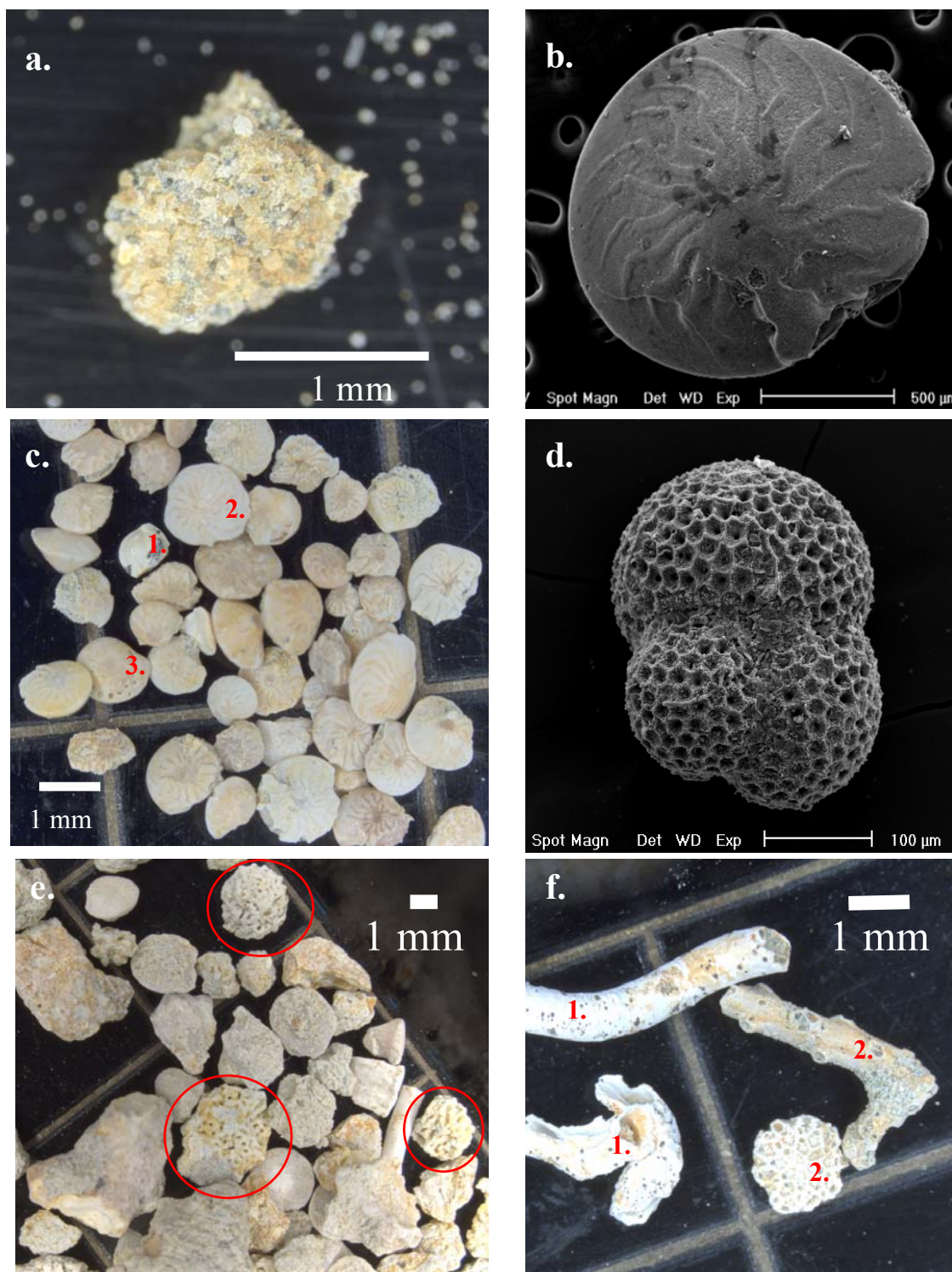
Figure 22: Grain types from the Gurabo Fm. a) composite cemented grain from 3.3 m in section; b) an SEM image of the most abundant benthic foraminifera, *Amphistegina lessonii*, from the Gurabo Fm; c) a combination of benthic foraminifera: 1. *Quinqueloculina bicostata*, 2. *Amphistegina hauerina*, and the predominant species is 3. *Amphestegina lessonii* from 55 m in the section; d) a common planktic foraminifera, *Globigerinoides ruber*, from 102.95 m in stratigraphic section; e) red algae, identified in red circles, from 142.8 m in the section; f) 1. worm tubes 2. bryozoans, branching and colonial, from 23.4 m in the section.
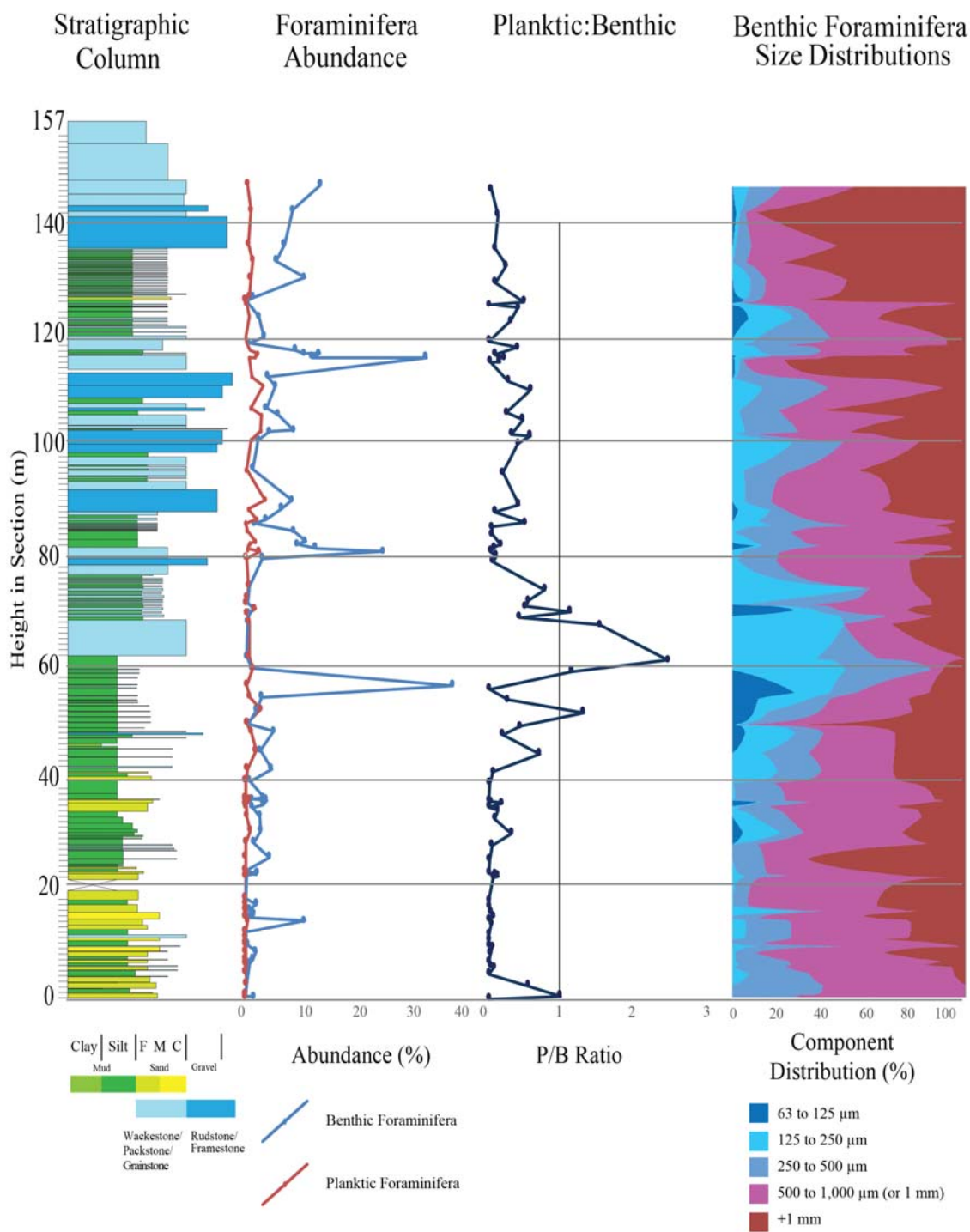
Figure 23: Stratigraphic plots that illustrate from left to right the stratigraphic column, foraminifera abundances through the Rio Mao section Gurabo Fm., planktic-to-benthic ratio, and the benthic foraminifera size-distribution.

Planktic-to-Benthic Ratio

The ratio of planktic-to-benthic foraminifera was assessed throughout the Rio Mao section (Figure 23). There is an increase in the ratio (more planktic-rich) in two distinct intervals: at the base of the section between 0-10 m and 45-75 m in the section. Benthic foraminifera were in greatest abundance in five intervals within the section at: 14.6 m, between 40-60 m, 80-85 m, 102-118 m, and 130-147.5 m (Figures 20 and 23). The benthic foraminifera occurrences in the interval 50-76 m tended to be of smaller diameter than those residing in the remainder of the stratigraphic column (Figure 23). The foraminifera had a maximum occurrence of 33.8% of the whole size fraction greater than mud (>63 μm). Benthic foraminifera represented an average of 4.2% of the grains and a standard deviation of 5.6% through the Rio Mao section (Table 4; Appendix B). Planktic foraminifera were less common with a maximum of 3% and standard deviation of 0.9% (Table 4; Appendix B).

Mollusks

The mollusks in the Rio Mao section were primarily composed of pectins and gastropods. These grains were not always fully intact for identification. The mollusks were distributed in seven discrete intervals throughout the section: 23.15-26.1 m, 42.0-48.7 m, 52-60.1 m, 68.5-72.0 m, 83.0-87.1 m, 101.5-103.2 m, and 116.25-126.5 m (Figure 20).

Coral Debris

Coral debris is a skeletal carbonate grain that was not readily traceable to specific types of coral. The debris in the Rio Mao section often had variable size, shapes, and levels of diagenetic alteration that made identification somewhat difficult. The coral debris was

most abundant in five intervals: 42-55 m, 60-70 m, 83-103 m, 111-116 m, and 127-157 m (Figure 20).

Recrystallized and Unidentifiable Grains

Recrystallized and unidentifiable grains were most-likely skeletal carbonate grains that were probably coral debris (Figure 20). These grains would likely be more easily identified in thin section.
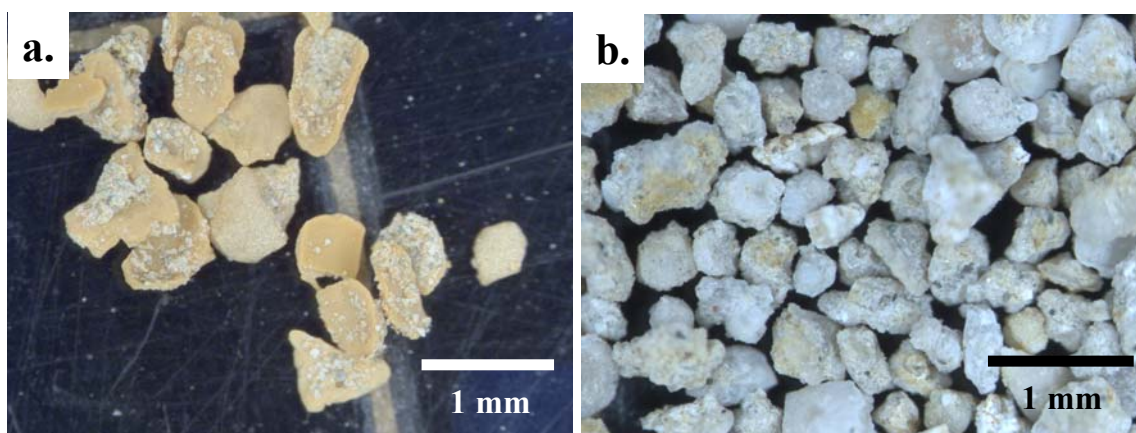
Figure 24: a) (125.95 m) calcite flakes with iron staining; b) (89.1 m) recrystallized and unidentifiable grains are typically white to off-white in color, have variability in shape and size.

'Other' Grains

This category includes the grains: bryozoans (Figure 22f), crab claws, calcite flakes (Figure 24a), echinoderm and sea urchin spines, epidote, mica, pyrite, and red algae (Figure 22e). Bryozoans were predominately located in four zones: 23-42 m, 60-62 m, 86-106 m, and 130-136 m (Figure 20). Crab claws were sparsely distributed at: 35.65 m, 117.6 m, and 125.95 m (Figure 20). Calcite flakes are precipitate grains found only at two stratigraphic intervals: 0.9 m and 125.95 m (Figures 20 and 24a). Echinoderms and sea urchin spines were located in low quantities throughout the Rio Mao section (Figure 20). Epidote was only present at the base of the section at 0.85 m and was identified through XRD and physical properties (color, lustre, hardness). Mica was predominantly in three

zones between: 3-37 m, 80-82 m, and 120-126 m (Figure 20). Pyrite exists at 75-82 m, 96-102 m, and 116-131 m. Red algae was present between 130-142.8 m (Figures 15(b,c), 16(d,e) and 22e). The most difficult types of grains to identify through the stereoscope within this category were bryozoans and red algae (Figures 22e and 22f). The bryozoans vary from branching to colonial, and the red algae are often encrusting or massive in this region (Figure 22f).

Component Summary

There were three main increases in abundance of quartz and CCG through the Rio Mao section at the ~0 m, 80 m, and 120 m (Figure 20). There was then a decrease in abundance of quartz and CCG upward through the section between each of these distinct intervals (Figure 20). The CCGs and quartz grains vary in abundance between 0-74.3% through the section with an average of 18.4% (Table 4). The second most abundant grain, on average through the section, is benthic foraminifera, 4.2%, that have an abundance that is variable between 0-33.8% (Table 4). Coral debris and mollusks can have high maximum abundances, but their average values are 3% and 1.7%, respectively (Table 4). Planktic foraminifera abundance varies between 0-3.6%, and recrystallized and unidentifiable grains vary between 0-13.7%, but their average is 2.3% (Table 4). The 'Others' vary between 0-8.2% with an average of only 1.1% through the section (Table 4).

Table 4: Component distributions, as a percent of sediments >63 micron, through the Rio Mao section Gurabo Fm.

		Components						
	Statistic	Quartz & CCG	Benthic Foraminifera	Planktic Foraminifera	Coral Debris	Mollusk	Recrystallized	Other
	Maximum	74.3	33.8	3.6	43.7	38.0	13.7	8.2
Gurabo	Average	18.4	4.2	0.7	3.0	1.7	2.3	1.1
Fm.	Standard Deviation	14.4	5.6	0.9	5.9	4.4	3.4	1.7
	Minimum	0.0	0.0	0.0	0.0	0.0	0.0	0.0

3.2.5 Coral Data

Coral abundances varied and were categorized by free-living, platy, massive, and branching corals through the Rio Mao section and are illustrated in Figure 25. There were predominately free-living corals at the base of the section at 25 m, 39.8 m, and 83.2 m (Figure 25). The contents of both platy and massive corals were greater than 40% at sample heights 62.5 m and 101.8 m in the section (Figure 25). Branching corals were found in samples from the middle and the upper part of the section (Figure 25). The two lower samples (25 and 39.8 m) had NO branching corals, as free-living corals were dominant. There was also greater coral diversity between 98.9-112.5 m in the section than in the four samples from lower in the Rio Mao section (Figure 25).

Coral Growth Forms and Diversity
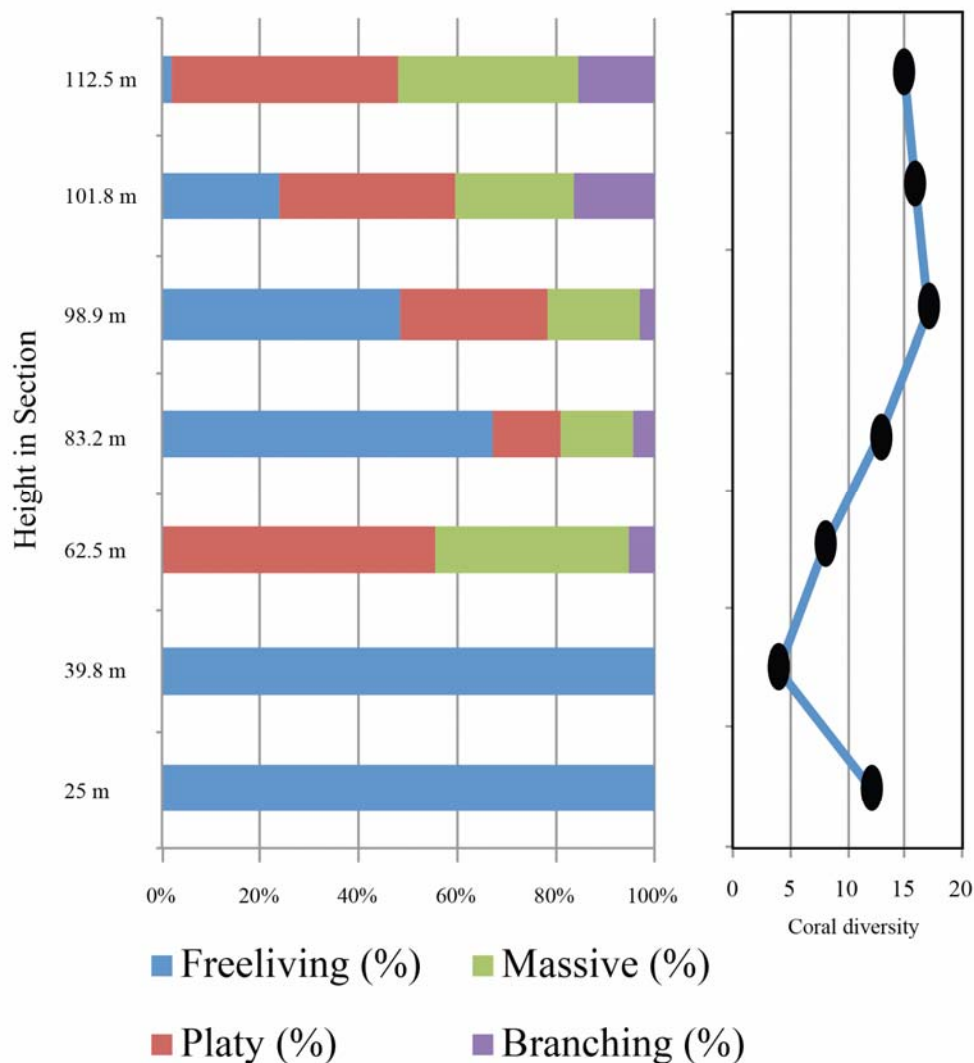
Figure 25: Coral distribution and classification through the Rio Mao sections Gurabo Fm.

3.3 Inorganic Stable Isotopes

Seventy-eight bulk samples analyzed for inorganic stable isotopes (Figure 26). The $\delta^{13}C_{Carb}$ contains values that range between -9.25 to 0.8‰. Each of the inorganic isotope curves, in Figure 27, contain error bars that represent the standard deviation, from the

average, for samples that had been analyzed more than once. The $\delta^{18}O_{Carb}$ values range between -4.08 to 0.83‰ (Figure 26).
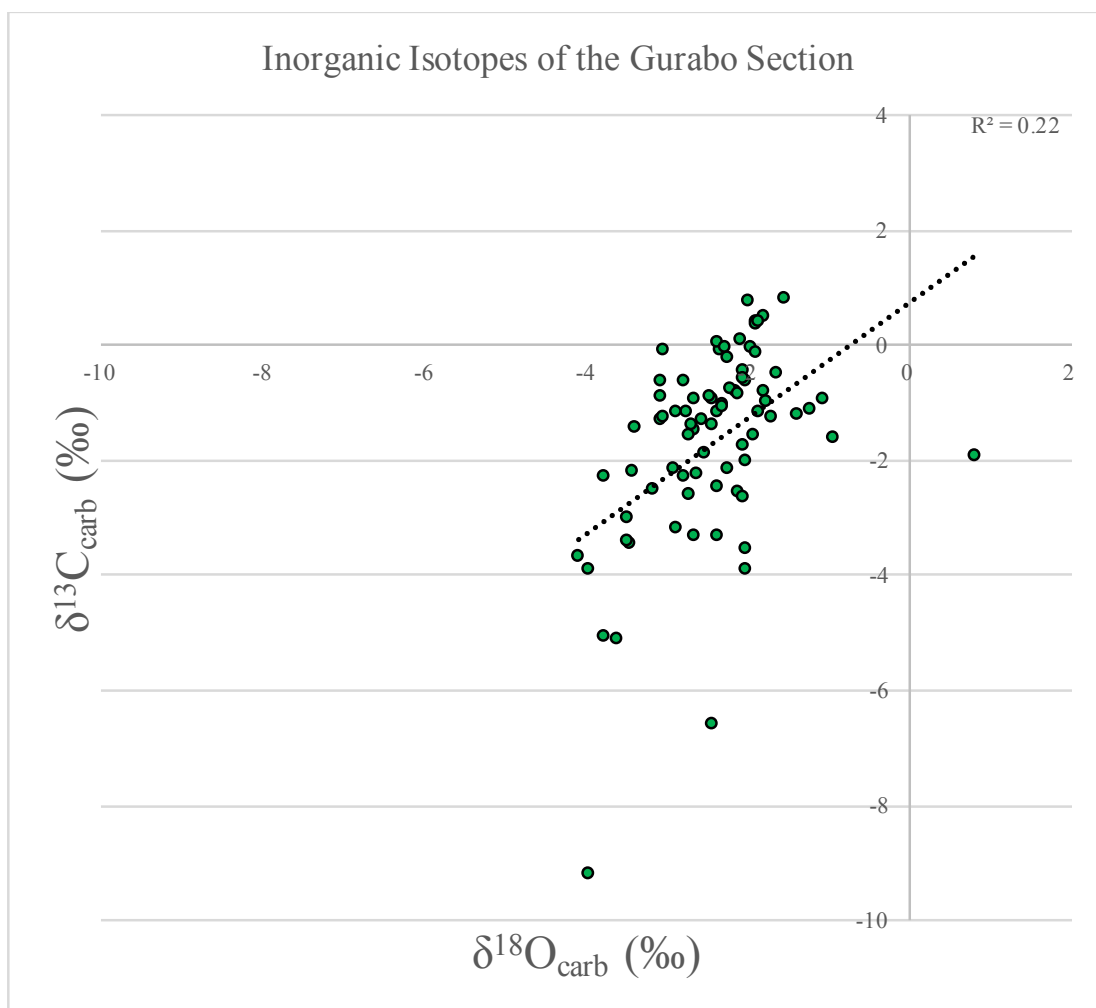
Figure 26: Comparison of inorganic carbon and inorganic oxygen of the bulk matrix samples through the Rio Mao section.
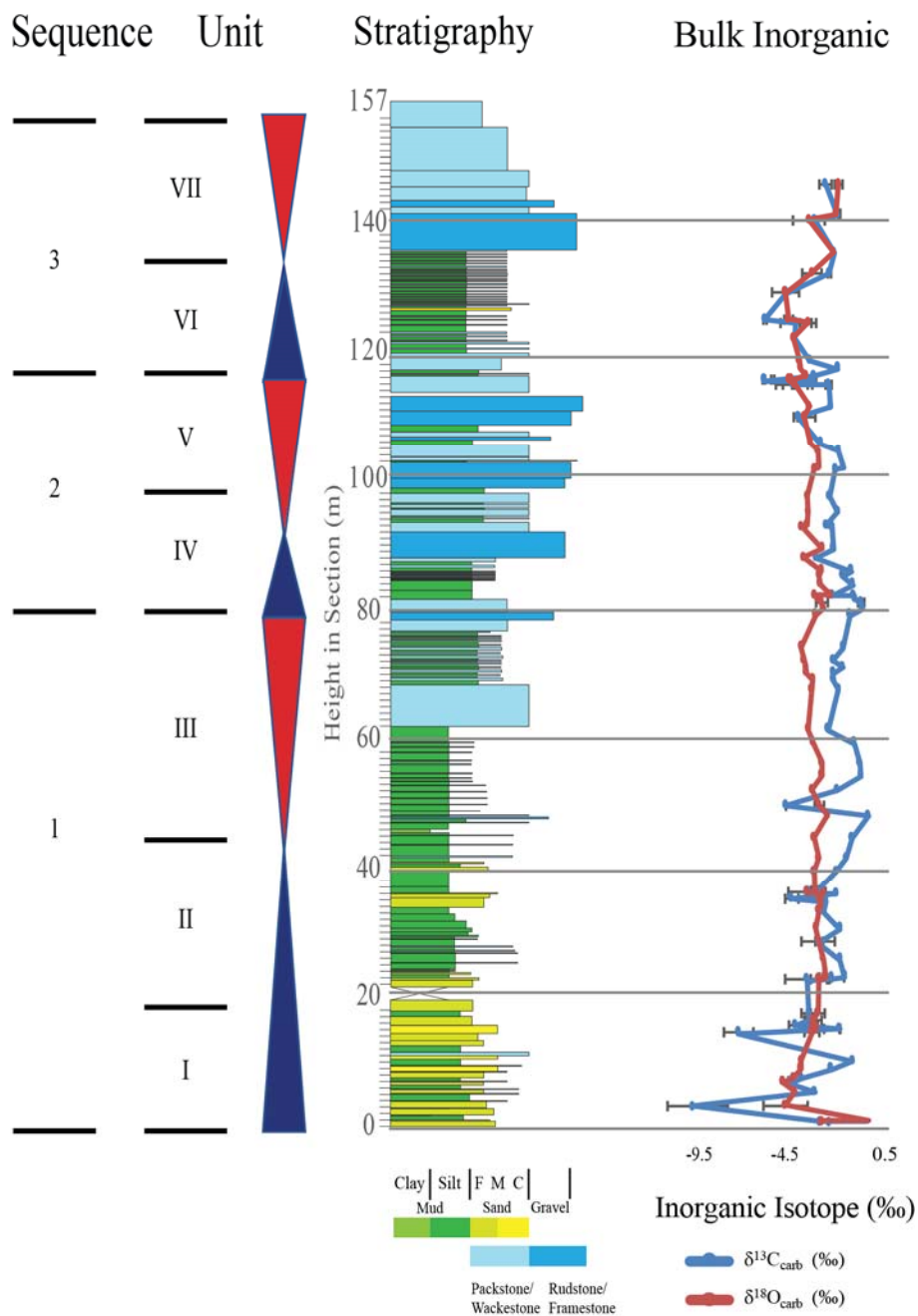
Figure 27: Bulk inorganic isotope data through the Rio Mao section indicates more negative carbon isotope values from 0-50 m and 116-125 m than in the remainder of the stratigraphic column. Each of the inorganic isotope curves contain error bars that represent the standard deviation, from the average, for samples that had been analyzed more than once.

3.3.1 Component Grain Inorganic Isotopes

The mixed-system has been analyzed by geochemically separating the bulk sedimentary matrix into its constituent granular components. The individual carbonate

components that contribute to the bulk inorganic isotope signature are: benthic foraminifera, bryozoans, CCG, coral debris, mollusks, planktic foraminifera, echinoderm spines, and worm tubes. For eighteen samples, the individual components were analyzed for inorganic isotope signatures. Using Equation 2 in methodology, the $\delta^{13}C_{Component}$ signature was multiplied by the abundance of that component, relative to the rest of the sample, and added to the subsequent other components to create a composite value for that sample. The same process was applied to each of the eighteen samples through the Rio Mao section to create a corresponding composite curve (Figure 28). The same process was applied to create a modeled primary signature by utilizing modern isotopic values for each component that was present within the eighteen Rio Mao samples (isotope values displayed in Appendix C).

The $\delta^{13}C_{Bulk}$ isotopic values through the Rio Mao section, the composite $\delta^{13}C$ curve, and the modeled primary signature are illustrated in Figure 28. The $\delta^{13}C_{Bulk}$ curve has values that range between -9.25 and 0.8‰ (Figure 29). The deconstructed components of this same mixed-system had $\delta^{13}C_{Components}$ values that span -20.86 to 2.69‰ (Figures 28 and 29).

Each of the components that were analyzed in more than one sample are illustrated as an average value with error bars that indicate the standard deviation for each type of sample (Figure 30). The correlation coefficient, R^2, values for fit of these components through the section are illustrated for components that had more than two samples analyzed in Table 6. The CCG component had the best fit to the bulk $\delta^{13}C$ isotopic signature (Table 6). Coral debris, planktic foraminifera, and benthic foraminifera had the next best

fits to the bulk isotopic signature, whereas mollusks and bryozoans had increasingly worse

fits to the bulk signature at their respective samples (Table 6).
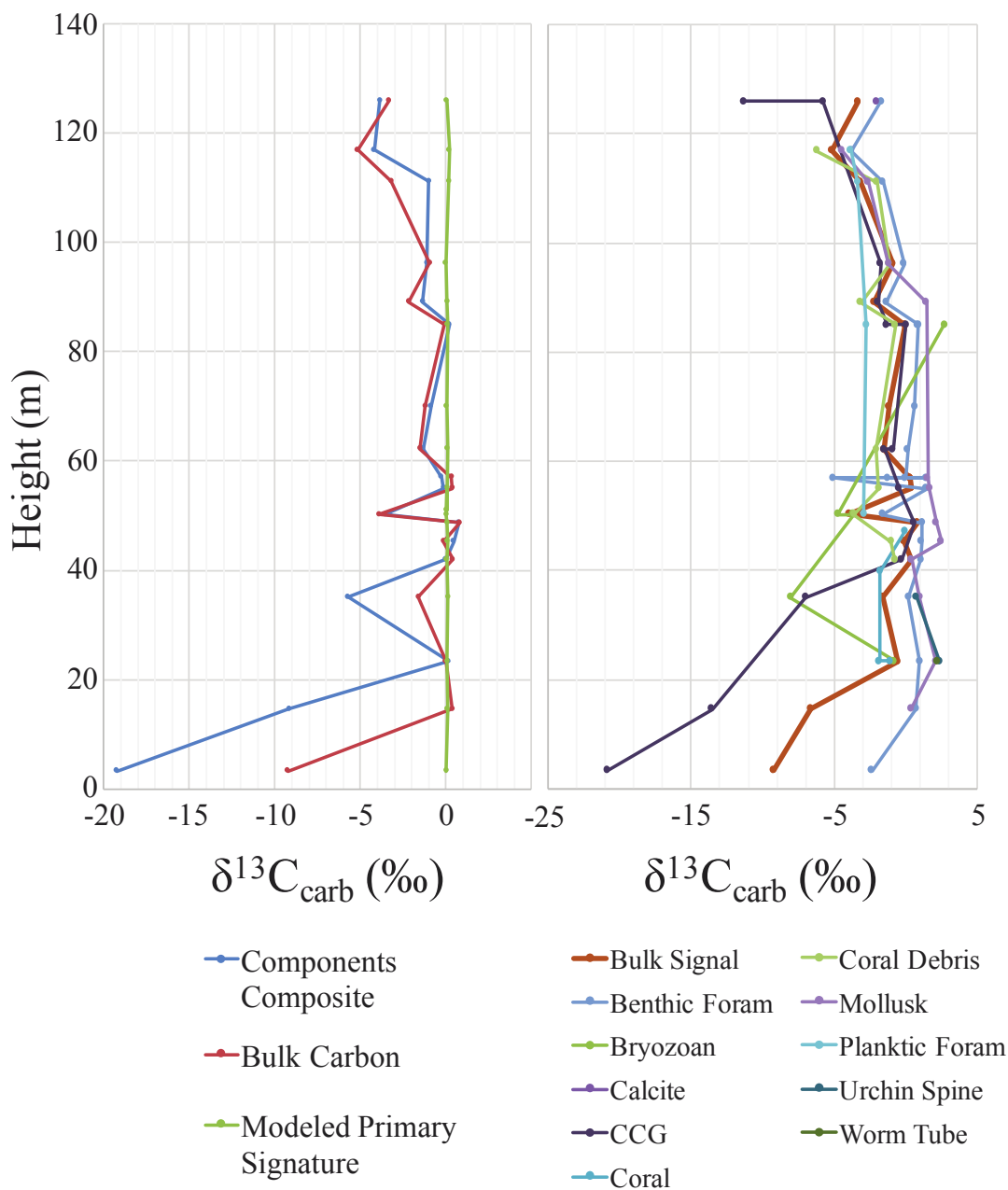
Figure 28: Graph on left displays a comparison of the bulk inorganic carbon isotope values to that of the modeled primary composite signature and the inorganic composite component values; whereas, the graph on the right illustrates the individual components isotopic signatures through the Rio Mao section Gurabo Fm that were utilized to create a components composite signature with Equation 2.
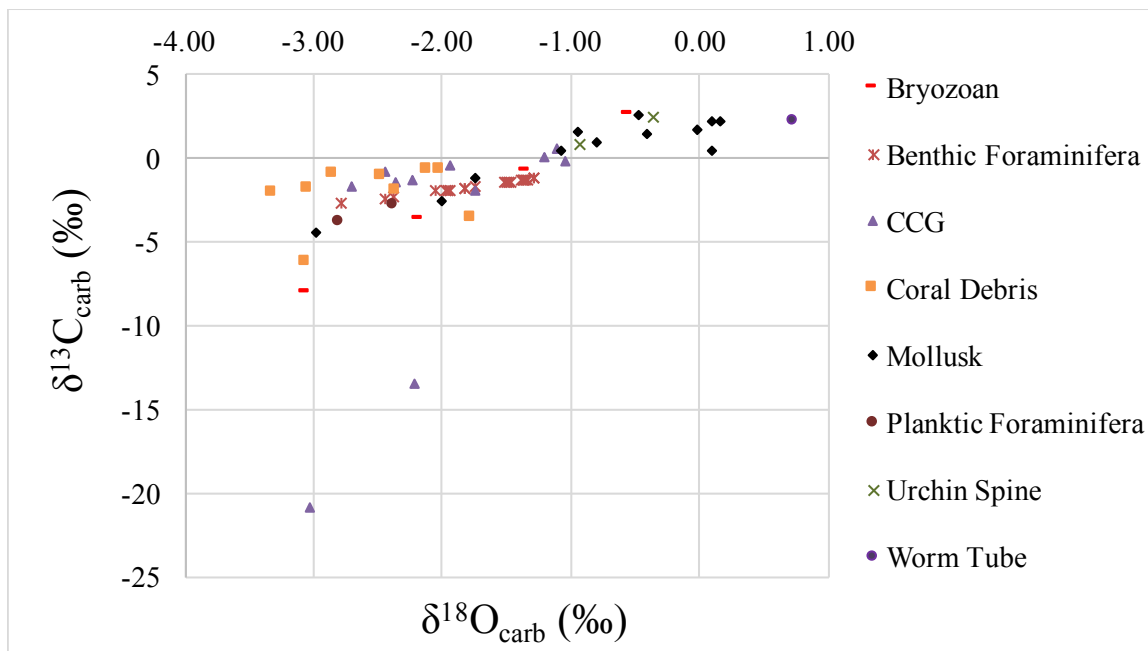
Figure 29: Component inorganic isotope comparison of oxygen and carbon stable isotopes. The CCG grains yield the most negative values of carbon.

Table 5: The correlation coefficient between the components inorganic isotope values to that of the bulk isotopic signature.

Component Correlations to Bulk Isotopic Signature		
Component	**R^2**	**Number of samples**
Benthic Foraminifera	0.44	19
Bryozoan	0.11	5
CCG	0.91	15
Coral	0.84	4
Coral Debris	0.77	10
Mollusk	0.38	12
Planktic Foraminifera	0.60	4
Urchin Spine	-	2
Worm Tube	-	1
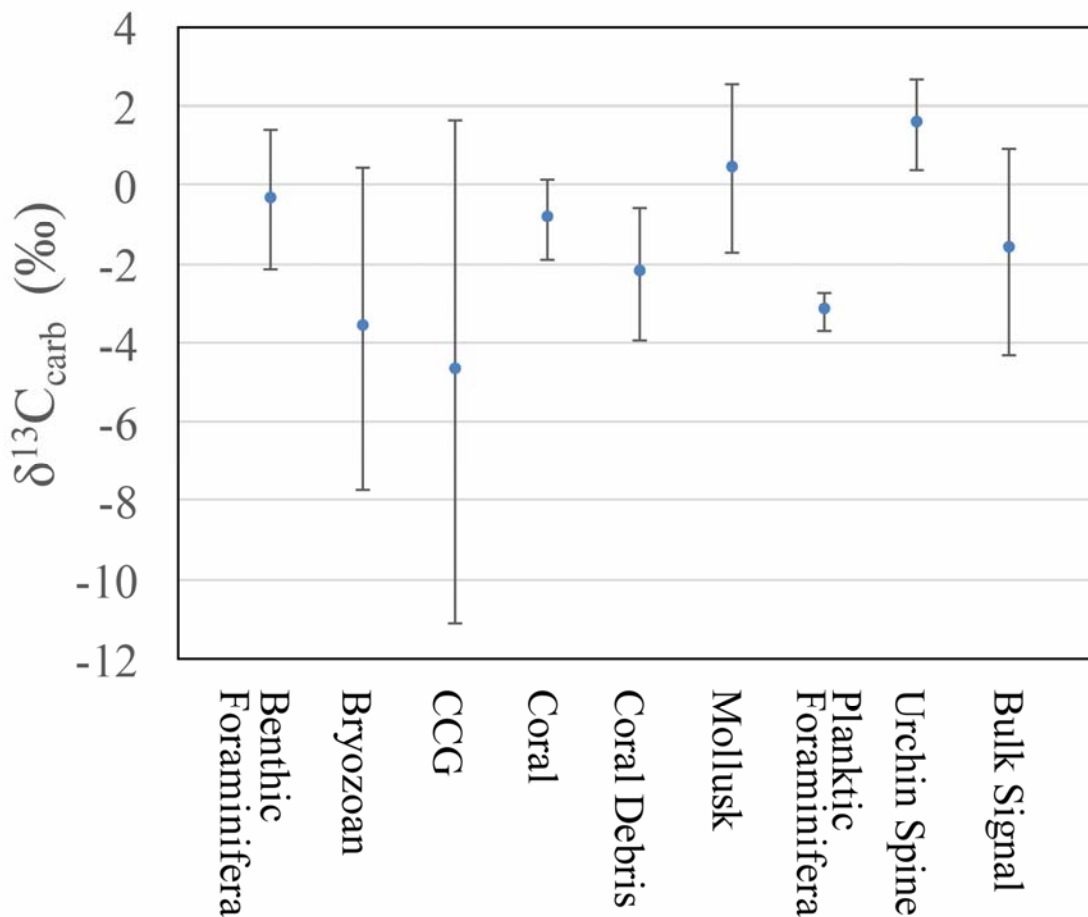
Figure 30: Inorganic carbon isotope values and standard deviation variance per component

3.4 Organic Isotope Data

The $\delta^{13}C$ value of organic carbon in the Rio Mao sections Gurabo Fm vary between -21.50 and -27.10‰. There were 57 corresponding samples tested for inorganic and organic carbon. There is a correlation of 0.24 between the $\delta^{13}C$ of inorganic and organic carbon, which yields a p-value <0.00001 and suggests that the datasets are significantly different. Values of total organic content (TOC) varied between 0-0.8% throughout the Rio Mao section (Figure 31). The organic carbon values were most positive near 45 m, 70 m, 85 m, and above 142 m (Figure 31).
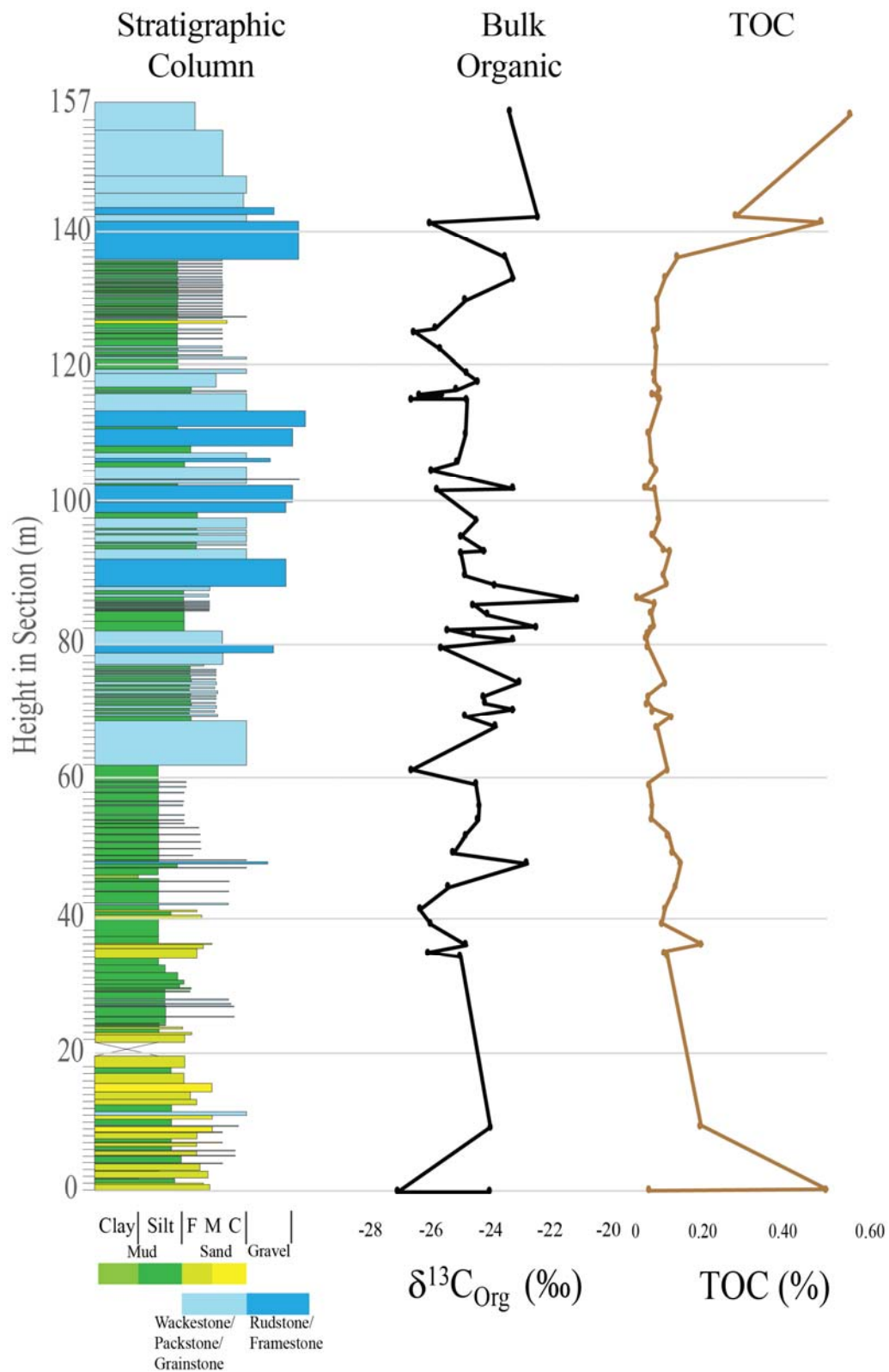
Figure 31: Bulk organic carbon and TOC comparison through the Rio Mao sections Gurabo Fm.

3.5 Strontium Chronostratigraphy

Three coral samples and one scaphopod sample that had high aragonite content (>93% aragonite) were sampled for $^{87}Sr/^{86}Sr$ isotopes. Corals that are high in aragonite content indicates that these samples likely contain the oceanic Sr signal from the time of deposition (Swart, 2015). The calculated age values of samples at 39.8 m range between 5.85-6.1 Ma. The most well-constrained sample contained a 95% confidence interval of between 5.7-5.96 Ma, which places the sample in the late Miocene according to (McArthur et al., 2001)(Table 6).

Table 6: List of values from Strontium dating in Unit 3 calculated from McArthur et al. (2001).

Sample Height (m)	$^{87}Sr/^{86}Sr$	± (95% CI)	Sr +	Sr -	Ma	Ma (late)	Ma (early)
39.8	0.709003	0.000007	0.709010	0.708996	5.85	5.7	5.96
39.8	0.708987	0.000029	0.709016	0.708958	6.1	5.59	6.88
39.8	0.708998	0.000010	0.709008	0.708989	5.96	5.75	6.06
47.1	0.709014	0.000015	0.709029	0.708999	5.63	5.23	5.91

Chapter 4. Discussion

4.1 Age and Correlation of the Gurabo Formation at Rio Mao

The age constraints from the Rio Mao section are two strontium-isotope age ranges from the basal portion of the stratigraphic section. These ages range between 5.6 to 6.3 Ma at 39.8 m, and 5.6 to 5.9 Ma at 47.1 m height in the section. The best age-dates for the Gurabo Formation is the integrated model from the Rio Gurabo transect where magnetostratigraphy, biostratigraphy, and strontium-isotope stratigraphy were used (McNeill et al. 2012). This integrated model provides ages that range from ~5.9 Ma at its base to ~4.5 Ma at the formation top. The two age ranges from the Rio Mao section, determined for the lower part of the Gurabo Formation, are consistent with the integrated age model (a Late Miocene age). The remaining approximately 100 m of the Gurabo Formation section at Rio Mao currently has no age control. However, if the Rio Mao section is correlated to the Rio Gurabo section, the section above 47.1 m is Early Pliocene (McNeill et al. 2012). The Rio Mao section likely contains deposits that reach ~4.0 Ma. At 4.0 Ma within the Rio Gurabo outcrop, a distinct erosional unconformity with gravel lag occurs, before deposition of the overlying Mao Formation. At Rio Mao, subaerial exposure separates the underlying Cercado Formation from the overlying Gurabo Formation, and this contact is visible ~1 km south of the Gurabo Fm study area (Figure 6). The contact with the Mao Formation is not well defined at Rio Mao, but likely lies along the road south of the city of Mao.

4.2 Depositional Sequences of the Rio Mao Section

Three sequences have been identified that illustrate the deepening upward (transgression) and shallowing upward (regression) transitions through an overall period of transgressive deposition. The interpretation is based on the concepts of T-R cycles from Embry (1995). The cycles were identified through analysis of depositional facies including bedding and sedimentary structures, coral fauna, and granular size and composition of the 157 m thick series of composite outcrops that comprise the Gurabo Fm within the Rio Mao section.

This mixed-system did not always have unambiguous cycle boundaries based on outcrops alone. Preliminary boundaries from outcrop were combined with the granular data to assist in refining specific boundaries (Schlager et al., 1994) (Figure 32; Appendix B).

4.2.1 Sequence 1 (0-81 m)

The sequence-1, S-1, transgression is denoted T-1, and comprises lithostratigraphic Unit I and II deposition (0-45 m in section; Figures 7-10 and 33). The base of the T-1 outcrop consists of a dense clay layer with abundant benthic foraminifera dominated by the genus *Amphistegina*, and indicative of deposition in a protected near-shore environment. Above this basal clay, the Mao section shows a marked increase in sand and silt sized siliciclastic sediments (primarily quartz). The quartz grains are often components of composite cemented grains (CCG) formed in situ during early marine diagenesis (Discussed in 4.5). While CCG grains are present in all sieve sizes, the quartz and feldspar grains that comprise them are predominately very fine sand, 63-125 μm (Figures 20 and 32; Appendix A and B). We interpret this large influx of siliciclastics to be a product of coastal erosion and transgressive recycling of the underlying Cercado Formation as sea

levels re-flooded the coastal plain. These very fine siliciclastic sands are admixed with in situ skeletal grains dominated by benthic foraminifera and mollusks, with minor contributions of free-living corals, and planktic foraminifera (Figure 32). The top of the transgression is marked by a condensed section composed of green mud with an abundant azooxanthellate coral fauna. While the presence of other zooxanthellate coral species suggests this is not below the photic zone, we do interpret this as a euphotic setting, and it is likely the most basinward position within the succession (Figures 9 and 10).
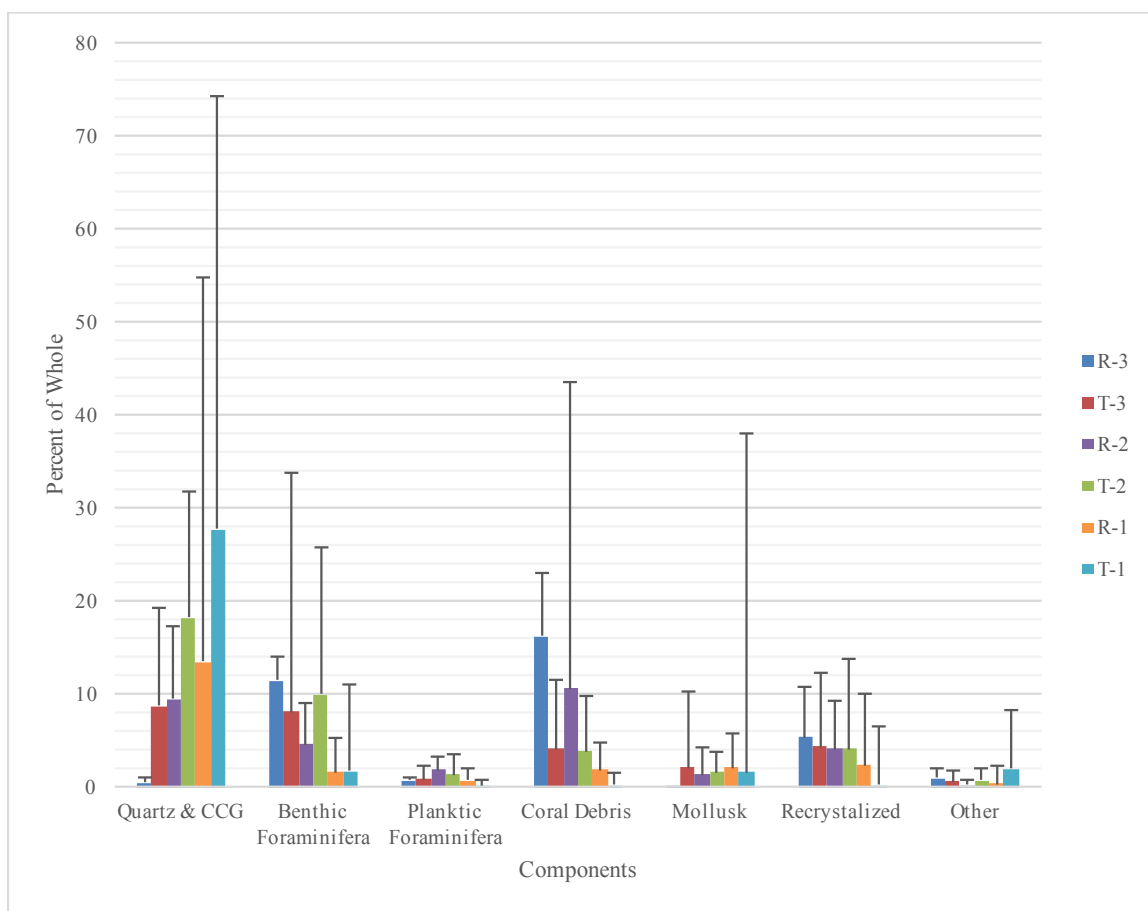
Figure 32: Components described in terms of their abundances within transgressive and regressive cycles. Greater abundances of quartz and CCG, benthic foraminifera, and mollusks tend to favor transgressive cycles; whereas, coral debris tends to favor regressive cycles.

The S-1 regression, R-1, is composed of lithostratigraphic Unit III (45-81 m in section). We interpret the base of the regressive hemicycle to be defined by a relative increase in siliciclastic sand and silt, benthic foraminifera, coral debris, and mollusks (Figures 10 and 32). The first expansive reef (~10 m height, 62-72 m) was subsequently deposited amongst an increase in abundance of carbonate grains (Figure 10 and 33). This zone is coincident with an increase in the planktic-to-benthic ratio as well as an increase in the proportion of small benthic foraminifera (Figures 24 and 33). This may be due to an increase in water depth as indicated by an increase in the planktic-to-benthic ratio (Milliman, 1974) and the reduced size distribution of the symbiont bearing foraminifera genus *Amphistegina* (Hallock et al., 1986), and reduced siliciclastic sedimentation. The reef is dominated by platy and massive corals, including: *Orbicella limbata*, *Porites mcdonaldi*, *Agaricia lamarcki*, *Leptoseris glabra*, *Stylophora minor*, and *Madracis decasptata*. The predominance of platy growth morphologies is characteristic of euphotic deeper forereef environments (Figure 10b). The reef unit is overlain by approximately 8 meters of alternating 10-30 cm thick beds of either indurated cohesive, silty-sand or lithified concretion beds of similar composition (Figure 33). The overall depauperate fauna within this interval may be indicative of relatively higher sedimentation rates. The lithified concretion beds likely reflect the pulsed nature of sedimentation with marine diagenesis and concretion formation associated with depositional hiatuses. The bedded concretion interval is overlain by shallow water corals and red algae. The shallow nature of this in situ reef deposit is further supported by prevalent red algal coatings on the coral debris. The top of the R-1 regression is capped by low-energy, shallow-water deposits with prevalent *Thalassinoides*-type calianassa burrows (Figure 11d). The top of S-1 had water

depth of only several meters, but no good evidence for subaerial exposure was found. A small incised channel occurs at the top of the sequence, and the channel may mark erosion associated with this event.

4.1.2 Sequence 2 (81-116 m)

The second transgression, T-2, is composed of lithostratigraphic Unit IV (81-96 m in section). The base of the hemicycle is a massive, well-sorted, light-tan colored mud and very-fine sand (Figure 12a). This basal mud is composed of benthic foraminifera followed by an increase in coral debris, mollusks, planktic foraminifera and recrystallized grains (Figures 12 and 33). Benthic foraminifera favor sandy bottom conditions and there were two large increases in their abundance in this sequence. The first increase in abundance was within the very fine sand and mud transgression and the second increase in abundance is at the top of the S-2 regression where there is an increase in coral debris (Figure 33). Both of these increases in abundance are similar as they coincide with large distributions of grains greater than mud-size (Figure 18). The top of this transgression is capped by a dense, mudstone and micrite matrix that contains large head corals, which is likely indicative of a deeper-water facies (Figure 12b). Beds near the top of T-2 display onlap stacking geometries indicative of retrogradation (Figure 12c).

The S-2 regression (R-2) is composed of lithostratigraphic Unit V (96-116 m). The S-2 regression begins within the northern side of RM-6, where there is a thick sequence that contains abundant corals, large benthic foraminifera, coral debris, and spiny oysters (~100 m height in section; Figure 14). The coral fauna is diverse with abundant large head corals and free-living corals (Figure 14). Coral rubble is deposited at 112-116 m height in the section that caps the top of the regression (Appendix B).

4.1.3 Sequence 3 (116-157 m)

T-3 is composed of lithostratigraphic Unit VI (116-136 m; Figure 15). At the base of this cycle, there was predominately quartz mud- to very fine- sand and CCGs. There was an absence of coral debris within the fine-quartz sand matrix, but there were large benthic foraminifera and a few scattered planktic foraminifera (Figure 33). Secondary pyrite and calcite flakes were diagenetically precipitated at 125.95 m height in section, which may be indicative of periodic exposure as these sediments are highly oxidized (Figures 25 and 33). Towards the top of the transgression there was an increase in abundance of benthic foraminifera, coral debris, and recrystallized grains between 125.95 m and 136 m (Figure 33). An increase in bryozoans and red algae mark the top of the interval as the transgression formed deeper-water facies (Figures 15 and 16a-c).

R-3 was composed of lithostratigraphic Unit VII (136-157 m; Figures 16d-f and 17). The R-3 regression shows trend toward more carbonate-rich sediment through an increase in coral debris and red algae toward the top of the sequence. At the base of the R-3 cycle there was prevalent coral debris and abundant deposition of red algae associated with a packstone and framestone matrix. The content of coral debris and benthic foraminifera continued to increase in abundance upward through the section, but due to lithification, additional samples could not be disaggregated for sedimentological analyses.

4.2.4 Summary of Rio Mao Section Sequences

In general, there is a greater abundance of carbonate skeletal grains within the regressive cycles of each sequence and greater abundances of siliciclastic deposition, or quartz and CCG, within transgressive cycles (Figures 32 and 33). Benthic foraminifera and mollusks are carbonate skeletal grains that are exceptions since they tend to deviate

from this generalization because they can be common in both transgressive and regressive settings (Figures 32 and 33). For example, benthic foraminifera have an affinity for sandy banks and sea grasses (e.g. Turtle grass), which are likely more common in transgressive cycles for this study area (Rose, 1977). In addition, Mount (1984) maintains that during siliciclastic deposition there are effects of increased turbidity, unstable substrates, and clogging of filter-feeding that encourage foraminifera-mollusk assemblages during these transgressive intervals.

The shelf during S-1 deposition was likely similar to a ramp, and reached water depths greater than that of S-2 and S-3 (Figure 35). This is supported by evidence in the ratio of planktic foraminifera relative to benthic foraminifera between 60-70 m height in the column, which is indicative of deepening water column and a shift towards middle-shelf deposition (Figure 33).

The first transgressive cycle had the greatest thickness of the three sequences, 45 m thick; whereas, T-2 and T-3 were much thinner, 15 m and 20 m, respectively (Figure 33). The latter two transgressions had greater carbonate content and reduced mud-size sediment within the bulk sedimentary matrix relative to T-1 (Figure 33). T-3 had a greater content of siliciclastic sediments, but this may be due to lobe shifting or many other changes in depositional conditions. There was a clear increase in carbonate skeletal grains within T-2 and T-3 relative to T-1, likely due to the evolution in shelf morphology from a higher to lower gradient (Figure 35). The R-2 and R-3 cycles bulk sediments contained a greater proportion of coral debris and carbonate content than R-1, and the latter two regressive cycles were slightly thicker than their paired transgressive cycles (Figures 33 and 35).

The regressive cycles in each of the three sequences contained the main reef assemblages. Each of these three cycles contained siliciclastic content, so none of the sequences were a 'clean-system' as described by the reciprocal sedimentation model (Figures 33 and 35). The concept of coeval deposition is better suited for this mixed system, but the framework of greater carbonate content within the regressive cycle, relative to its corresponding transgressive cycle, continues to hold true along the shelf. The lithofacies within each cycle are controlled by the hydrodynamics of the system where transgressive cycles that have greater turbidity tend to be more siliciclastic-rich; whereas, regressive cycles tend to be more carbonate-rich.

In the surrounding area, Klaus et al. (2008) provided coral classifications within the context of transgressive and regressive cycles by way of the relative abundance of free-living coral relative to mixed-types of coral assemblages. In the Rio Mao section, S-1 has lower coral diversity and contains primarily free-living coral within the transgression (Figure 26). The free-living coral assemblages occur in more restricted or soft-bottom grassflat environments and may have extended into depths as great as 20-30 m (Klaus et al., 2008). Platy corals are suggestive of deeper water depths as this growth morphology allows the coral to maximize the light capture. Platy corals dominate the basal regressive portion of S-1 with massive and branching corals becoming more abundant toward the top of the sequence (Figure 34). Though branching corals were in lesser abundance than platy corals (Figure 34). The S-1 regression is the zone in which the reef was becoming better established.

Sequence two, S-2, transition is marked by a muddy-sand lithofacies overlying the shallow-water *Thalassinoides* unit, and the transition is interpreted to mark deepening

water depth. During the subsequent transgression, the shelf was better suited for coral reef development in S-2, and this was evident by the increase in coral diversity (Figure 34). Throughout the transgression, the coral population once again contained primarily free-living corals. In the upper part of S-2, the coral diversity increases up-section as decreasing populations of free-living coral were replaced by increasing proportions of platy, massive and branching corals (Figure 34). It is estimated that the S-2 reefal assemblage developed at approximately 5 to 4.5 Ma. The top of S-2 is marked by shallow water carbonate-rich lithofacies and the change to more siliciclastic sediment in the overlying S-3 sequence.

4.3 Timing of Sequences and Correlation to Global Sea Level

Sediment supply is closely linked to eustatic fluctuations, and we have two strontium-isotope tie points within S-1. These tie points place the top of the S-1 transgression between 5.8-6 Ma and the base of the section may date back to 6.2 Ma. There were at least three sea level inundations (Miller et al., 2011) that contributed to the formation of three distinct sequences of deposition that comprise the Gurabo Fm along the Rio Mao (Figure 5).

A generalized framework of transgressive and regressive cycles has been applied to the Rio Mao section Gurabo Fm. These cycles are interpreted as deepening upward and shallowing upward, respectively. The varying degrees of coeval deposition may be used in relation to the sea level curve to further estimate the correlation between reef formation and sea level.

In the surrounding area, Klaus et al. (2008) provided coral classifications within the context of transgressive and regressive cycles by way of the relative abundance of free-living coral relative to mixed-types of coral assemblages. In the Rio Mao section, S-1 has

lower coral diversity and contains primarily free-living coral within the transgression (Figure 26). The free-living coral assemblages occur in more restricted or soft-bottom grass flat environments and may have extended into depths as great as 20-30 m (Klaus et al., 2008). Platy corals are suggestive of deeper water depths as this growth morphology allows the coral to maximize the light capture. Platy corals dominate the basal regressive portion of S-1 with massive and branching corals becoming more abundant toward the top of the sequence (Figure 34). Though branching corals were in lesser abundance than platy corals (Figure 34). The S-1 regression is the zone in which the reef was becoming better established. It is estimated that the S-1 reef formed approximately 5.5 Ma.

The shelf was better suited for coral reef development in S-2, and this was evident by the increase in coral diversity (Figure 34). Throughout the transgression, the coral population once again contained primarily free-living corals. In the regressive portion of S-2, the coral diversity increased up-section as decreasing populations of free-living coral were replaced by increasing proportions of platy, massive and branching corals (Figure 34). It is estimated that the S-2 reefal assemblage developed at approximately 4.52 Ma.

A third, and final sea level fall and subsequent rise, likely comprises the third and final sequence of deposition. This third sequence is likely capped at an average of about 4.13 Ma as is suggested from correlation to previous studies further to the west (McNeill et al., 2012).
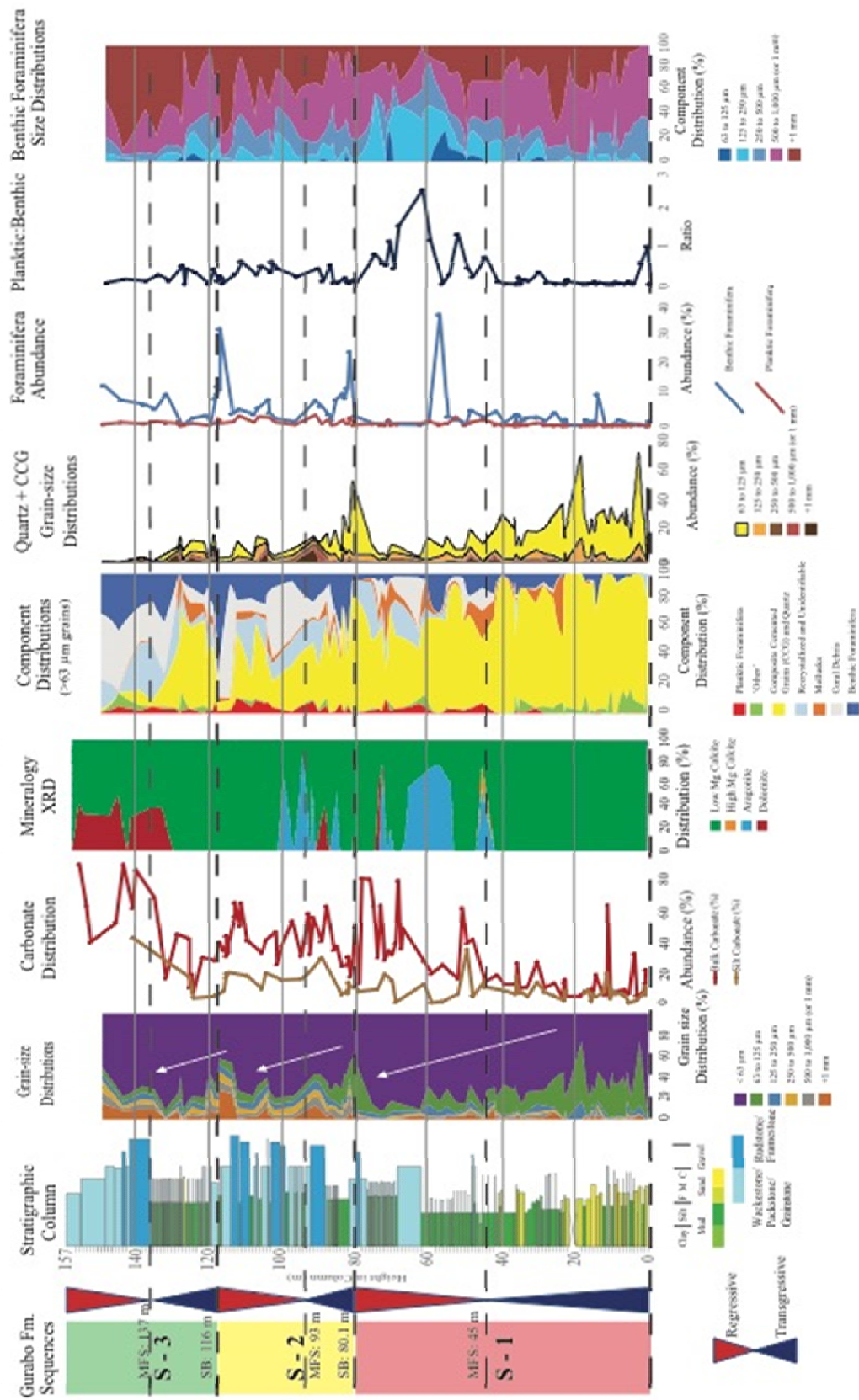
Figure 33: Sedimentological deconstruction of the Gurabo Fm. through sequence stratigraphic analysis of the grain-size distribution, carbonate content, XRD mineralogy, grain type distribution, quartz and CCG grain distribution, foraminifera abundance, planktic-to-benthic ratio, and the benthic foraminifera size distribution
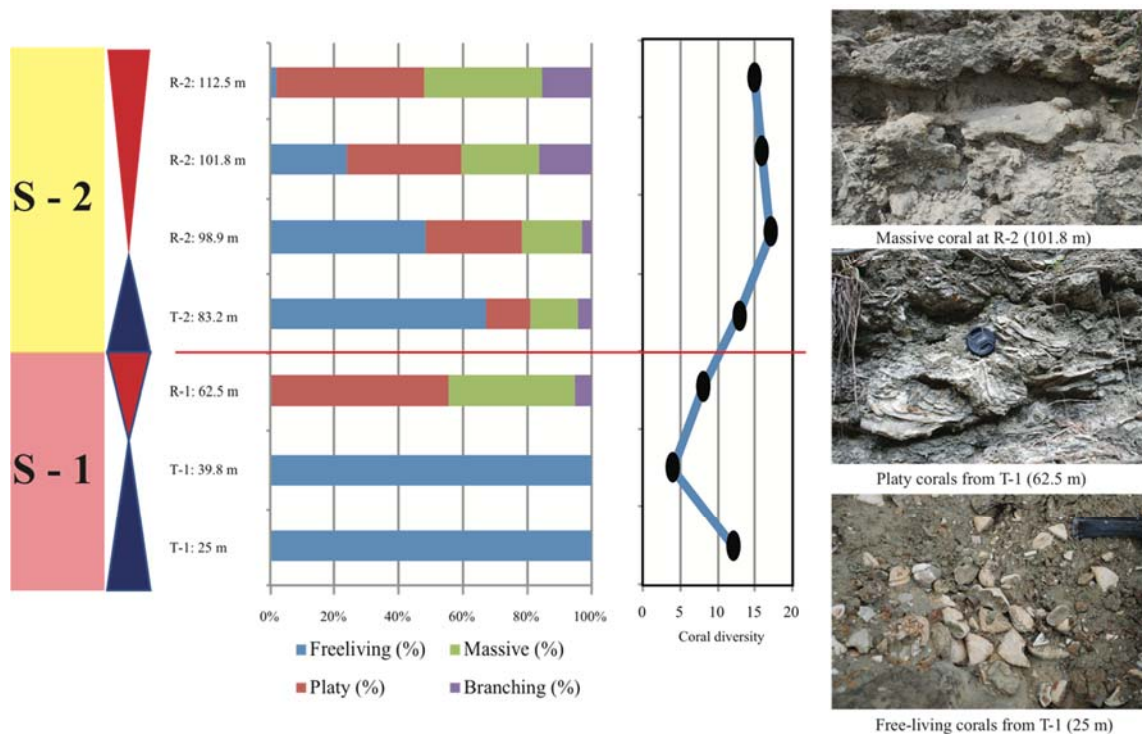
Figure 34: Coral distribution by classification through the first two sequences of the Rio Mao section.

4.3 Evolution of Gurabo Fm Shelf

There is much facies heterogeneity along the shelf due to changing shelf morphology and hydrodynamics. Eustatic fluctuations, sediment flux, and accommodation space are variable through time. These influences are considered a cornerstone to the foundation for sequence stratigraphic principles and depositional interpretation relative to a shoreline position. In order to reconstruct a paleo-shelf, it is crucial to consider: shelf morphology, lithofacies, reef framework (and relative abundances of coral that comprise subsequent reefs), reef thicknesses and lateral extents, and sea level implications at the time of deposition. The narrow shelf (6 km wide) in the Cibao Basin during the late Miocene to early Pliocene is predominately within the inner shelf to middle shelf transition. The

following discussion postulates the paleo-conditions during deposition of the mixed-system.

4.3.1 Implications of a Narrow Shelf Along the Rio Mao section Gurabo Fm.

The narrow shelf likely had restricted water circulation. These restricted conditions may be from a combination of low tidal range (+/- 1 m), shallow waters (~45 m maximum), and protection from the northern Cordillera Septentrional mountains that caused the Basin to have narrow- to complete-closure of the northeastern inlet to the Atlantic Ocean (Figures 2 and 3). Restricted current conditions decrease hydrodynamic effects that in turn minimize sedimentation movement along the shelf from tidal effects (Maxwell & Swinchatt, 1970). This allows for an expectation that carbonate detritus should remain within a minimal range of the reef it was precipitated amongst.

Minimal tidal circulation along the narrow shelf would likely cause temperature and salinity changes to be more pronounced due to seasonality; whereas, that of a more open marine hydrodynamic shelf such as the Great Barrier Reef (GBR), Australia would have less of an impact from seasonality as it has much larger tidal ranges (~4 m) (Maxwell & Swinchatt, 1970). In the Cibao Basin, the seasonal changes would increase cyclic duration relative to the GBR and allow for more prolonged and subtle changes in depositional facies.

Weathering of igneous and metamorphic sediments of the Cordillera Central mountains, to the South, deposited fine siliciclastic grains through fluvial transport to the inner marine shelf. Supply of sedimentation was likely controlled by temporal variations of inclement weather, sea level fluctuations and the subsequent accommodation space variability as the shelf morphology evolved (Figure 35). Increases in rain water or drops

in sea level increase fluvial deposition of siliciclastic sediments to the inner shelf when the supply exceeds the accommodation space. When sedimentation is siliciclatic-rich, CCGs have been found most-likely to form. These grains were bound by precipitation of carbonate cement. The CCGs likely formed by a combination of cementing processes that include: a rise in pH of the environment, as discussed by Correns (1950), Garrels (1960), Krauskopf (1967) and Bucke & Mankin (1971), and also by an increase in temperature, as suggested by Siever (1962) and Bucke & Mankin (1971), to drive pH conditions for early diagenesis to at least 9.0 (as cited in Blanche & Whitaker, 1978). These CCGs are also likely to have formed during sulfate reduction of organic material during periods of hiatuses in deposition as suggested by Coleman (1985) (Discussed further in 4.4).

The conditions to reach pH values for this type of early diagenesis in siliciclastic formations is found in the Brent Sands Formation of the North Sea basin (Blanche & Whitaker, 1978). The North Sea location is at a higher latitude and can more easily reach these values in open ocean conditions due to the more basic input of glacial melt. The restricted inner shelf conditions in the Cibao Basin can also replicate these conditions due to fresh water input on the inner shelf during the interpreted transgressions, or water deepening in outcrop interpretation, for these types of diagenesis to take place.

4.3.2 Paleo-Shelf Lithofacies Reconstruction

In general, reef morphology and diversity is controlled by substrate, water depth and eustatic fluctuations, sea water chemistry (mainly pH, temperature, and salinity), water clarity, and the energy of the current system that passes through the reef. The reef framework can be generally characterized by the growth of marine organisms interbedded with calcareous sands, silts and muds (Tucker et al., 1990). Reef thicknesses may be

associated with either regional subsidence and sea level rise, or both. Reefs favor idealized conditions, generalized above, and these conditions are most likely to exist within the highstand systems tract, or regressive cycles, as there is generally less clastic mud sedimentation in this cycle.

In mixed-systems, reef development occurs rarely under idealized conditions, an indication of reefal tolerance. In this study, each of the three depositional sequences differ in their composition, and this is illustrated through shelf evolution as the sequences grade from predominately clastic to predominately carbonate (Figure 33).

The Miocene-Pliocene shelf mixed-system was located at the Rio Mao near a fluvial source, and in the S-1 transgression, despite the high influx of quartz deposited on the shelf margin, it provided the substrate for free-living coral. Colonial corals were not present in this cycle because they would have likely been smothered by mud-rich clastic sedimentation or inimical water conditions. The shelf during S-1 deposition was likely similar to a ramp, and reached water depths greater than that of S-2 and S-3 (Figure 35). This is supported by evidence in the ratio of planktic foraminifera relative to benthic foraminifera between 60-70 m height in the column, which is indicative of deepening water column and a shift towards middle-shelf deposition (Figure 33).

The first transgressive cycle had the greatest thickness of the three sequences, 45 m thick; whereas, T-2 and T-3 were much thinner, 15 m and 20 m, respectively (Figure 33). The latter two transgressions had greater carbonate content and reduced mud-size sediment within the bulk sedimentary matrix relative to T-1 (Figure 33). T-3 had a greater content of siliciclastic sediments, but this may be due to lobe shifting or many other changes in depositional conditions. There was a clear increase in carbonate skeletal grains within T-

2 and T-3 relative to T-1, likely due to the evolution in shelf morphology from a higher to lower gradient (Figure 35). The R-2 and R-3 cycles bulk sediments contained a greater proportion of coral debris and carbonate content than R-1, and the latter two regressive cycles were slightly thicker than their paired transgressive cycles (Figures 33 and 35).

The regressive cycles in each of the three sequences contained the main reef assemblages. Each of these three cycles contained siliciclastic content, so none of the sequences were a 'clean-system' as described by the reciprocal sedimentation model (Figures 33 and 35). The concept of coeval deposition is better suited for this mixed system, but the framework of greater carbonate content within the regressive cycle, relative to its corresponding transgressive cycle, continues to hold true along the shelf. The lithofacies within each cycle are controlled by the hydrodynamics of the system where transgressive cycles that have greater turbidity tend to be more siliciclastic-rich; whereas, regressive cycles tend to be more carbonate-rich.

4.4 Geochemistry and Diagenesis

The goal was to utilize the point count data and the isotopic values for the components to reconstruct the $\delta^{13}C_{Bulk}$ signal (Equation 2). This creates an understanding of which sedimentary components control the bulk isotopic signal. The isotopic values of individual components exhibit their respective diagenetic fractionation and provides the means to interpreting their environmental influences that occurred during and after deposition of the Miocene-Pliocene Rio Mao section. The methodology employed in this study - deconstructing the geochemistry of the bulk isotopic signal by its constituent grains was similar to the modern analysis by (Gischler et al., 2009).
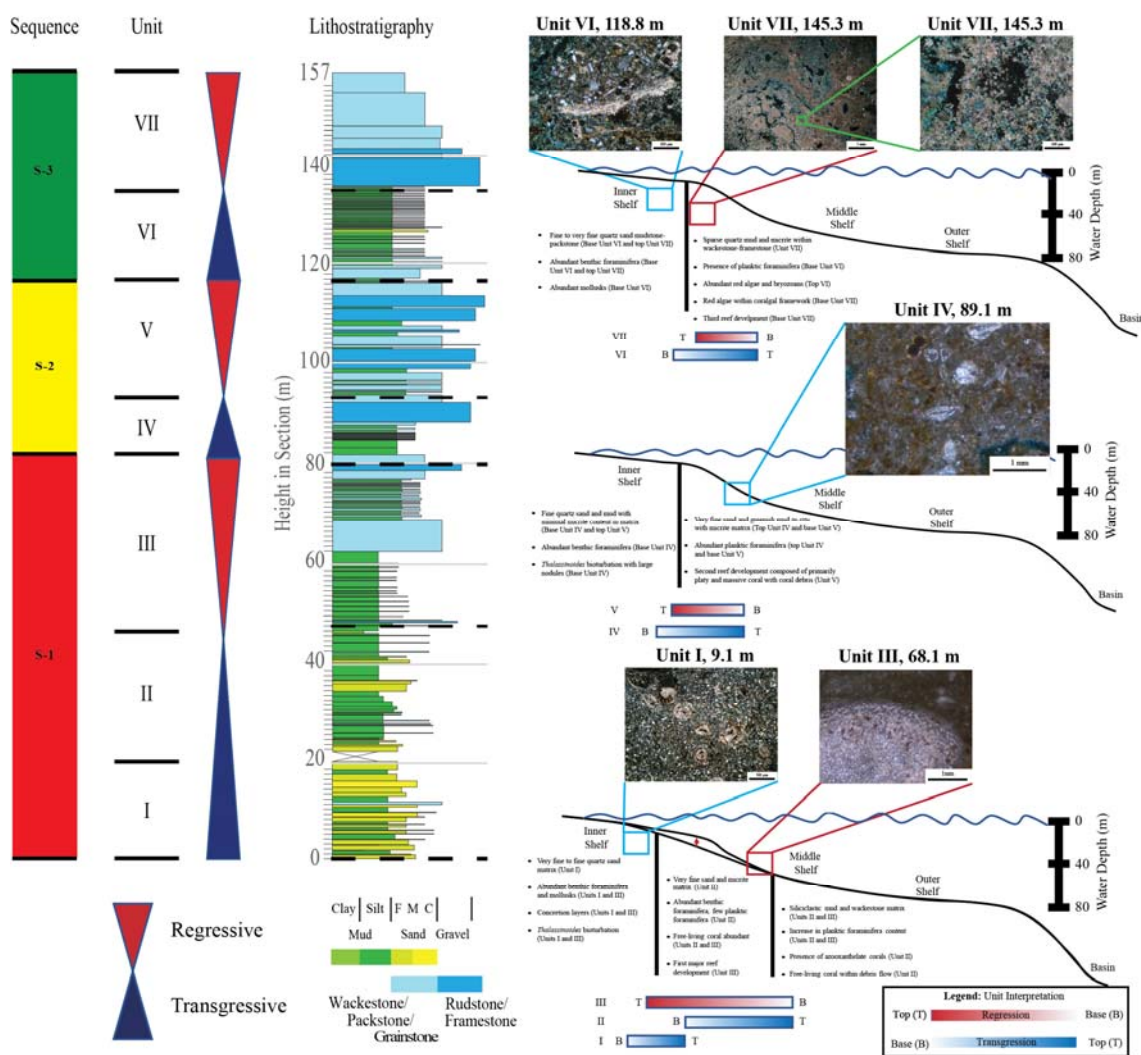
Figure 35: Lithofacies positions and shelf morphology through the Rio Mao section Gurabo Fm three sequences. The transition from a more siliciclastic-rich S-1 ramped inner shelf to the carbonate-rich S-2 and S-3 inner shelves that have less relief. The lithofacies may be different in similar positions on the shelf because of a change in hydrodynamics interpreted through transgressive-regressive cycles.

Variations in inorganic δ13C values were primarily utilized for geochemical interpretation in this shelf study due to the increased residence time of water on the shelf (Weber & Woodhead, 1971). The prominent controls on the δ13C is the value of the dissolved inorganic carbon (DIC), the weathering of carbonate rocks, and the oxidation of organic material within the marine environment (Swart, 2015; Figure 36). Throughout the succession, there are varying degrees of meteoric diagenesis that cause δ18O values to shift

to more negative values than the primary marine DIC values (Miller et al., 2005; Zachos et al., 2001)(Figure 36).

The skeletal components considered were: benthic foraminifera, bryozoans, calcite flakes, coral debris, mollusks, planktic foraminifera, sea urchin spines, and worm tubes (Figures 22 and 24). Each of these sedimentary grain types within the 18 samples through the Rio Mao's Gurabo Fm were analyzed for inorganic carbon stable isotope values (Figure 36). This allowed for a comparative analysis between a modeled primary signature curve, the bulk inorganic carbon profile, and the component composite curve of the sediments that comprise the corresponding samples (Figure 28).

This comparative analysis assists in determining where in the stratigraphic succession diagenetically altered grains exist. The modeled primary signature reflects an anticipated isotope curve for an identical mixed-system that has not undergone diagenetic alteration. The illustration displays that there are significant deviations, greater than 1-2‰, from the primary signature in both the bulk carbon profile and composite component profiles between 0-20 m, 50 m, and 116-126 m (Figures 28, 36 and 37). The major deviations from the primary signal are diagenetically induced dissolution and precipitation of LMC as can be seen by the isotopic shift to more negative values.

The sediments between 0-20 m and 116-126 m are predominately composed of terrestrially sourced quartz and composite cemented grains (CCG) in these transgressive cycles (i.e. T-1 and T-3) (Figures 28 and 36). In both the T-1 and T-3 cycles, the CCG isotopic signatures vary between -20.86 to -11.3‰, and these extremely negative $\delta^{13}C$ values provided evidence to interpret that marine authigenic precipitation cemented the CCGs at low rates of burial (Coleman, 1985) (Figure 28). Additionally, these grains are

likely microbiologically mediated from the processes of sulfate reduction and calcite precipitation (Coleman, 1985) (Figures 21 and 36).

In Figures 33 and 36, it is evident that regressive cycles there was greater carbonate content within the constituent sedimentary matrix resulting in an isotopic shift to more positive carbon isotopic values (Figure 28). These shifts in granular isotopic signatures may best be described through diagenetic partitioning of differing sedimentary layers (Eberli et al., 2000). A generalization of transgressive and regressive cycles simplifies the interpretation between these facies-dependent isotopic interpretations (Figure 36).
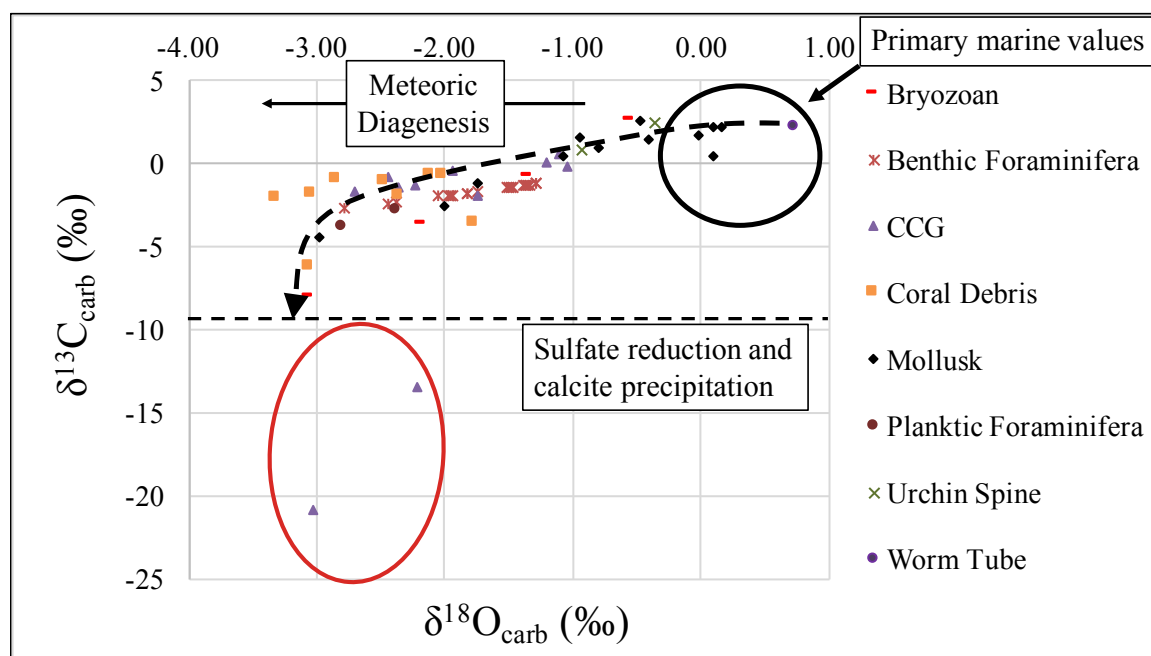
Figure 36: Inorganic isotopic composition of the components from 18 samples in the Rio Mao section Gurabo Fm. Illustration of microbially-induced sulfate reduction and calcite precipitation within CCGs and normal meteoric influence in carbonate grains described by K.C. Lohman's Inverted J.
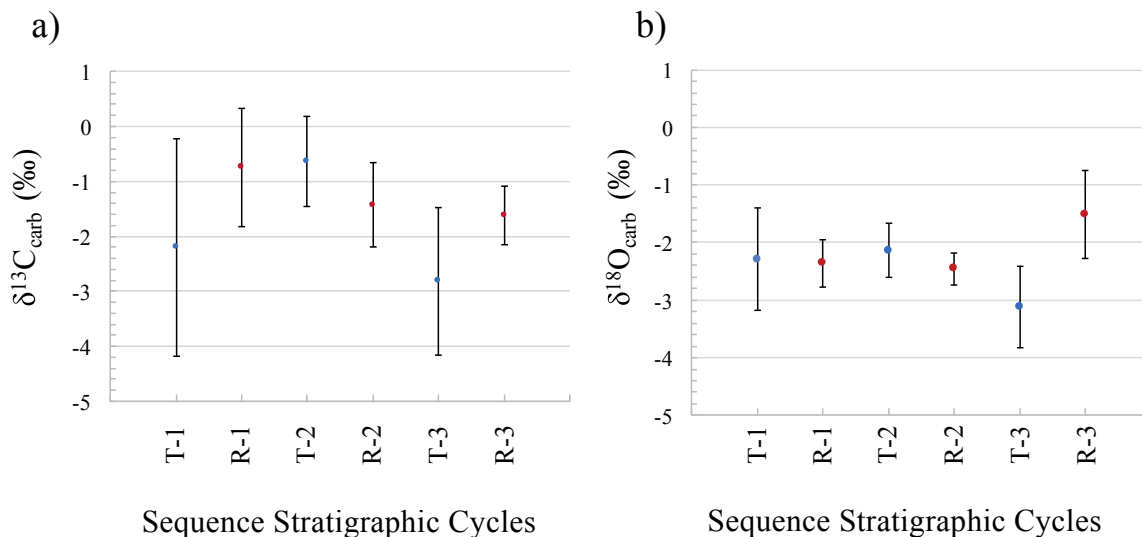
Figure 37: a) The carbon isotope mean and standard deviation through each of the transgressive and regressive cycles of the Rio Mao's Gurabo Fm b) Corresponding oxygen isotope mean and standard deviation through each of the three transgressive-regressive cycles in the Rio Mao section Gurabo Fm.

4.4.1 Comparison of Transgressive-Regressive Cycles

A comparison of the statistical significance, p-values, of the oxygen and carbon isotopes are described through cross-plots between the respective transgressive and regressive cycles within each sequence (Table 7; Appendix E). In this table, a statistically significant difference between the two compared cycles isotopic composition is indicated in green (>0.05), and the statistically insignificant difference between the cycles compared isotopic composition is indicated in red. Table 7 suggests that there is a statistically significant difference in the values for inorganic carbon between the transgressive and regressive pairs for each sequence. Table 7 also proves that there is only a significant difference in the oxygen isotopic composition within the S-3 transgressive-regressive pair; whereas, in S-1 and S-2, the paired cycles were not significantly different. The statistical comparisons in Table 7 provide the evidence to support the conceptual interpretations and comparison of the inorganic isotope cycles from Figures 36 and 37 (Appendix G).

Table 7: A statistical cross-plot of the p-values for each compared transgressive, T, and regressive, R, cycles' $\delta^{13}C$ and $\delta^{18}O$ isotopic compositions. This table illustrates that in the $\delta^{13}C$ the cycles within each sequence are significantly different (indicated in green) for each compared pair, and in the $\delta^{18}O$ that only the third sequence is significantly different; whereas, the first two sequences paired cycles are insignificantly different (indicated in red).

	T_1R_1	T_2R_2	T_3R_3
$\delta^{13}C$ (‰)	.004	.036	.023
$\delta^{18}O$ (‰)	.72	.07	.001

4.4.2 Bulk Isotope Analysis in T-R Cycles

Warm tropical waters in the Early Pliocene and heightened calcium carbonate content in the interstitial water assists in creating the conditions necessary for precipitation of carbonate reefs and carbonate cement (Blanche & Whitaker, 1978; Bucke & Mankin, 1971; Correns, 1950; Garrels, 1960; Krauskopf, 1967). An illustration of the abundance of carbonate skeletal grains relative to siliciclastic quartz and CCGs throughout the Rio Mao section is depicted in Figure 34. This figure shows that there was a great abundance of quartz and CCG within the transgressive portions, and an increase in abundance of carbonate skeletal grains in the regressive cycles for each of the three sequences.

The reason that diagenetic precipitation occurred in the transgressive sequence is because the porous, well-sorted fine sand in the transgressions generally had heightened susceptibility to marine water infiltration. There is also greater turbidity anticipated in transgressions (Mount, 1984). Through time of burial and intermittent hiatuses in deposition, bacterial sulfate reduction increased and exhausted the oxidation of organic matter, and during this process, the mineralized water within the pore space precipitated LMC cement (Coleman, 1985; Lohmann, 1988; Swart, 2015). This microbiologically

mediated LMC cement that binds the CCGs on the shelf drives the inorganic bulk isotopic profile in the transgressive cycle due to the susceptibility of the facies to diagenesis.

There was a marked difference in the S-2 transgression as it contained a more positive $\delta^{13}C$ value relative to that of S-1 and S-3 (Figure 27). The composition of the CCGs within this interval were less oxidized relative to that of the S-1 and S-3 intervals (Figure 21). The composite grains had $\delta^{13}C$ values of ~0‰, which may indicate that they had greater carbonate content and were formed in the early stage of diagenesis within shallow oxygenated waters (Coleman, 1985) (Figure 21b-c). The S-2 transgression also likely had less oxidation (more positive $\delta^{13}C_{Organic}$) of organic matter that may have been due to changes in geological conditions. Alternatively, a decrease, or change in type of organic matter in S-2 may have limited the ability for sulfate reduction in this interval. Each of the three transgressive cycles inorganic isotopic profiles were driven by the CCGs due to their respective differences in diagenetic conditioning (Figures 26 and 38).

Within the regressive cycles, there is an increase in carbonate content, and the δ13CCarbonate values typically shift to more positive values because the original signature of the DIC is better preserved (Figures 36 and 37). In Figure 28, within the S-1 regressive cycle, 45-80 m, the component composite curve and the bulk isotopic curve were nearly identical. These two curves deviate to more negative values than the primary signature when there is diagenetic influence. These diagenetic carbonates are not representative of the original DIC since the negative excursion in the δ13CCarbonate values are likely from the pore waters that were dominated by the product of the oxidation of organic matter as seen by the negative excursion in the corresponding δ13COrganic samples (Figure 36;
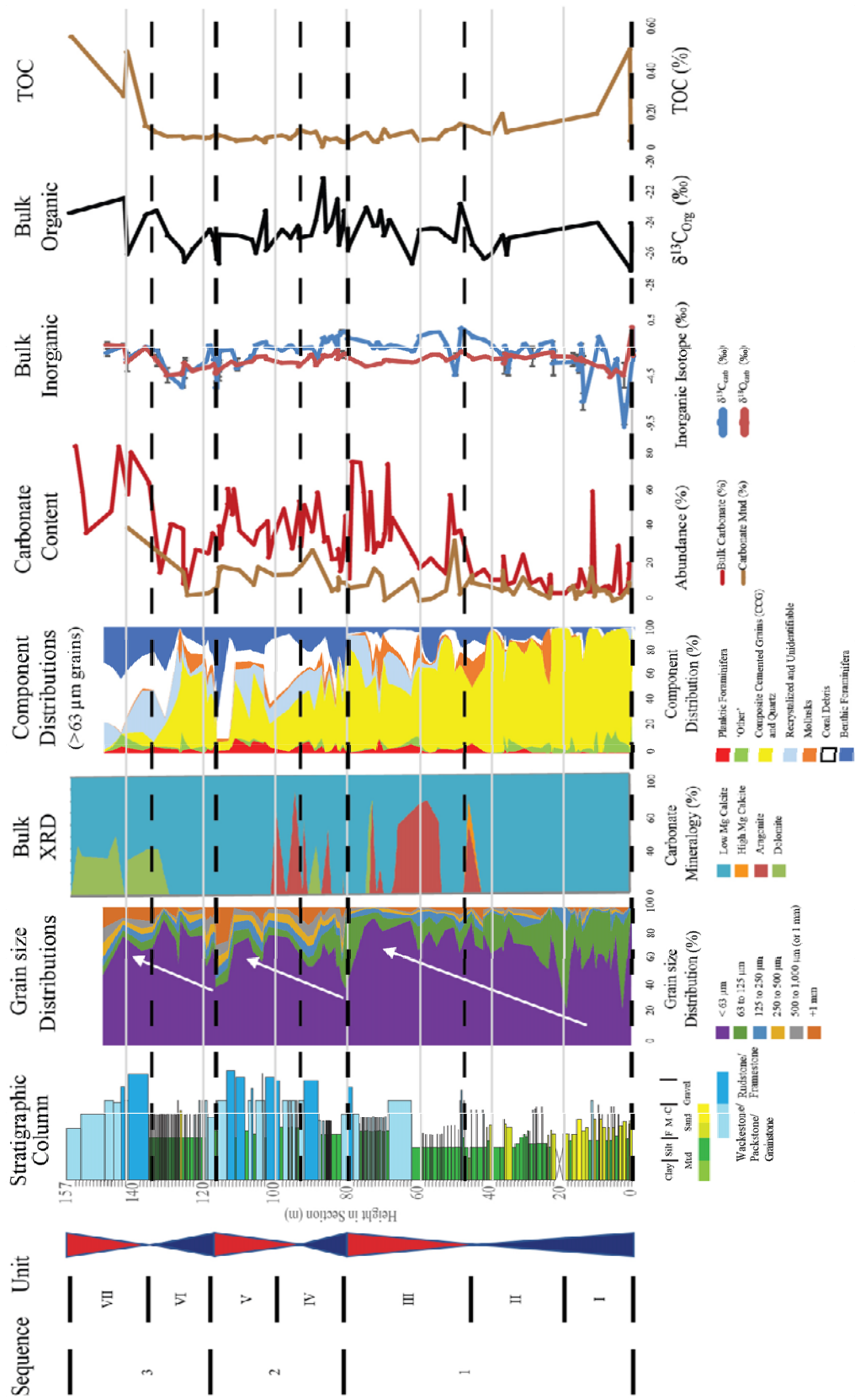
Figure 38: A comparison of grain size distribution, XRD, components distribution, carbonate content, bulk inorganic stable isotopes, bulk organic carbon, and TOC through the Rio Mao section Gurabo Fm's three sequences.

Swart, 2015). The S-2 regression had less organic content than that of R-1, and perhaps the increase in skeletal carbonate grains within the matrix made R-2 less susceptible to diagenesis than the more clastic-rich R-1 (Figure 38). The more diagenetically susceptible, clastic-rich, R-1 contained slightly more negative values in $\delta^{13}C$ (Figures 30, 36, 37 and Appendix E). Each of these first two regressive cycles were best characterized by the isotopic composition of coral debris as these grains most similarly reflected both the primary signal and diagenetic signals of the bulk isotopic signature in these cycles (Figures 26 and 36; Table 5).

In the first two sequences, the $\delta^{18}O$ contents were consistent, which provided the necessary information to deduce that that the mixed-system did not have upwelling of nutrients that could have influenced the depositional processes (Figure 38). Instead, it may be inferred that the depositional system was relatively simple and was controlled by only two sources: siliciclastic deposition through fluvial means, and through the precipitation of biogenic carbonate through differential mineral solubility throughout the Rio Mao section Gurabo Fm (Figure 36) (Lohmann, 1988).

The S-3 regression could only be examined through bulk isotopic analysis and thin section because the grains in this cycle could not be disaggregated (Figures 16d-f and 17). In considering the bulk inorganic isotope data, the S-3 regression had a drastic shift to more positive values in both the inorganic $\delta^{13}C$ the $\delta^{18}O$ relative to the remainder of the section (Figures 36, 37 and 38). The positive excursions in isotopic compositions were due to the presence of dolomite within the sample (Figures 16d-f, 19, 37, and 38). Dolomite presence is observed as minerals within the matrix, and they are typically less than 10 μm diameter

(Figure 16d-f). It is interpreted that the dolomite replaced portions of the micrite matrix. This most-commonly occurred at or near vuggy pore spaces in the thin section.

4.4.3 Summary of Geochemical Discussion

There is a facies dependent diagenetic partitioning between the transgressive and regressive cycles on the shelf. Eberli (2000) discussed that the disparity in the diagenetic potential of different sedimentary layers controls the subsequent diagenesis. Diagenesis within changing lithofacies for both the transgressive and regressive cycles caused a deviation to more negative values in the inorganic carbon isotope relative to the primary signature unless there was diagenetic precipitation of dolomite.

Within transgressive cycles, increased siliciclastic (quartz, feldspar, and mica) content may provide a heightened connectivity of the pore system. The connectivity of the pore system increases the susceptibility of the formation to water infiltration. Sulfate reduction and oxidation of organic material within saturated pore waters provide the condition for microbiologically mediated LMC cement precipitation. These diagenetically altered grains caused the $\delta^{13}C_{Bulk}$ to shift to more negative values in S-1 and S-3. The early diagenesis in the S-2 transgression that likely spurned from an increase in carbonate content that caused more positive $\delta^{13}C_{Bulk}$ values. Each of these transgressive sequences were best characterized by the isotopic composition of the CCGs as these grains most similarly reflected both diagenetic signals incurred.

When there is an increase in carbonate content, the $\delta^{13}C$ values shift to more positive values because the original signature of the DIC is better preserved. The presence of dolomite can cause shifts to more positive values in oxygen and carbon isotopes relative to those of calcite or aragonite. However, in the zones where the carbonate content is

greatest and there is less mud in the matrix to buffer the sediments from diagenesis - there can be shifts in the $\delta^{13}C$ to more negative values (Figure 36). When samples are analyzed within the context of sedimentary composition and a stratigraphic framework, stable isotope geochemistry can assist in understanding diagenetic causation.

Chapter 5. Implications

Mixed-system sedimentation is complex and has many heterogeneities. Lithofacies changes are not simply shelf-position dependent, but the hydrodynamic regime from transgressive versus regressive characterization provides context into the lithofacies positions along the shelf (Figure 35). The proportions of siliciclastic relative to carbonate sediments throughout the three sequences that comprise the Rio Mao section's Gurabo Fm can be a case study for shelf deposition by providing a lithofacies representation of the coeval sedimentation model for the mixed-system within a stratigraphic framework (Figures 33 and 35).

Sedimentary porosity and likely permeability provide conduits for the susceptibility of lithologic units to diagenesis. These units can be anticipated when considered within transgressive and regressive cycles. Transgressive cycles are carbonate deficient and have an abundance of quartz; whereas, the regressive cycles are more carbonate-rich (Figure 38). Each of the cycles are more susceptible to diagenetic alteration when there is sufficient porosity and permeability to aid water infiltration to and through the sediments. This is evident in the siliciclastic-rich transgressions by the microbiologically mediated LMC cement that binds the CCGs together and drives the bulk inorganic isotope signal to more negative values, and by the skeletal carbonate grains that have an isotopic shift to more negative values within zones that have lower quantities of mud that lessen their ability to buffer the grains from diagenesis in regressions.

During these regressive intervals, coral debris best reflects both the primary and diagenetic signals indicated by the bulk inorganic isotope signature. Whereas, in the

transgressive intervals, diagenetic signals of LMC cement in CCGs drive the bulk isotopic signature of this mixed-system.

This sedimentology study has created a model for the proportions of mixing between carbonate and siliciclastic sedimentation. Once the chronostratigraphic ages are further constrained, the Rio Mao section Gurabo Fm can be used as a case study for sedimentation rates for both carbonate and siliciclastic sediments through their temporal coeval deposition. Through the current study, zones of diagenetic partitioning have been identified due to lithofacies variations within the deposition of the overall transgressive mixed-system. The sedimentology and lithofacies analysis has led to a reconstructed paleo-shelf in accordance with the interpreted lithostratigraphic succession along the Rio Mao section Gurabo Fm (Figure 35). This paleo-reconstruction is best considered when applied to a narrow shelf (~6 km) that has minimal tidal influence and restricted circulation from the deep ocean.

Bibliography

Blanche, J. B., & Whitaker, J. H. (1978). Diagenesis of Part of the Brent Sand Formation (Middle Jurassic) of the Northern North Sea Basin. *Journal of the Geological Society*, *135*(1), 73–82. https://doi.org/DOI: 10.1144/gsjgs.135.1.0073

Bowin, C. O. (1966). Geology of Central Dominican Republic. In *Geological Society of America Memoirs* (Vol. 98, pp. 11–85). Geological Society of America. https://doi.org/10.1130/MEM98-p11

Bucke, D. P. J., & Mankin, C. J. (1971). Clay-Mineral Diagenesis Within Interlaminated Shales and Sandstones. *Journal of Sedimentary Petroleum*, *41*, 971–81.

Burgess, P. M., & Steel, R. J. (2017). How To Interpret, Understand, and Predict Stratal Geometries Using Stratal-Control Spaces and Stratal-Control-Space Trajectories. *Journal of Sedimentary Research*, *87*(4), 325–337. https://doi.org/10.2110/jsr.2017.19

Calais, E., Mazabraud, Y., Mercier De Lepinay, B., Mann, P., Mattioli, G. S., & Jansma, P. E. (2002). Strain Partitioning and Fault Slip Rates in the Northeastern Caribbean From GPS Measurements. *Geophysical Research Letters*, *29*(18), 4. https://doi.org/10.1029/2002GL015397

Coleman, M. L. (1985). Geochemistry of Diagenetic Non-Silicate Minerals: Kinetic Considerations. *Philosophical Transactions of the Royal Society of London. Series A Mathematical and Physical Sciences*, *315*, 39–56. https://www.jstor.org

Correns, C. W. (1950). *On The Geochemistry of Diagenesis, I. The Behavior of CaCO3 and SiO2*. Geochim. Cosmochim. Acta 1.

Draper, G., Jackson, T. A., & Donovan, S. K. (1994). Geologic Provinces of the Caribbean Region. *Caribbean Geology: An Introduction*, 3–12.

Droxler, A. W., & Jorry, S. J. (2011). Deglacial Origin of Barrier Reefs Along Low-Latitude Mixed Siliciclastic and Carbonate Continental Shelf Edges. *Annual Review of Marine Science*, *5*(1), 120928130849008. https://doi.org/10.1146/annurev-marine-121211-172234

Droxler, A. W., & Jorry, S. J. (2013). Deglacial Origin of Barrier Reefs Along Low-Latitude Mixed Siliciclastic and Carbonate Continental Shelf Edges. *Annual Review of Marine Science*, *5*(1), 165–190. https://doi.org/10.1146/annurev-marine-121211-172234

Dunbar, G. B., & Dickens, G. R. (2003). Late Quaternary Shedding of Shallow-Marine Carbonate Along a Tropical Mixed Siliciclastic-Carbonate Shelf: Great Barrier Reef, Australia. *Sedimentology*, *50*(6), 1061–1077. https://doi.org/10.1046/j.1365-3091.2003.00593.x

Dunham, R. J. (1962). Classification of Carbonate Rocks According To Depositional Texture. *Classification of Carbonate Rocks - A Symposium*, 108–121.

Eichenseer, H. T., Walgenwitz, F. R., & Biondi, P. J. (1999). Stratigraphic Control on Facies and Diagenesis of Dolomitized Oolitic Siliciclastic Ramp Sequences (Pinda Group, Albian, Offshore Angola) 1, *11*(11), 1729–1758.

Embry, A. F. (1995). Sequence Boundaries and Sequence Hierarchies: Problems and Proposals (pp. 1–11). https://doi.org/10.1016/S0928-8937(06)80059-7

Evans, C. (1986). Facies Evolution in a Neogene Transpressional Basin: Cibao Valley. *Dominican Republic [Ph. D. Thesis]: Coral Gables,*. https://scholar.google.com/scholar?q=C.C.+Evans+1986+dominican+republic+thesis&btnG=&hl=en&as_sdt=0%2C10

Flood, P. G., Orme, G. R., & Scoffin, T. P. (1978). An Analysis of the Textural Variability Displayed by Inter-Reef Sediments of the Impure Carbonate Facies in the Vicinity of the Howick Group. *Philosophical Transactions of the Royal Society of London. Series A Mathematical and Physical Sciences*, (291), 73–83. https://www.jstor.org

Francis, J. M. (2007). *Late Quaternary Sediment Dispersal and Accumulation of Slopes of the Great Barrier Reef Mixed Siliciclastic-Carbonate Depositional System, Gulf of Papua, Papua New Guinea and North Queensland Margin, Australia*. Rice University.

Garrels, R. M. (1960). *Mineral Equilibria*. New York: Harper & Bros.

Gischler, E., Swart, P. K., & Lomando, A. J. (2009). Stable Isotopes of Carbon and Oxygen in Modern Sediments of Carbonate Platforms, Barrier Reefs, Atolls and Ramps: Patterns and Implications. *Perspectives in Carbonate Geology* (pp. 61–74). John Wiley & Sons, Ltd. https://doi.org/10.1002/9781444312065.ch5

González, L. A., & Lohmann, K. C. (n.d.). Carbon and Oxygen Isotopie Composition of Holocene Reefal Carbonates. http://geology.gsapubs.org/content/13/11/811.full.pdf

Hallock, P., Forward, L. B., & Hansen, H. J. (1986). Influence of Environment on the Test Shape of Amphistegina. *Journal of Foraminiferal Research*, *16*(3). http://jfr.geoscienceworld.org/content/16/3/224

Haq, B. U., Hardenbol, J., & Vail, P. R. (1987). Chronology of Fluctuating Sea Levels Since the Triassic. *Science (New York, N.Y.)*, *235*(4793), 1156–1167. https://doi.org/10.1126/science.235.4793.1156

Heubeck, C., Mann, P., Dolan, J., & Monechi, S. (1991). Diachronous Uplift and Recycling of Sedimentary Basins during Cenozoic Tectonic Transpression, Northeastern Caribbean Plate Margin. *Sedimentary Geology*, *70*(1), 1–32. https://doi.org/10.1016/0037-0738(91)90063-J

Hodell, D. A., & Kennett, P. (1986). Late Miocene-Early Pliocene Straitgraphy and Paleoceanography of the South Atlantic and Southwest Pacific Oceans: A Synthesis, *1*(3), 285–311.

Hsu, K. J., Ryan, W. B. F., & Cita, M. B. (1973). Late Miocene Desiccation of the Mediterranean. *Nature*, *242*, 240–244.

Klaus, J. S., McNeill, D. F., Budd, A. F., & Johnson, K. G. (2008). Assessing Community Change in Miocene to Pliocene Coral Assemblages of the Northern Dominican Republic. In R. H. Nehm & A. F. Budd (Eds.), *Evolutionary Stasis and Change in the Dominican Republic Neogene* (pp. 193–223). Dordrecht: Springer Netherlands. https://doi.org/10.1007/978-1-4020-8215-3_9

Krauskopf, K. B. (1967). *Introduction to geochemistry*. New York: McGraw-Hill Book Co.

Lohmann, K. C. (1988). Geochemical Patterns of Meteoric Diagenetic Systems and Their Application to Studies of Paleokarst. In N. P. James & P. W. Choquette (Eds.), *Paleokarst* (pp. 58–80). New York, NY: Springer New York. https://doi.org/10.1007/978-1-4612-3748-8_3

Maurrasse, F. (1982). Survey of the Geology of Haiti: Guide to the Field Excursions in Haiti: Miami, Florida, Miami Geological Society, p. 103. *Caribbean Geology*.

Maxwell, W. G. H., & Swinchatt, J. P. (1970). Great Barrier Reef: Regional Variation in a Terrigenous-Carbonate Province. *Geological Society of America Bulletin*, *81*(3), 691. https://doi.org/10.1130/0016-7606(1970)81[691:GBRRVI]2.0.CO;2

McArthur, J. M., Howarth, R. J., & Bailey, T. R. (2001). Strontium Isotope Stratigraphy: LOWESS Version 3: Best Fit to the Marine Sr-Isotope Curve for 0-509 Ma and Accompanying Look-Up Table for Deriving Numerical Age. *The Journal of Geology*, *109*(2), 155–170. https://doi.org/10.1086/319243

McNeill, D. F., Klaus, J. S., Budd, A. F., Lutz, B. P., & Ishman, S. E. (2012). Late Neogene Chronology and Sequence Stratigraphy of Mixed Carbonatesiliciclastic Deposits of the Cibao Basin, Dominican Republic. *Bulletin of the Geological Society of America*, *124*(1–2), 35–58. https://doi.org/10.1130/B30391.1

McNeill, D. F., Klaus, J. S., Evans, C. C., & Budd, A. F. (2008). An Overview of the Regional Geology and Stratigraphy of the Neogene Deposits of the Cibao Valley, Dominican Republic. R. H. Nehm & A. F. Budd (Eds.), *Evolutionary Stasis and Change in the Dominican Republic Neogene* (pp. 21–45). Dordrecht: Springer Netherlands. https://doi.org/10.1007/978-1-4020-8215-3_2

McNeill, D. F., Klaus, J. S., O'Connell, L. G., Coates, A. G., & Morgan, W. A. (2013). Depositional Sequences And Stratigraphy of the Colon Carbonate Platform: Bocas Del Toro Archipelago, Panama. *Journal of Sedimentary Research*, *83*(2), 183–195. https://doi.org/10.2110/jsr.2013.13

Miller, K. G., Kominz, M. A., Browning, J. V., Wright, J. D., Mountain, G. S., Katz, M. E., … Pekar, S. F. (2005). The Phanerozoic Record of Global Sea-Level Change. *Science*, *310*(5752). http://science.sciencemag.org/content/310/5752/1293

Miller, K. G., Mountain, G. S., Wright, J. D., & Browning, J. V. (2011). A 180-Million-Year Record of Sea Level and Ice Volume Variations from Continental Margin and Deep-Sea Isotopic Records. *Oceanography*, *2426*(2), 40–53. https://doi.org/10.5670/oceanog.2011.26

Milliman, J. (1974). Marine Carbonates, Part I. *Heidelberg7 Springer-Verlag*.

Mount, J. F. (1984). Mixing of Siliciclastic and Carbonate Sediments in Shallow Shelf Environments. *Geology*, *12*, 432–435. https://gsw.silverchair-cdn.com/gsw/Content_public/Journal/geology/12/7/10.1130_0091-7613(1984)12_432_MOSACS_2.0.CO;2/2/i0091-7613-12-7-432.pdf?Expires=1502213404&Signature=W0hjE4~laYoj3jl7vyPKRBIMyzwwP6BCpohANcoZRUXyO943Tizjerv-D1L82kCKvqQd6huKmSm3icFowv

Pourmand, A., Prospero, J. M., & Sharifi, A. (2014). Geochemical Fingerprinting of Trans-Atlantic African Dust Based on Radiogenic Sr-Nd-Hf Isotopes and Rare Earth Element Anomalies. *Geology*, *42*(8), 675–678. https://doi.org/10.1130/G35624.1

Prasada Rao, C. (1993). Carbonate Minerals, Oxygen and Carbon Isotopes in Modern Temperate Bryozoa, Eastern Tasmania, Australia. *Sedimentary Geology*, *88*(1–2), 123–135. https://doi.org/10.1016/0037-0738(93)90153-V

Puga-bernabe, N., Droxler, W., Webster, J. M., Gischler, E., Harper, B. B., Tiwari, M., … Hohl, U. (2015). Mixed Carbonate–Siliciclastic Sedimentation Along the Great Barrier Reef Upper Slope: A Challenge to the Reciprocal Sedimentation Model. *Journal of Sedimentary Research*, *85*, 1019–1036. https://doi.org/10.2110/jsr.2015.58.1

Purdy, E. G., & Gischler, E. (2003). The Belize Margin Revisited: 1. Holocene Marine Facies. *International Journal of Earth Sciences*, *92*(4), 532–551. https://doi.org/10.1007/s00531-003-0324-0

Reolid, J., Betzler, C., Braga, J. C., Martín, J. M., Lindhorst, S., & Reijmer, J. J. G. (2014). Reef Slope Geometries and Facies Distribution: Controlling Factors (Messinian, SE Spain). *Facies*, *60*(3), 737–753. https://doi.org/10.1007/s10347-014-0406-4

Richard G. Fairbanks, Mark Sverdlove, Rosemary Free, Peter, H. Wiebe, & A. W. H. B. (1982). Vertical Distribution and Isotopic Franctionation of Living Planktonic Foraminifera From the Panama Basin. *Nature*, *298*. https://www.nature.com/nature/journal/v298/n5877/pdf/298841a0.pdf

Rose, P. R. (1977). *Diagnostic Foraminiferal Assemblages of Shallow-Water Modern Environments, South Florida and the Bahamas*. Miami : Comparative Sedimentology Laboratory, Division of Marine Geology and Geophysics, Rosenstiel School of Marine & Atmospheric Science, University of Miami. https://searchworks.stanford.edu/view/971080

Saunders, J. B. (1986). *Neogene Paleontology in the Northern Dominican Republic*. Paleontological Research Institution. https://catalog.loc.gov/vwebv/citeRecord?searchId=2528&recPointer=0&recCount=25&searchType=0&bibId=972299

Schlager, W., Reijmer, J. J. G., & Droxler, A. (1994). Highstand Shedding of Carbonate Platforms. *Journal of Sedimentary Research*, *B64*(3), 270–281. https://doi.org/10.1306/D4267FAA-2B26-11D7-8648000102C1865D

Mehterian, S., Pourmand, A., Sharifi, A., Lahijani, H., Naderi, M., & Swart, P. (2017). Speleothem Records of Glacial/Interglacial Climate from Iran Forewarn of Future Water Availability in the Interior of the Middle East. https://www.sciencedirect.com/science/article/pii/S0277379116305571

Swart, P. K. (2015). The Geochemistry of Carbonate Diagenesis: The Past, Present and Future. *Sedimentology*, *62*(5), 1233–1304. https://doi.org/10.1111/sed.12205

Swart, P. K., Eberli, G. P., Malone, M. J., & Sarg, J. F. (2000). The Record of Neogene Sea-Level Changes in the Prograding Carbonates Along the Bahamas Transect—Leg 166 Synthesis. *Proceedings of the Ocean Drilling Program, 166 Scientific Results*, *166*(1), 167–177. https://doi.org/10.2973/odp.proc.sr.166.128.2000

Tcherepanov, E. N., Droxler, A. W., Lapointe, P., & Mohn, K. (2008). Carbonate Seismic Stratigraphy of the Gulf of Papua Mixed Depositional System: Neogene Stratigraphic Signature and Eustatic Control. *Basin Research*, *20*(2), 185–209. https://doi.org/10.1111/j.1365-2117.2008.00364.x

Tucker, M. E., Wright, V. P., & Dickson, J. A. D. (1990). *Carbonate Sedimentology*. Blackwell Scientific Publications.

Van Couvering, J. a, Castradori, D., Cita, M. B., Hilgen, F. J., & Rio, D. (2000). The Base of the Zanclean Stage and of the Pliocene Series. *Episodes*, *23*, 179–187. http://www.stratigraphy.org/upload/bak/Zanclean.pdf%5Cnfiles/1617/Zanclean.pdf

Vokes, E. (1979). The Age of the Baitoa Formation, Dominican Republic, Using Mollusca for Correlation. *Tulane Stud. Geol. Paleontol*. https://scholar.google.com/scholar?hl=en&q=vokes+1979+dominican+republic&btnG=&as_sdt=1%2C10&as_sdtp=

Weber, J. N., & Woodhead, P. M. J. (1971). Diurnal Variations in the Isotopic Composition of Dissolved Inorganic Carbon in Seawater from Coral Reef Environments. *Geochimica et Cosmochimica Acta*, *35*(9), 891–902. https://doi.org/10.1016/0016-7037(71)90003-2

Zachos, J., Pagani, M., Sloan, L., Thomas, E., & Billups, K. (2001). Trends, Rhythms, and Aberrations in Global Climate 65 Ma to Present. *Science*, *292*(5517), 686–693. https://doi.org/10.1126/science.1059412

APPENDIX A: Point-Count Distribution

POINT COUNT DISTRIBUTION

Sedimentologic grain distribution within each sequence of the Rio Mao section Gurabo Fm.

Sequence	Statistic	Components (%)						
		Quartz & CCG	Benthic Foraminifera	Planktic Foraminifera	Coral Debris	Mollusk	Recrystalized	Other
Gurabo Fm.	Max	74.3	33.8	3.6	43.7	38.0	13.7	8.2
	Avg	18.4	4.2	0.7	3.0	1.7	2.3	1.1
	Min	0.0	0.0	0.0	0.0	0.0	0.0	0.0
S-3	Max	19.4	33.8	2.3	23.2	10.4	12.3	2.1
	Avg	7.7	8.5	0.9	5.7	1.9	4.5	0.6
	Min	0.0	0.2	0.0	0.0	0.0	0.0	0.0
S-2	Max	31.8	25.8	3.6	43.7	4.3	13.7	2.1
	Avg	14.1	7.5	1.6	7.1	1.5	4.1	0.5
	Min	3.6	1.4	0.1	0.0	0.0	0.0	0.0
S-1	Max	74.3	11.1	1.9	4.8	38.0	10.1	8.2
	Avg	23.4	1.7	0.3	0.7	1.8	0.9	1.4
	Min	1.0	0.0	0.0	0.0	0.0	0.0	0.0

The components of the Gurabo Fm. statistically analyzed through each sequences transgressive and regressive cycles and each component is illustrated as percent of whole sample (all grains >63 μm).

Sequence	Cycle	Statistic	Components (%)						
			Quartz & CCG	Benthic Foraminifera	Planktic Foraminifera	Coral Debris	Mollusk	Recrystalized	Other
Gurabo Fm.		Max	74.3	33.8	3.6	43.7	38.0	13.7	8.2
		Avg	18.4	4.2	0.7	3.0	1.7	2.3	1.1
S-3	Regressive	Max	0.9	14.1	1.1	23.2	0.2	10.7	2.1
	Regressive	Avg	0.5	11.5	0.8	16.2	0.1	5.4	1.0
	Transgressive	Max	19.4	33.8	2.3	11.7	10.4	12.3	1.8
	Transgressive	Avg	6.5	17.8	1.7	4.3	2.4	1.8	0.4
S-2	Regressive	Max	17.3	9.0	3.3	43.7	4.3	9.4	0.9
	Regressive	Avg	9.5	4.6	1.9	10.6	1.4	4.1	0.3
	Transgressive	Max	31.8	25.8	3.6	9.8	3.8	13.7	2.1
	Transgressive	Avg	18.2	10.0	1.3	3.9	1.7	4.1	0.7
S-1	Regressive	Max	54.9	5.3	1.9	4.8	5.8	10.1	2.3
	Regressive	Avg	13.6	1.7	0.8	1.8	2.2	2.4	0.3
	Transgressive	Max	74.3	11.1	0.9	1.4	38.0	6.5	8.2
	Transgressive	Avg	27.7	1.7	0.1	0.2	1.6	0.3	1.9
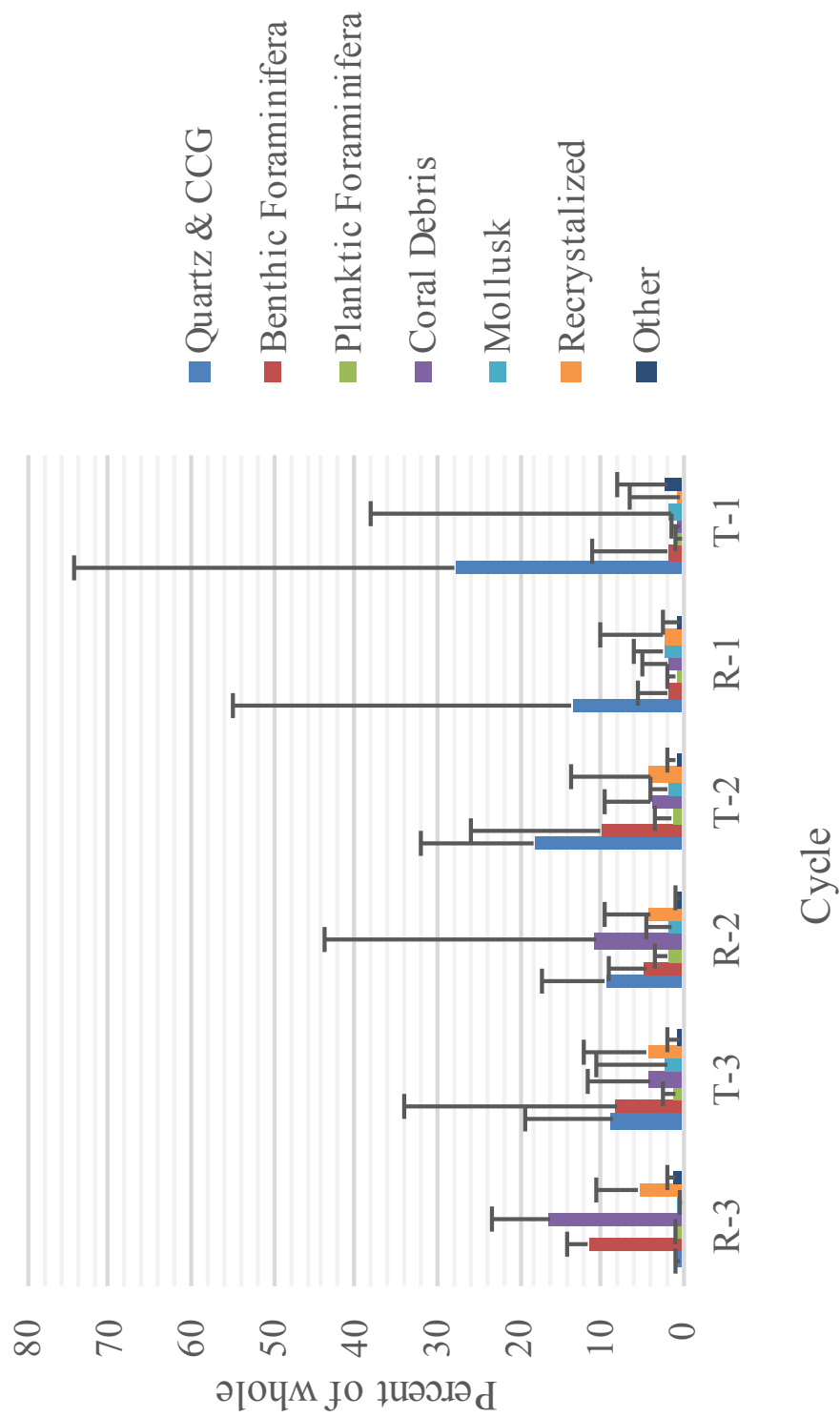
Graph indicating the compositional variances of each of the components within their transgressive and regressive cycles.

APPENDIX B: Carbon Isotopes through Gurabo Fm.
(Inorganic and Organic)

CARBON ISOTOPES IN TRANSGRESSIVE AND REGRESSIVE CYCLES
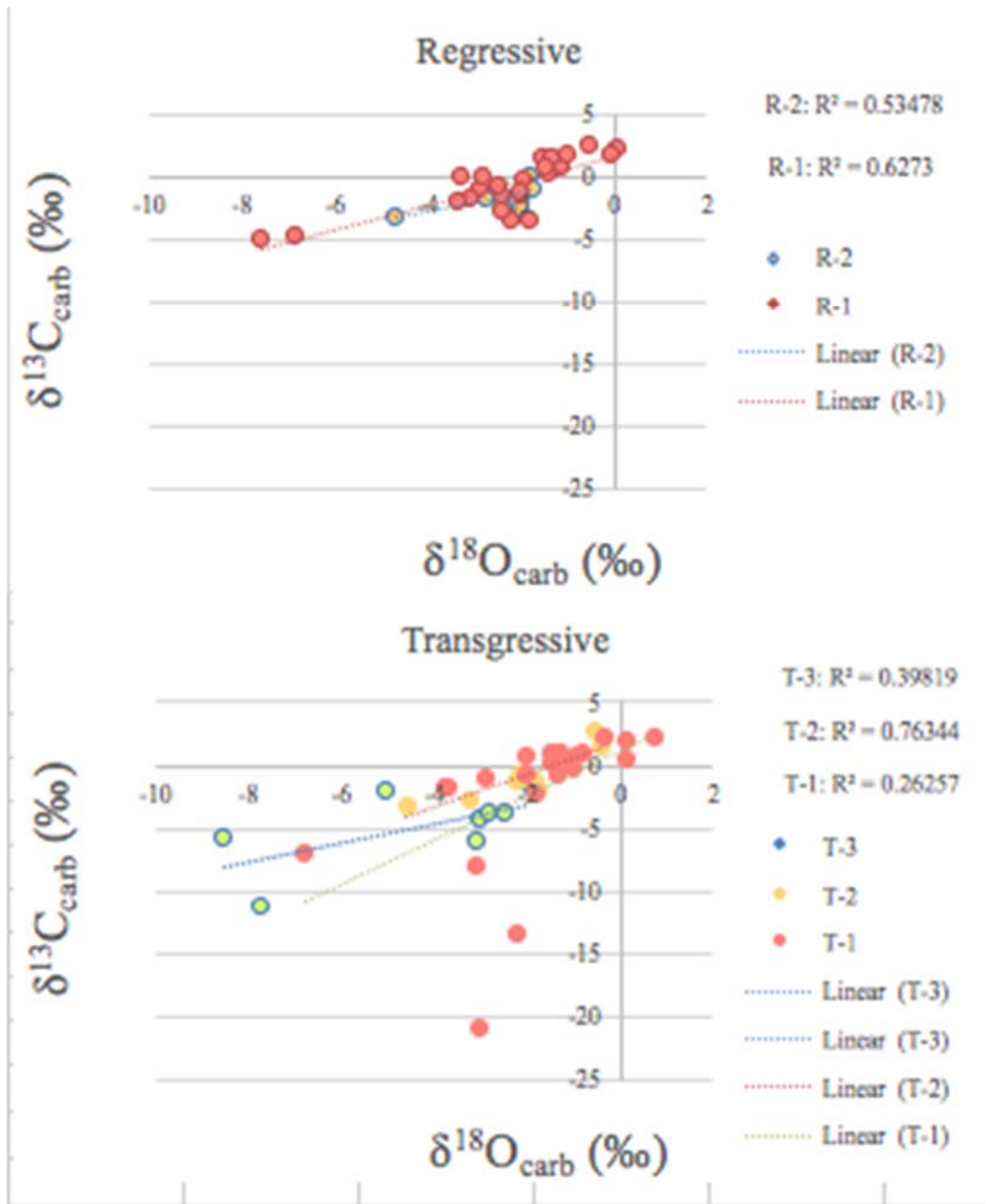
The component inorganic isotope values described as a function of transgressive and regressive cycles through the three sequences. The T-1 and T-3 components were more diagenetically altered due to low Mg calcite precipitation that cements the CCG clastic grains; whereas, the regressive cycle is relatively unaltered.

APPENDIX C: Isotopic Signatures of Mixed-System

ISOTOPIC SIGNATURES OF MIXED-SYSTEM

Inorganic carbon values utilized for each component in primary signature reconstruction of the Miocene-Pliocene mixed-system.

Component Type	$\delta^{13}C_{Carbonate}$ (‰)	Source
Benthic Foraminifera	0.3	(Milliman, 1974), pg 84
Planktic Foraminifera	1	(Richard G. Fairbanks, Mark Sverdlove, Rosemary Free, Peter, H. Wiebe, 1982)
Coral Debris	-0.09	(Milliman, 1974) pg 96
Mollusk	0	(Milliman, 1974) (pg 116)
Quartz Grain	N/A	
Recrystalized	N/A	
CCG	N/A	
Bryozoans	2.2	(Prasada Rao, 1993)
Calcite	N/A	
Sea urchin	0.725	(Milliman, 1974) pg 134
Worm tube	-1.8	(González & Lohmann, n.d.)
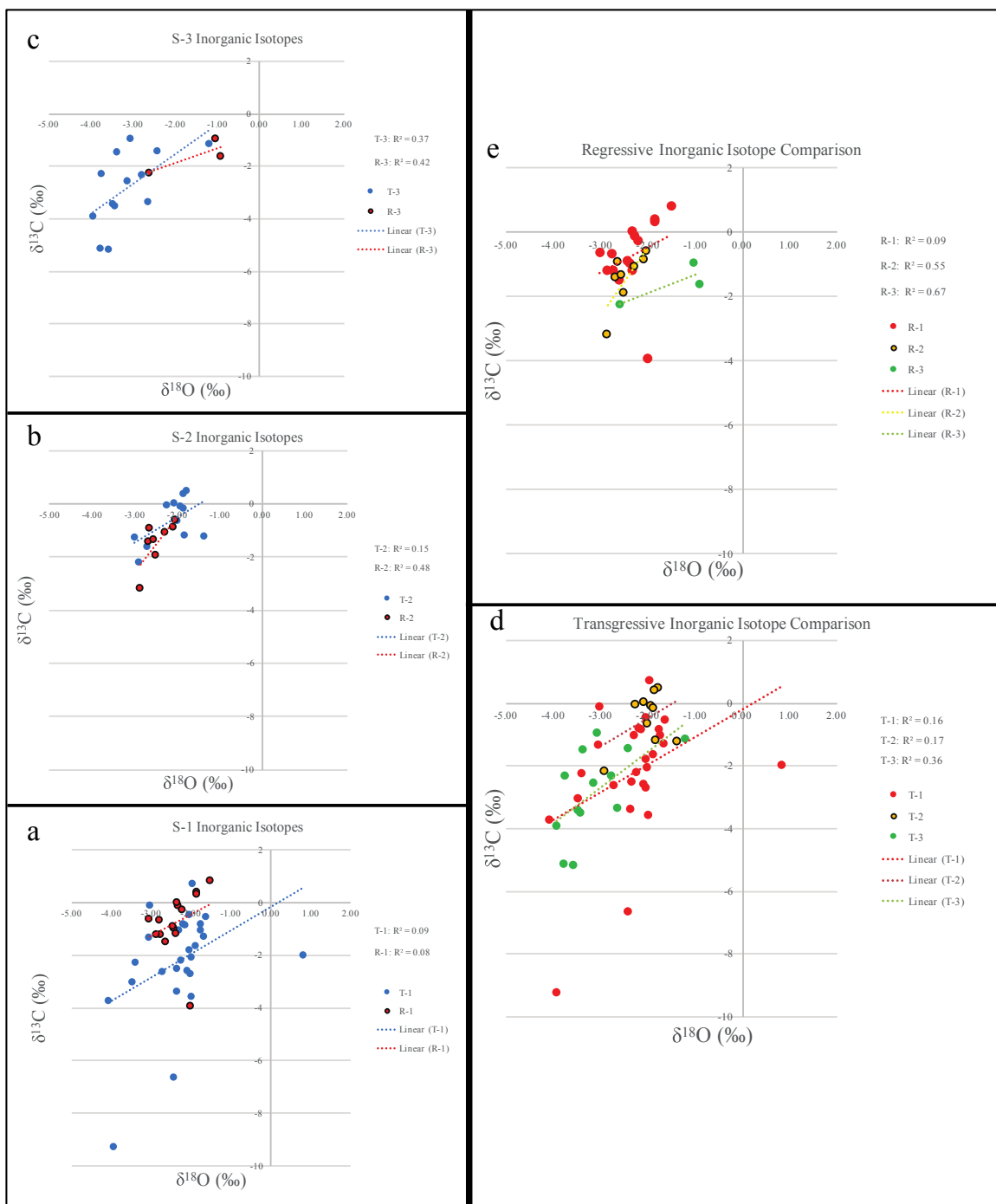
Bulk inorganic isotope cross-plots of $\delta^{13}C$ and $\delta^{18}O$ through the Gurabo Fm. a-c) comparing the isotopes in terms of sequences d-e) comparing the isotopes in terms of cycles to conceptually determine the diagenetically altered zones of the Gurabo Fm.

APPENDIX D: Carbonate Content

CARBONATE CONTENT

Bulk carbonate content was lowest in S-1 and increases through each subsequent sequence as the platform became better established throughout the deposition of the Gurabo Fm.

Sequence	Statistic	Bulk Carbonate Content (%)
Gurabo Fm.	Max	80.9
	Avg	28.6
	Min	1.3
S-3	Max	80.9
	Avg	42.5
	Min	6.3
S-2	Max	58.5
	Avg	34.1
	Min	11.4
S-1	Max	72.7
	Avg	21.9
	Min	2.6

The bulk and mud carbonate content through each sequence statistically analyzed by transgressive and regressive cycles.

Sequence	Cycle	Statistic	Bulk Carbonate Content (%)	Carbonate Mud Content (%)
S-3	Regressive	Maximum	80.9	37.9
	Regressive	Average	61.1	N/A
	Regressive	Sample Number	10	1
	Transgressive	Maximum	61.3	17.6
	Transgressive	Average	28.8	11.1
	Transgressive	Sample Number	14	6
S-2	Regressive	Maximum	58.5	18.1
	Regressive	Average	39.5	14.4
	Regressive	Sample Number	14	5
	Transgressive	Maximum	56.5	12.0
	Transgressive	Average	29.0	8.1
	Transgressive	Sample Number	15	7
S-1	Regressive	Maximum	72.7	31.3
	Regressive	Average	40.7	8.9
	Regressive	Sample Number	24	11
	Transgressive	Maximum	57.2	17.1
	Transgressive	Average	10.8	5.7
	Transgressive	Sample Number	41	31

Ratio of mud-to-bulk carbonate values within the carbonate-rich intervals that have mud-size carbonate values present. The mud-derived carbonate contains 30-40% of the bulk carbonate signature in these intervals.

Height in section (m)	Statistic	Ratio
85-120	Max	0.6
	Avg	0.4
	Min	0.1
	Sample size	13
68-79	Max	0.6
	Avg	0.4
	Min	0.2
	Sample size	4
48-52	Max	0.8
	Avg	0.3
	Min	0.0
	Sample size	3
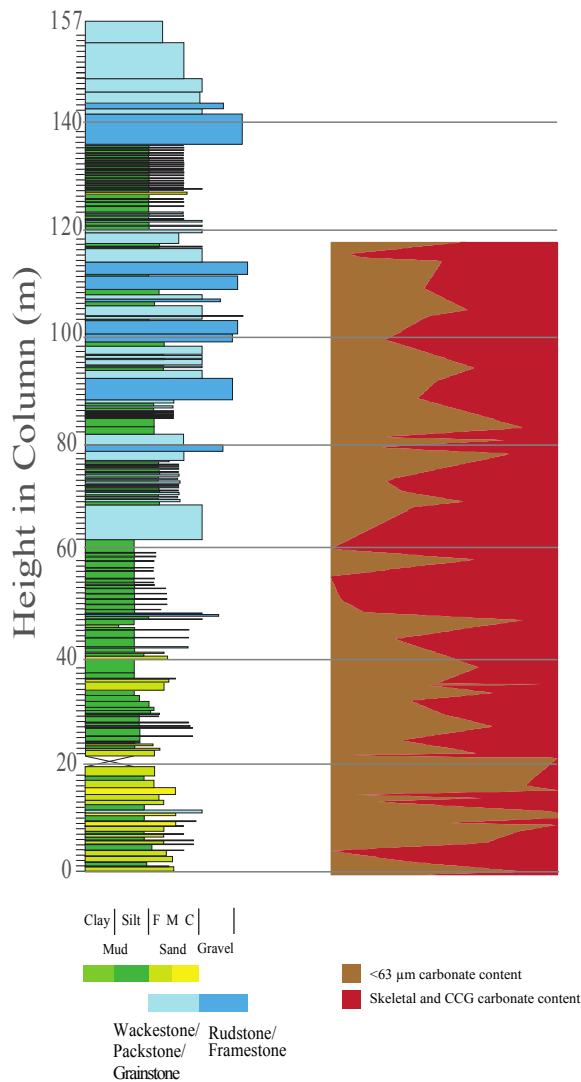
Bulk (red) and mud carbonate (brown) content through the Rio Mao section Gurabo Fm.
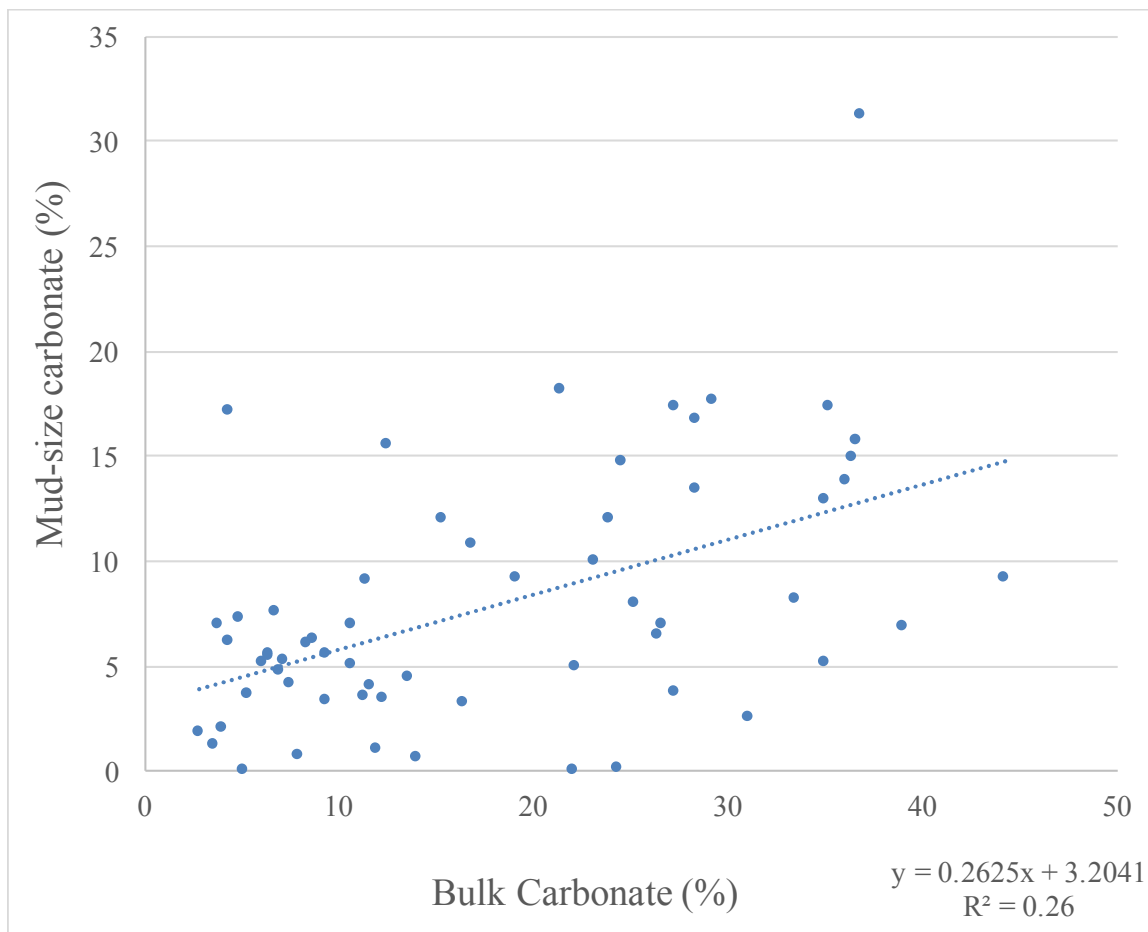
The lack of correlation between bulk to mud-derived carbonate through the Rio Mao section Gurabo Fm.

APPENDIX E: Statistical significance tables

A statistical cross-plot of the p-values for each compared transgressive, T, and regressive, R, cycles' $\delta^{13}C$ isotopic composition. This plot illustrates that the cycles within each sequence are significantly different for each pair.

Carbon						
	R-1	R-2	R-3	T-1	T-2	T-3
R-1	-					
R-2	0.087	-				
R-3	0.034	0.643	-			
T-1	**0.004**	0.106	0.212	-		
T-2	0.661	**0.0364**	0.014	0.001	-	
T-3	0.00012	0.007	**0.023**	0.249	0	-

A statistical cross plot of the p-values for each compared transgressive, T, and regressive, R, cycles $\delta^{18}O$ isotopic composition. This plot proves that the paired T-R cycle for S-3 was inherently different, but the S-1 and S-2 cycle pairs have similar oxygen isotope values.

Oxygen						
	R-1	R-2	R-3	T-1	T-2	T-3
R-1	-					
R-2	0.5	-				
R-3	0.008	0.015	-			
T-1	**0.72**	0.4	0.017	-		
T-2	0.2	**0.07**	0.076	0.49	-	
T-3	0.001	0.006	**0.001**	0.002	0.0004	-

VITA

Brandon Glenn Burke was born in Houston, Texas, on February 8, 1989. His parents are Glenn Patrick Burke and Vicki Samuels Burke. He received his elementary education at River Oaks Baptist School and his secondary education at Episcopal High School. In August 2008 he began his undergraduate career at Iowa State University where he studied geology and was a varsity member of the golf team. He transferred to Rice University in 2009 and received his B.S. degree in Earth Science through the Geophysics track in May 2013. In August 2015, he commenced his graduate studies at the Rosenstiel School of Marine and Atmospheric Science of the University of Miami where he was granted an M.S. degree in August 2018.

Permanent Address: 5913 Katy Street, Houston, Texas   77007